

N73-11999

NASA CONTRACTOR
REPORT



NASA CR-2157

NASA CR-2157

CALCULATIVE TECHNIQUES FOR
TRANSONIC FLOWS ABOUT CERTAIN CLASSES
OF WING-BODY COMBINATIONS - PHASE II

by Stephen S. Stahara and John R. Spreiter

Prepared by

NIELSEN ENGINEERING & RESEARCH, INC.

Mountain View, Calif. 94040

for Ames Research Center

NATIONAL AERONAUTICS AND SPACE ADMINISTRATION • WASHINGTON, D. C. • DECEMBER 1972

1. Report No. NASA CR-2157	2. Government Accession No.	3. Recipient's Catalog No.	
4. Title and Subtitle Calculative Techniques for Transonic Flows About Certain Classes of Wing-Body Combinations - Phase II		5. Report Date December 1972	
		6. Performing Organization Code	
7. Author(s) Stephen S. Stahara and John R. Spreiter		8. Performing Organization Report No.	
		10. Work Unit No.	
9. Performing Organization Name and Address Nielsen Engineering and Research, Inc. 850 Maude Avenue Mountain View, CA 94040		11. Contract or Grant No. NAS 2-6259	
		13. Type of Report and Period Covered Contractor Report	
12. Sponsoring Agency Name and Address National Aeronautics & Space Administration Washington, D.C. 20546		14. Sponsoring Agency Code	
15. Supplementary Notes			
16. Abstract Theoretical analysis and associated computer programs were developed for predicting properties of transonic flows about certain classes of wing-body combinations. The procedures used are based on the transonic equivalence rule and employ either an arbitrarily-specified solution or the local linearization method for determining the nonlifting transonic flow about the equivalent body. The class of wind planform shapes include wings having sweptback trailing edges and finite tip chord. Theoretical results are presented for surface and flow-field pressure distributions for both nonlifting and lifting situations at Mach number one.			
17. Key Words (Suggested by Author(s)) Transonic Flow Aerodynamics Wing-Body Combinations Transonic Equivalence Rule Local Linearization		18. Distribution Statement UNCLASSIFIED-UNLIMITED	
19. Security Classif. (of this report) UNCLASSIFIED	20. Security Classif. (of this page) UNCLASSIFIED	21. No. of Pages 114	22. Price* 3.00

CALCULATIVE TECHNIQUES FOR TRANSONIC FLOWS

ABOUT CERTAIN CLASSES OF WING-BODY COMBINATIONS -- PHASE II

By Stephen S. Stahara and John R. Spreiter*
Nielsen Engineering & Research, Inc.

SUMMARY

Theoretical analysis and the development of associated computer programs were carried out for the purpose of developing computational techniques for predicting properties of transonic flows about certain classes of wing-body combinations. The procedures used are based on the transonic equivalence rule and employ either an arbitrarily-specified solution or the local linearization method for determining the nonlifting transonic flow about the equivalent body. Theoretical results obtained by using the local linearization method are presented for surface and flow-field pressure distributions for certain members of the general classes of configurations studied, for both nonlifting and lifting situations, at $M_\infty = 1$.

The computational programs developed under this report are documented and presented in a general user's manual included as part of the report.

INTRODUCTION

Stimulated by the need for accurate prediction of transonic flows about realistic aircraft configurations, recent research is producing significant advances in the ability to predict theoretically both two and three-dimensional transonic flows about a wide variety of aerodynamic shapes. While current emphasis seems to be placed on the development of numerical techniques (refs. 1, 2, 3, 4, 5), it has become clear that, although significant accuracy limitations need not exist for advanced computer programs, these techniques do have cost limitations with regard to both accuracy and the use of alternate methods. Consequently, in

*Professor, Departments of Applied Mechanics and Aeronautics and Astronautics, Stanford University, Stanford, California. (Consultant at Nielsen Engineering & Research, Inc.)

order to enhance these computational efforts, the parallel development of proven analytical and analytic/numeric methods to provide accurate first approximations, for example, in the systematic study of a large number of configurations, is clearly warranted.

Previous investigations by Nielsen Engineering & Research, Inc. (NEAR) in reference 6, where the local linearization method and the transonic equivalence rule were applied to predict surface and flow-field properties of several general classes of axisymmetric and nonaxisymmetric bodies for both lifting and nonlifting situations, and in reference 7, where those results were extended to include several classes of wing-body combinations, have demonstrated the effectiveness of such a combined approach.

While the ultimate goal of the present investigation is to develop computational techniques for the prediction of the flow field, pressure distribution, and aerodynamic characteristics of three-dimensional, lifting, wing-body combinations, the purposes of this study are to extend the results of reference 7 to include a more general class of wing planform shapes, specifically, wings having (1) sweepback trailing edges, and (2) finite tip chords. In addition, the computer programs developed in reference 7 were to be further enhanced with regard to minimization of computational time and applicability to wider classes of equivalent body shapes and equivalent body transonic solutions.

LIST OF SYMBOLS

a	major axis of elliptic cross section of indented body
a_{sb}	major axis of elliptic cross section of smooth (non-indented) body
AR	aspect ratio
b	minor axis of elliptic cross section of indented body
c	equal to $\sqrt{a^2 - b^2}$
c_w	wing chord
c	Euler's constant

$C_{D_{eb}}$	drag coefficient of equivalent body of revolution, $D_{eb}/q_\infty S_m$ eq. (22)
C_{D_t}	total drag coefficient, $D_t/q_\infty S_m$
$C_{D_{\alpha=0}}$	drag coefficient at zero lift, $D_{\alpha=0}/q_\infty S_m$
C_L	lift coefficient, $L/q_\infty S_m$
C_p	pressure coefficient, $(p - p_\infty)/\frac{1}{2} \rho_\infty U_\infty^2$
$C_{p_{eb}}$	pressure coefficient due to equivalent body of revolution
C_m	pitching moment coefficient about nose, $M_y/q_\infty S_m l$ (positive nose-up)
C_{tip}	wing tip chord
C_{R_t}	wing root chord
D	maximum diameter of equivalent body of revolution
D_{eb}	drag of equivalent body of revolution
D_i	drag due to lift
D_t	total drag
$D_{\alpha=0}$	total drag at zero lift
k	equal to $M_\infty^2(\gamma + 1)/U_\infty$
K	complete elliptic integral of first kind
ℓ	complete body length
L	lift
m	exponent describing wing ordinates, eqs. (8), (9)
$M_{cr,i}$	lower critical Mach number on equivalent body of revolution
$M_{cr,u}$	upper critical Mach number on equivalent body of revolution
M_y	pitching moment about nose, positive nose-up

M_∞	free-stream Mach number
n	exponent describing equivalent body ordinates and related to location of point of maximum thickness, eqs. (11), (12), (13), (14)
P_∞	free-stream pressure
q_1, q_2, q_3 q_4, q_5, q_6	quantities defined by eqs. (55), (56), (57)
q_∞	free-stream dynamic pressure
r	radial distance in crossflow plane, $\sqrt{y^2 + z^2}$
R_b	radius of indented body of revolution
R_{eb}	radius of equivalent body of revolution
R_1	radius of circular body in transformed (σ_1) plane, eq. (33)
s	semispan of wing which, depending on axial location, represents either leading ($s = s_\ell$) or trailing ($s = s_t$) edge
s_ℓ	semispan of wing leading edge
s_t	semispan of wing trailing edge
s_1	semispan of wing in transformed (σ_1) plane, eq. (34)
$s_{1\ell}$	semispan of wing leading edge in transformed (σ_1) plane
s_{1t}	semispan of wing trailing edge in transformed (σ_1) plane
S_b	area distribution of indented body of revolution
S_{eb}	area distribution of equivalent body of revolution
S_m	maximum area distribution of equivalent body of revolution, $\pi D^2/4$
TR	wing planform taper ratio, C_{tip}/C_{R_t}
u, v, w	perturbation velocity components parallel to the x, y, z axes, respectively

u_B, v_B, w_B	perturbation velocity components associated with solution for transonic flow about equivalent body of revolution
$u_{2,B}, v_{2,B}, w_{2,B}$	perturbation velocity components associated with two-dimensional incompressible solution of expansion or contraction of equivalent cross section in crossflow plane
$u_{2,t}, v_{2,t}, w_{2,t}$	perturbation velocity components associated with two-dimensional incompressible solution of expanding or contracting cross section in crossflow plane
$u_{2,\alpha}, v_{2,\alpha}, w_{2,\alpha}$	perturbation velocity components associated with two-dimensional incompressible solution of translating cross section in crossflow plane
U_∞	free-stream velocity
$w_{2,t}$	complex potential describing two-dimensional incompressible flow about expanding or contracting cross section in crossflow plane
$w_{2,\alpha}$	complex potential describing two-dimensional incompressible flow about translating cross section in crossflow plane
x, y, z	body-fixed Cartesian coordinate system with x axis direction rearward and aligned with longitudinal axis of body, y axis directed to the right facing forward, and z axis directed vertically upward
x_s	location of point closest to origin where $S''_{eb}(x) = 0$
x_b	axial location of body base
x_{rle}	axial location of wing leading edge root chord
x_{rle_1}	axial location of point where wing leading edge pierces body surface
x_{rte}	axial location of wing trailing-edge root chord
x_{rte_1}	axial location of point where wing trailing edge pierces body surface
x_{sm_1}	axial location of wing tip chord leading edge
x_{sm_2}	axial location of wing tip chord trailing edge
\bar{x}	axial distance from wing leading edge

\bar{y}	lateral distance from wing leading edge
z_w	wing ordinates, eqs. (8), (9)
α	angle of attack
β_{le}	wing leading-edge sweep angle
β_{te}	wing trailing-edge sweep angle
γ	ratio of specific heats
θ	polar angle in crossflow plane
λ	ratio of major to minor axes of elliptic cross section, a/b
ξ, ξ_1	dummy variables
ρ_∞	free-stream density
σ	complex variable in crossflow plane, $y + iz$
σ_1	complex variable in transformed crossflow plane, $y_1 + iz_1$
τ_{eb}	thickness ratio of equivalent body of revolution, D/ℓ
τ_w	thickness-to-chord ratio of wing profile, eq. (10)
ϕ	perturbation velocity potential
ϕ_B	perturbation velocity potential associated with transonic flow about equivalent body of revolution
ϕ_2	perturbation velocity potential associated with two-dimensional incompressible solutions to translation and growth of cross section in crossflow plane
$\phi_{2,B}$	perturbation velocity potential associated with two-dimensional incompressible solution for expansion or contraction of equivalent cross section in crossflow plane
$\phi_{2,t}$	perturbation velocity potential associated with two-dimensional incompressible solution for expansion or contraction of cross section in crossflow plane
$\phi_{2,\alpha}$	perturbation velocity potential associated with two-dimensional incompressible solution for translation of cross section in crossflow plane

ANALYSIS

General Considerations

Because the current work is an extension of that of reference 7, the basic theory and equations used are discussed in depth in that reference and their derivation will not be repeated here. For convenience, however, those points relevant to the present work will be outlined.

The coordinate system used for all of the three-dimensional flows considered herein is a body-fixed Cartesian system centered at the body nose with the x axis directed rearward and aligned with the longitudinal axis of the body, the y axis directed to the right, facing forward, and the z axis directed vertically upward, as shown in figure 1. For lifting situations, the free-stream direction is taken to be inclined at any arbitrary small angle α to the x axis and confined to the $x-z$ plane so that there is no sideslip. The governing partial differential equation for the perturbation potential ϕ is given by

$$(1 - M_\infty^2) \phi_{xx} + \phi_{yy} + \phi_{zz} = \frac{M_\infty^2 (\gamma + 1)}{U_\infty} \phi_x \phi_{xx} \quad (1)$$

where M_∞ is the free-stream Mach number, γ the ratio of specific heats, and U_∞ the free-stream velocity. The pressure coefficient C_p in the above reference frame is given by

$$C_p = - \frac{2}{U_\infty^2} (\phi_x + \alpha \phi_z) - \frac{1}{U_\infty^2} (\phi_y^2 + \phi_z^2) \quad (2)$$

The transonic equivalence rule enables the perturbation potential ϕ to be expressed in the form

$$\phi = \phi_{2,\alpha} + \phi_{2,t} - \phi_{2,B} + \phi_B \quad (3)$$

where each of the individual components has the meaning indicated in figure 1. Since $\phi_{2,\alpha}$, $\phi_{2,t}$, and $\phi_{2,B}$ satisfy the two dimensional incompressible Laplace equation

$$(\phi_{2,i})_{yy} + (\phi_{2,i})_{zz} = 0 \quad (4)$$

(where the subscript i depends upon the particular potential in question), they are independent of Mach number. Hence, the only portion of the solution dependent upon M_∞ is ϕ_B and this term represents the solution to the full transonic equation (1) for the nonlifting flow about the equivalent body of revolution. Because the equivalence rule places no essential restrictions on the methods of calculating ϕ_B , its solution may be determined in a variety of ways. For example, it can be given by an exact numerical solution, by experimental data, by an approximate analytic solution, or by a combined analytic/numeric solution such as the local linearization method. One of the tasks of the present work is to extend the applicability of the computer programs developed in reference 7 to include general, arbitrarily-specified solutions for ϕ_B , and the method of doing this is detailed in the user's manual. If the local linearization method is used to determine ϕ_B , or more conveniently, $u_B = (\phi_B)_x$, then one of the following set of three first-order nonlinear differential equations must be integrated according to whether $M_\infty \approx 1$, $M_\infty < M_{cr,l}$, or $M_{cr,u} < M_\infty$, where $M_{cr,l}$, $M_{cr,u}$ are the lower and upper critical Mach numbers, respectively.

Thus, for accelerating flows with $M_\infty \approx 1$

$$\begin{aligned} \frac{d}{dx} \left(\frac{u_B}{U_\infty} \right) = & \frac{S'_{eb}(x) S''_{eb}(x)}{4\pi S_{eb}(x)} + \exp \left\{ \frac{4\pi}{S''_{eb}(x)} \left[\frac{u_B}{U_\infty} + \frac{M_\infty^2 - 1}{M_\infty^2(\gamma + 1)} \right. \right. \\ & \left. \left. - \frac{S''_{eb}(x)}{4\pi} \ln \frac{M_\infty^2(\gamma + 1) S_{eb}(x) e^C}{4\pi x} - \frac{1}{4\pi} \int_0^x \frac{S''_{eb}(\xi) - S''_{eb}(\xi)}{x - \xi} d\xi \right] \right\} \end{aligned} \quad (5)$$

for purely subsonic flows ($M_\infty < M_{cr,l}$)

$$\frac{d}{dx} \left(\frac{u_B}{U_\infty} \right) = \frac{S_{eb}'''(x)}{4\pi} \ln (1 - M_\infty^2 - ku_B) + \frac{d}{dx} \left[\frac{S_{eb}''(x)}{4\pi} \ln \frac{S_{eb}(x)}{4\pi x(\ell - x)} + \frac{1}{4\pi} \int_0^\ell \frac{S_{eb}''(x) - S_{eb}''(\xi)}{|x - \xi|} d\xi \right] \quad (6)$$

and for purely supersonic flows ($M_{cr,u} < M_\infty$)

$$\frac{d}{dx} \left(\frac{u_B}{U_\infty} \right) = \frac{S_{eb}'''(x)}{4\pi} \ln (M_\infty^2 - 1 + ku_B) + \frac{d}{dx} \left[\frac{S_{eb}''(x)}{4\pi} \ln \frac{S_{eb}(x)}{4\pi x^2} + \frac{1}{2\pi} \int_0^x \frac{S_{eb}''(x) - S_{eb}''(\xi)}{x - \xi} d\xi \right] \quad (7)$$

where C in equation (5) is Euler's constant ≈ 0.577 , k in equations (6) and (7) is equal to $M_\infty^2(\gamma + 1)/U_\infty$, $S_{eb}(x)$ represents the area distribution of the equivalent body, and primes indicate differentiation with respect to the appropriate variable. These differential equations have been programmed for computation in reference 6 where details regarding starting conditions, numerical techniques, accuracy, limitations, etc. are provided.

Wing and Body Geometry

The classes of wing-body configurations examined in reference 7 and in this study are composed of finite thickness wing and either circular or elliptic cross-sectional bodies in which the bodies are area-rule indented along the wing-body junction in such a manner that the total cross-sectional area distribution (body plus wing) remains identical to that of a smooth body having a certain specified profile. The general class of wings considered have symmetric planforms consisting of straight leading and trailing edges, swept at arbitrary angles β_{le} and β_{te} respectively, to the y axis. In reference 7, the planform shapes were restricted to wings having either straight or sweptforward trailing edges and zero taper ratio. This work extends that class to wings with sweptback trailing edges and taper ratio between zero and one, as shown in figures 2 and 3. The wing profiles are represented by expressions of the form

$$\frac{z_w}{c_w} = \frac{\tau_w^{m/(m-1)}}{2(m-1)} \left(\frac{x}{c_w} - \left(\frac{x}{c_w} \right)^m \right) \quad (8)$$

or

$$\frac{z_w}{c_w} = \frac{\tau_w^{m/(m-1)}}{2(m-1)} \left(1 - \frac{x}{c_w} - \left(1 - \frac{x}{c_w} \right)^m \right) \quad (9)$$

where c_w is the local chord, x the distance from the leading edge, m is a constant ≥ 2 , and τ_w is the wing thickness-to-chord ratio. In addition, the wings are assumed to maintain a constant thickness-to-chord ratio across the span, with the consequence that the wing profiles at all spanwise locations are geometrically similar. Thus,

$$\frac{\tau_w}{2} = \frac{(z_w(x,y))_{\max}}{c_w(y)} = \frac{(z_w(x,0))_{\max}}{C_{Rt}} \quad (10)$$

where C_{Rt} is the wing root chord.

Two categories of body shape are considered. Figure 2(a) and (b), illustrates two members of the first category which have indented bodies that are circular in cross section, while figure 3(a) and (b) illustrates two members of the second category which have indented bodies that are elliptic in cross section and that maintain a constant ratio $\lambda (=a/b)$ of semimajor to semiminor axis along the entire body length. In reference 7, the profiles of the equivalent bodies of revolution of the wing-circular body combinations are described by the expressions

$$\frac{R_{eb}}{\ell} = \frac{\tau_{eb} n^{n/(n-1)}}{2(n-1)} \left[\frac{x}{\ell} - \left(\frac{x}{\ell} \right)^n \right] \quad (11)$$

where the exponent n is given in terms of the location of maximum radius by

$$\left(\frac{x}{\ell} \right)_{R_{max}} = \left(\frac{1}{n} \right)^{1/(n-1)} \quad (12)$$

or

$$\frac{R_{eb}}{\ell} = \frac{\tau_{eb} n^{n/(n-1)}}{2(n-1)} \left[1 - \frac{x}{\ell} - \left(1 - \frac{x}{\ell} \right)^n \right] \quad (13)$$

where

$$\left(\frac{x}{\ell} \right)_{R_{max}} = 1 - \left(\frac{1}{n} \right)^{1/(n-1)} \quad (14)$$

while the equivalent bodies of the wing-elliptic body combinations are parabolic-arc bodies, i.e. equations (11) or (13) with $n = 2$. This work extends the class of equivalent body profiles for both the circular and elliptic body shapes to include arbitrarily specified functions subject to certain closure and continuity restrictions on the derivatives that are discussed in the appropriate section of the included user's manual.

Straight or Sweptforward Trailing
Edge Planforms

Circular bodies. - For finite thickness wing-circular body combinations having wings with finite tip chords and trailing edges that are either straight or sweptforward, the complex potentials, $w_{2,a}$, $w_{2,t}$, and $w_{2,B}$ can be readily determined from the work of reference 7.

$$w_{2,a} = -iU_\infty \alpha \left\{ \left[\left(\sigma + \frac{R_b^2}{\sigma} \right)^2 - \left(s + \frac{R_b^2}{s} \right)^2 \right]^{1/2} - \sigma \right\} \quad (15)$$

$$\begin{aligned} \frac{w_{2,t}}{U_\infty} &= \frac{1}{\pi} \int_{R_b}^s \frac{dZ_w(x, \xi)}{dx} \ln \left[\frac{(\sigma^2 - \xi^2)(\sigma^2 - \frac{R_b^4}{\xi^2})}{\sigma^4} \right] d\xi \\ &\quad + \frac{1}{2\pi} \left[S'_{eb}(x) + 4 Z_w(x, R_b) \frac{dR_b}{dx} \right] \ln \sigma \end{aligned} \quad (16)$$

$$\frac{w_{2,B}}{U_\infty} = \frac{S'_{eb}(x)}{2\pi} \ln \sigma \quad (17)$$

where σ is the complex variable in the crossflow plane

$$\sigma = y + iz \quad (18)$$

R_b is the indented body radius, s - depending upon axial location - represents the local wing semispan of either the leading ($s = s_t$) or trailing ($s = s_{t'}$) edge, and Z_w represents the wing ordinates. The velocity components associated with these potentials can be found by substituting those expressions into the general formulas:

$$u_{2,i} = \frac{\partial \phi_{2,i}}{\partial x} = R.P. \frac{\partial w_{2,i}}{\partial x} \quad (19)$$

$$(v - w)_{2,i} = (\phi_y - i\phi_z)_{2,i} = \frac{dw_{2,i}}{d\sigma} \quad (20)$$

where the subscript i depends upon the particular potential in question and R.P. signifies the real part of a complex quantity.

These operations have been carried out and the resulting expressions, which are quite lengthy, are given in reference 7. It should be noted that, in the evaluation of the velocity components associated with the thickness problem (w_2, t), different sets of expressions are necessary depending on whether the point of interest is (1) at a general location, (2) on the wing surface, or (3) at the wing-body junction. These distinctions are required in order to account properly for the Cauchy singularities which appear in several of the integrals associated with the thickness velocity components. No such distinctions are required for the lifting ($w_{2,\alpha}$) or equivalent thickness ($w_{2,B}$) problems.

Because of the symmetry of the class of wing-body combinations considered, nonlifting flows will produce no lateral forces or moments. The only force will be the longitudinal drag force which can be determined through the general formula,

$$D_{\alpha=0} = D_{eb} - \frac{\rho_\infty}{2} \left(\oint_{C_t} \phi_{2,t} \frac{\partial \phi_{2,t}}{\partial n} d\sigma_t - \oint_{C_B} \phi_{2,B} \frac{\partial \phi_{2,B}}{\partial n} d\sigma_B \right) \quad (21)$$

where D_{eb} represents the drag of the equivalent body while the other two terms involve the line integral along their respective contours (C_t is the contour defined by the cross section of the wing-body combination while C_B is the contour about the equivalent area circular cylinder) of the product of the appropriate velocity potential and the normal velocity associated with it. We note that the drag indicated by equation (21) refers to the inviscid drag of the configuration minus the base pressure drag. As pointed out in reference 8, there exist many shapes of aerodynamic interest for which the two integrals involved cancel. In particular, we note that if the equivalent body and the original body have the same shape and surface slope at the base, as is the case for configurations studied here, then since both integrals are carried out over the same contour along which $\phi_{2,t} = \phi_{2,B}$ and $\partial \phi_{2,t}/\partial n = \partial \phi_{2,B}/\partial n$, the integrals cancel and $D_{\alpha=0} = D_{eb}$. If we define a drag coefficient C_D based upon the maximum cross-sectional area of the equivalent body, S_m , then

$$C_{D_{\alpha=0}} = C_{D_{eb}} = \frac{D_{eb}}{\frac{\rho_\infty}{2} U_\infty^2 S_m} = \frac{1}{S_m} \int_0^{X_b} C_{P_{eb}} S'_{eb}(x) dx \quad (22)$$

where X_b is the axial location of the body base and $C_{P_{eb}}$ is the pressure coefficient on the surface of the nonlifting equivalent body and is equal to

$$C_{P_{eb}} = -2 \frac{u_B}{U_\infty} - \left(\frac{dR_{eb}(x)}{dx} \right)^2 \quad (23)$$

For the lifting situation, an exact analysis of the aerodynamic forces and moments, even within the framework of small disturbance theory, is quite formidable. The general formulas for determining the coefficients of lift, pitching moment, and drag are given by

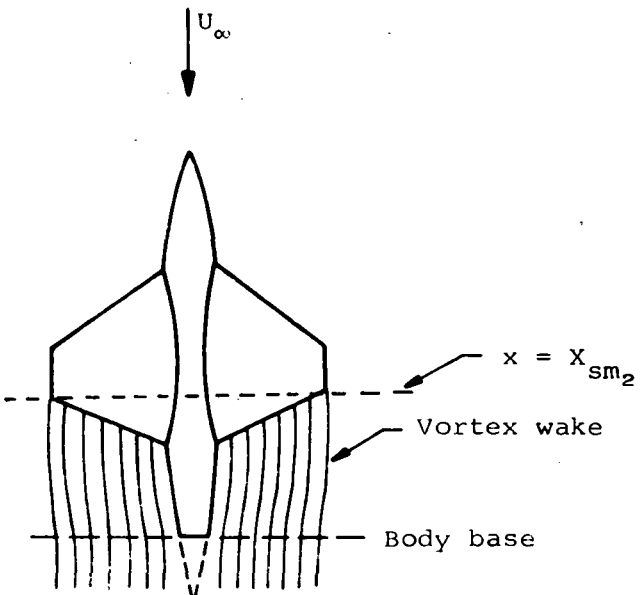
$$C_L = \frac{L}{S_m q_\infty} = -\frac{2}{U_\infty} \oint_C \phi_{2,\alpha} d\sigma_C \quad (24)$$

$$C_m = \frac{M_y}{q_\infty \cdot S_m \cdot l} = \frac{-1}{q_\infty \cdot S_m \cdot l} \int_0^X \xi \frac{dL(\xi)}{d\xi} d\xi \quad (25)$$

$$C_{D_t} = \frac{D_t}{q_\infty S_m} = \frac{D_{eb}}{q_\infty S_m} - \frac{1}{S_m U_\infty^2} \left(\oint_C \phi_{2,\alpha} \frac{\partial \phi_{2,\alpha}}{\partial n} d\sigma_C + \oint_C \phi_{2,t} \frac{\partial \phi_{2,t}}{\partial n} d\sigma_t \right. \\ \left. - \oint_B \phi_{2,B} \frac{\partial \phi_{2,B}}{\partial n} d\sigma_B \right) \quad (26)$$

where now the contour C , while still taken at the base of the body, must now account for the vortex wake which springs from the wing trailing edge and, as before, the drag given by equation (26) represents the inviscid drag minus the base pressure drag. Because the vortex lines near the body surface must follow the streamlines of the flow around the body, the vortex wake will not proceed parallel to the x axis,

in general, as it does in many simpler cases considered in slender body theory; but will move away from or toward the body axis to follow the lateral expansion or contraction of the flow field near the body as shown below.



The resulting flow at the body base is influenced by the wake and, consequently, is no longer independent of the flow at cross sections preceding it. The solution of problems of this type is discussed briefly in reference 9. In general, they are quite difficult to solve and since they are by no means unique to transonic slender body flows, their exact solution is clearly beyond the scope of the present investigation. Because the analysis presented here, however, remains valid up to the axial location of the wing tip trailing edge $x = X_{sm_2}$ (i.e. as long as the edge of the wing remains a leading edge) an estimate can be made of these quantities by making the assumption that beyond that point the vortex sheet remains parallel to the x axis and does not vary with x . With this premise in mind, we can proceed to evaluate equations (24), (25), and (26). Carrying through the indicated operations (see ref. 7 for details), we arrive at the result that the coefficients of lift, drag, and pitching moment are given by

$$C_L = \frac{2\pi\alpha}{S_m} \left(s_\ell^2 + \frac{R_b^4}{s_\ell^2} - R_{eb}^2 \right) \Big|_{x = X_{sm_2}} \quad (27)$$

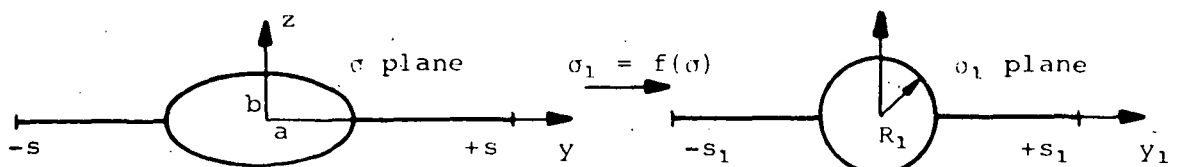
$$C_{D_t} = C_{D_{\alpha=0}} + \frac{\alpha}{2} C_L \quad (28)$$

$$C_m = \frac{2\pi\alpha}{S_m \cdot \ell} \left[-x \left(s_\ell^2 + \frac{R_b^4}{s_\ell^2} - R_{eb}^2 \right) \right] \Big|_{x = X_{sm_2}} + \int_0^{X_{rle_1}} R_{eb}^2 d\xi$$

$$+ \int_{X_{rle_1}}^{X_{sm_2}} \left(s_\ell^2 + \frac{R_b^4}{s_\ell^2} - R_{eb}^2 \right) d\xi \quad (29)$$

where the drag coefficient at zero lift $C_{D_{\alpha=0}}$ is given by equation (22) and X_{rle_1} is the axial location of the point where the wing leading edge pierces the body surface.

Elliptic bodies. - The basic analysis of wing-body combinations composed of wings having finite tip chords with trailing edges that are either straight or sweptforward and bodies having indented elliptic cross sections such that the total cross-sectional area distribution equals the area of the original smooth body with elliptic cross section proceeds in a manner analogous to that used for the circular body shapes. Apparently, the most direct approach consists of reducing the elliptic cross section to a circular one by use of the appropriate Joukowski transformation and then applying the methods used for the circular shapes. The transformation required to take the ellipse into the circle shown below



is given by

$$\sigma_1 = \frac{\sigma + \sqrt{\sigma^2 - c^2}}{2} \quad (30)$$

where

$$c^2 = a^2 - b^2 \quad (31)$$

and

$$\sigma_1 = y_1 + iz_1 \quad (32)$$

This takes the ellipse into a circle of radius

$$R_1 = \frac{(a + b)}{2} \quad (33)$$

and the semispan s into the shortened semispan

$$s_1 = \frac{s + \sqrt{s^2 - c^2}}{2} \quad (34)$$

The potentials $w_{2,\alpha}$, $w_{2,t}$, and $w_{2,B}$ are then given by

$$\frac{w_{2,\alpha}}{U_\infty} = -ia \left\{ \left[\left(\sigma_1 + \frac{R_1^2}{\sigma_1} \right)^2 - \left(s_1 + \frac{R_1^2}{s_1} \right)^2 \right]^{1/2} - 0 \right\} \quad (35)$$

$$\begin{aligned} \frac{w_{2,t}}{U_\infty} &= \frac{1}{\pi} \int_{R_1}^{s_1} \frac{dZ_w(x, \xi_1 + \frac{c^2}{4\xi_1^2})}{dx} \ln \left[\frac{(\sigma_1^2 - \xi_1^2)(\sigma_1^2 - \frac{R_1^4}{\xi_1^2})}{\sigma_1^4} \right] \left(1 - \frac{c^2}{4\xi_1^2} \right) d\xi_1 \\ &\quad + \left(\frac{S'_{eb}(x)}{2\pi} + 2 Z_w(x, a) \frac{da}{dx} \right) \ln \sigma_1 \end{aligned} \quad (36)$$

$$\frac{w_{2,B}}{U_\infty} = \frac{S'_{eb}(x)}{2\pi} \ln \sigma \quad (37)$$

The velocity components associated with these potentials are found through the operations

$$u_{2,i} = R.P. \frac{\partial w_{2,i}}{\partial x} \quad (38)$$

$$(v - w)_{2,i} = \frac{d w_{2,i}}{d \alpha_1} \frac{d \alpha_1}{d \alpha} \quad (39)$$

These have been carried out and are given in reference 7 where it must be remembered in those formulas that depending upon axial location s_1 represents either the leading ($s_1 = s_{1L}$) or trailing ($s_1 = s_{1T}$) edge in the transformed plane. For the case of nonlifting flows about these classes of symmetric configurations, no lateral forces or moments exist so that the only force present is the longitudinal drag force. This can be determined through the use of equation (21) where now the contributions of the two line integrals do not cancel since the contour over which the product $\psi_{2,t} \partial \phi_{2,t} / \partial n$ is evaluated is the elliptic cross section at the base of the body whereas the contour for evaluating $\psi_{2,B} \partial \phi_{2,B} / \partial n$ is the circular cross section of the equivalent body. Carrying out the indicated operations, we find that the drag coefficient of this general class of nonlifting elliptic wing-body combinations is

$$C_{D_{u=0}} = C_{D_{eb}} - \frac{1}{S_m} \left(\frac{S'_{eb}(x)}{2\pi} \right)^2 2 \left[\frac{2}{\lambda} \ln \left(\frac{a(\lambda + 1)}{2\lambda} \right) K \left(\frac{\sqrt{\lambda^4 - 1}}{\lambda^2} \right) - \pi \ln R_{eb} \right] \quad (40)$$

where $C_{D_{eb}}$ is the drag coefficient of the nonlifting equivalent body and is given by equation (22), and $K(\xi)$ is the complete elliptic integral of the first kind.

For lifting flows at small angles of attack about these configurations, if we apply the same assumptions regarding the trailing vortex wake as were made for the circular body case, then the evaluation of equations (24), (25), and (26) provides the following results for the lift, pitching moment, and drag coefficients.

$$C_L = \frac{2\pi\alpha}{S_m} \left\{ \left(\frac{s_\ell + \sqrt{s_\ell^2 - c^2}}{2} \right)^2 \left[1 + \frac{2c^2}{(s_\ell + \sqrt{s_\ell^2 - c^2})^2} + \left(\frac{a+b}{s_\ell + \sqrt{s_\ell^2 - c^2}} \right)^4 \right] - R_{eb}^2 \right\} \Big|_{x=X_{sm_2}} \quad (41)$$

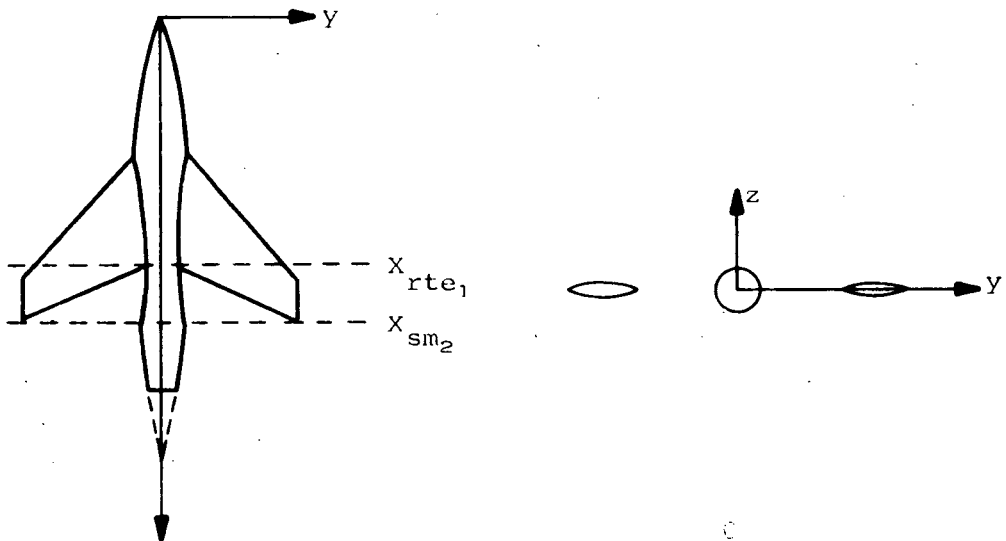
$$C_m = \frac{2\pi\alpha}{S_m \cdot \ell} \left(-x \left\{ \left(\frac{s_\ell + \sqrt{s_\ell^2 - c^2}}{2} \right)^2 \left[1 + \frac{2c^2}{(s_\ell + \sqrt{s_\ell^2 - c^2})^2} + \left(\frac{a+b}{s_\ell + \sqrt{s_\ell^2 - c^2}} \right)^4 \right] - R_{eb}^2 \right\} \Big|_{x=X_{sm_2}} + \lambda \int_0^{X_{r\ell e_1}} R_{eb}^2(x) dx \right. \\ \left. + \int_{X_{r\ell e_1}}^{X_{sm_2}} \left\{ \left(\frac{s_\ell + \sqrt{s_\ell^2 - c^2}}{2} \right)^2 \left[1 + \frac{2c^2}{(s_\ell + \sqrt{s_\ell^2 - c^2})^2} + \left(\frac{a+b}{s_\ell + \sqrt{s_\ell^2 - c^2}} \right)^4 \right] - R_{eb}^2 \right\} dx \right) \quad (42)$$

$$C_{D_t} = C_{D_{\alpha=0}} + \frac{\alpha}{2} C_L \quad (43)$$

where $C_{D_{\alpha=0}}$ is the drag coefficient at zero lift and is given by equation (40).

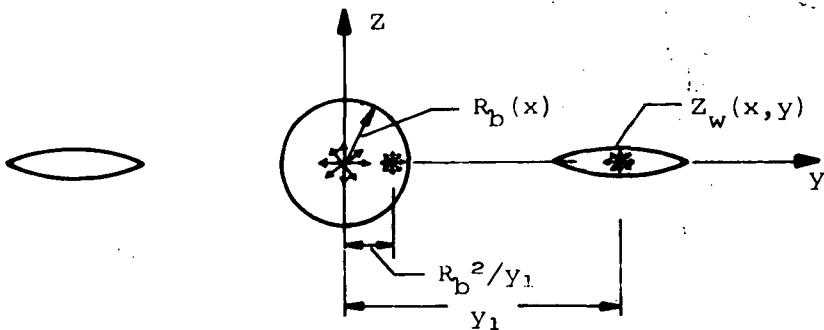
Sweptback Trailing Edge Planforms

Circular bodies. - For finite thickness wing-indented circular body combinations having sweptback trailing edges, as illustrated below,



new potential solutions are required to account for the gap between wing and body cross sections which appear in the crossflow plane between the axial locations $x = X_{rte_1}$ and $x = X_{sm_2}$. For lifting flows, the analysis is complicated even with the previously made assumption that the vortex sheet emanating from the trailing edge remains parallel to the x axis beyond the point $x = X_{sm_2}$. This is due to the presence of the vortex sheet in the gap between the wing and body from X_{rte_1} to X_{sm_2} . Consequently, the flow at any axial station beyond X_{rte_1} is influenced by the wake ahead of it and is no longer independent of the flow at preceding cross sections. Thus, the simplified analysis which was valid for lifting flows about wings with straight or sweptforward trailing edges - i.e. for cases where the edge of the wing always remained a leading edge - does not apply here. A new potential solution for W_2, α' is required and this is beyond the work scope of the present investigation.

One of the primary goals of this study, however, is to determine the potential $w_{2,t}$ associated with the thickness problem for configurations of this type. For $x < x_{rte_1}$, equation (16) is valid. For $x_{rte_1} < x < x_{sm_2}$, a new potential must be developed to account for the gap between the wing and body. This is accomplished by using an extension of the method developed by Stocker in reference 10. That method is based upon the method of singularities and models the wing thickness by placing a continuous distribution of two-dimensional incompressible sources (or sinks) along the wing chordal plane together with their appropriate images within the body. The body itself is represented by a source (or sink) at the origin. Although originally developed for a wing attached to a body, this method can accommodate such a wing body as shown below



by distributing sources (or sinks) only along the wing and appropriately imaging them within the body. This method thus provides the following expression for the complex potential $w_{2,t}(x,y,z)$:

$$\frac{w_{2,t}}{U_\infty} = \frac{1}{\pi} \int_{s_t}^{s_l} \frac{dz_w(x, \xi)}{dx} \ln \left[\frac{(\sigma^2 - \xi^2)(\sigma^2 - \frac{R_b^4}{\xi^2})}{\sigma^2} \right] d\xi + \frac{s_b'(x)}{2\pi} \ln \sigma$$

$(x_{rte_1} < x < x_{sm_2}) \quad (44)$

Since for sweptback trailing edges with $x_{rte_1} < x < x_{sm_2}$, the equivalent body area distribution and actual body area distribution are related through the expression

$$S_{eb}(x) = S_b(x) + 4 \int_{s_t}^{s_l} z_w(x, y) dy \quad (45)$$

we can write the alternate form

$$\frac{w_2, t}{U_\infty} = \frac{1}{\pi} \int_{s_t}^{s_l} \frac{dz_w(x, \xi)}{dx} \ln \left[\frac{(\sigma^2 - \xi^2)(\sigma^2 - \frac{R_b^4}{\xi^2})}{\sigma^4} \right] d\xi + \frac{S'_{eb}(x)}{2\pi} \ln \sigma$$

$(x_{rte_1} < x < x_{sm_2}) \quad (46)$

The velocity components associated with this potential are determined through equations (19) and (20). As in the case of straight or sweptforward trailing edges, proper account must be taken of the familiar Cauchy singularity which appears in several of the integrals associated with these velocity components on the wing surface. If, because of the symmetry of these configurations, we restrict attention to the first quadrant of the crossflow plane ($y \geq 0, z \geq 0$), the following results are obtained. For points at any general location but not on the wing surface,

$$\begin{aligned}
\frac{u_2, t}{U_\infty} = & \frac{1}{2\pi} \left(\int_{s_t}^{s_\ell} \frac{d^2 Z_w(x, \xi)}{dx^2} \times \right. \\
& \ln \left\{ \frac{\left[z^2 + (y - \xi)^2 \right] \left[z^2 + (y + \xi)^2 \right] \left[z^2 + (y - \frac{R_b^2}{\xi})^2 \right] \left[z^2 + (y + \frac{R_b^2}{\xi})^2 \right]}{(z^2 + y^2)^4} \right\} d\xi \\
& + 4R_b \frac{dR_b}{dx} \int_{s_t}^{s_\ell} \frac{dZ_w(x, \xi)}{dx} \frac{1}{\xi} \left[\frac{y + \frac{R_b^2}{\xi}}{z^2 + (y + \frac{R_b^2}{\xi})^2} - \frac{y - \frac{R_b^2}{\xi}}{z^2 + (y - \frac{R_b^2}{\xi})^2} \right] d\xi \\
& + \frac{dZ_w(x, s_\ell)}{dx} \frac{ds_\ell}{dx} \times \\
& \ln \left\{ \frac{\left[z^2 + (y - s_\ell)^2 \right] \left[z^2 + (y + s_\ell)^2 \right] \left[z^2 + (y - \frac{R_b^2}{s_\ell})^2 \right] \left[z^2 + (y + \frac{R_b^2}{s_\ell})^2 \right]}{(z^2 + y^2)^4} \right\} \\
& - \frac{dZ_w(x, s_t)}{dx} \frac{ds_t}{dx} \times \\
& \ln \left\{ \frac{\left[z^2 + (y - s_t)^2 \right] \left[z^2 + (y + s_t)^2 \right] \left[z^2 + (y - \frac{R_b^2}{s_t})^2 \right] \left[z^2 + (y + \frac{R_b^2}{s_t})^2 \right]}{(z^2 + y^2)^4} \right\} \\
& \left. + \frac{s''_{eb}(x)}{2} \ln [z^2 + y^2] \right) \tag{47}
\end{aligned}$$

$$\frac{v_2, t}{U_\infty} = \frac{1}{\pi} \left\{ \int_{s_t}^{s_\ell} \frac{s_\ell \cdot dZ_w(x, \xi)}{dx} \left[\frac{y - \xi}{z^2 + (y - \xi)^2} + \frac{y + \xi}{z^2 + (y + \xi)^2} + \frac{y - \frac{R_b^2}{\xi}}{z^2 + (y - \frac{R_b^2}{\xi})^2} \right. \right. \\ \left. \left. + \frac{y + \frac{R_b^2}{\xi}}{z^2 + (y + \frac{R_b^2}{\xi})^2} \right] d\xi + \frac{y}{z^2 + y^2} \left(-4 \int_{s_t}^{s_\ell} \frac{dZ_w(x, \xi)}{dx} d\xi + \frac{s'_{eb}(x)}{2} \right) \right\} \quad (48)$$

$$\frac{w_2, t}{U_\infty} = \frac{1}{\pi} \left\{ z \int_{s_t}^{s_\ell} \frac{dZ_w(x, \xi)}{dx} \left[\frac{1}{z^2 + (y - z)^2} + \frac{1}{z^2 + (y + \xi)^2} + \frac{1}{z^2 + (y - \frac{R_b^2}{\xi})^2} \right. \right. \\ \left. \left. + \frac{1}{z^2 + (y + \frac{R_b^2}{\xi})^2} \right] d\xi + \frac{z}{z^2 + y^2} \left(-4 \int_{R_b}^{s_\ell} \frac{dZ_w(x, \xi)}{dx} d\xi + \frac{s'_{eb}(x)}{2} \right) \right\} \quad (49)$$

For points on the wing surface, i.e. $z = 0$, $s_t < y < s_\ell$:

$$\frac{u_2, t}{U_\infty} = \frac{1}{2\pi} \left\{ \int_{s_t}^{s_\ell} \frac{d^2 Z_w(x, \xi)}{dx^2} \ln \left[\frac{(y + \xi)^2 (y + \frac{R_b^2}{\xi})^2 (y - \frac{R_b^2}{\xi})^2}{y^4} \right] d\xi \right. \\ \left. + \int_{s_t}^{s_\ell} \left(\frac{d^2 Z_w(x, \xi)}{dx^2} - \frac{d^2 Z_w(x, y)}{dx^2} \right) \ln \left[\left(\frac{y - \xi}{y} \right)^2 \right] d\xi \right. \\ \left. + 4R_b \frac{dR_b}{dx} \frac{1}{y} \int_{s_t}^{s_\ell} \frac{dZ_w(x, \xi)}{dx} \left[\frac{1}{\xi + \frac{R_b^2}{y}} - \frac{1}{\xi - \frac{R_b^2}{y}} \right] d\xi \right. \\ \left. + 2 \frac{d^2 Z_w(x, y)}{dx^2} \left\{ (s_\ell - y) \left[\ln \left(\frac{s_\ell - y}{y} \right) - 1 \right] + (y - s_t) \left[\ln \left(\frac{y - s_t}{y} \right) - 1 \right] \right\} \right\}$$

(Continued on next page)

$$\begin{aligned}
& + \frac{dZ_w(x, s_\ell)}{dx} \frac{ds_\ell}{dx} \ln \left[\frac{(s_\ell - y)^2 (s_\ell + y)^2 (y - \frac{R_b^2}{s_\ell})^2 (y + \frac{R_b^2}{s_\ell})^2}{y^8} \right] \\
& - \frac{dZ_w(x, s_t)}{dx} \frac{ds_t}{dx} \ln \left[\frac{(y - s_t)^2 (y + s_t)^2 (y - \frac{R_b^2}{s_t})^2 (y + \frac{R_b^2}{s_t})^2}{y^8} \right] \\
& + \frac{s_{eb}''(x)}{2} \ln(y^2) \Bigg\} \quad (50)
\end{aligned}$$

$$\begin{aligned}
\frac{v_{2,t}}{U_\infty} = & \frac{1}{\pi} \left[\int_{s_t}^{s_\ell} \frac{dZ_w(x, \xi)}{dx} \left(\frac{1}{y + \xi} + \frac{1}{y + \frac{R_b^2}{\xi}} + \frac{1}{y - \frac{R_b^2}{\xi}} \right) d\xi \right. \\
& - \int_{s_t}^{s_\ell} \left(\frac{\frac{dZ_w(x, \xi)}{dx}}{\xi - y} - \frac{dZ_w(x, y)}{dx} \right) d\xi - \frac{dZ_w(x, y)}{dx} \ln \left(\frac{s_\ell - y}{y - s_t} \right) \\
& \left. + \frac{1}{y} \left(-4 \int_{s_t}^{s_\ell} \frac{dZ_w(x, \xi)}{dx} d\xi + \frac{s_{eb}'(x)}{2} \right) \right] \quad (51)
\end{aligned}$$

$$\frac{w_{2,t}}{U_\infty} = \frac{dZ_w(x, y)}{dx} \quad (52)$$

We note that in this case no singularities occur on the body surface or in the gap between the wing and body. At the leading and trailing edges of the wing, however, the characteristic logarithmic singularity associated with two-dimensional incompressible flow at a sharp edge appears.

As before, the thickness potential for the equivalent body cross section $w_{2,B}$ is given by equation (17). Because of the symmetry of these configurations, nonlifting flows will produce no lateral forces or

moments but only a longitudinal drag force. Since, as is the usual case of realistic wing-body combinations, the configurations considered herein have the body base located aft of the trailing edge of the wing tip chord (i.e. $x_b > x_{sm_2}$), the drag coefficient at zero lift is given by

$$C_{D_{a=0}} = C_{D_{eb}} \quad (53)$$

where $C_{D_{eb}}$ is the drag coefficient of the equivalent body of revolution and is given by equation (22).

Elliptic bodies.- For the wing-body combinations with indented elliptic cross section and sweptback trailing edges, equation (36) for $w_{2,t}$ applies for $x < X_{rte_1}$. For $X_{rte_1} < x < x_{sm_2}$, use of the Joukowski transformation, equation (30), provides the result that

$$\frac{w_{2,t}(\sigma_1)}{U_\infty} = \frac{1}{\pi} \int_{S_1 t}^{S_1 l} \frac{dZ_w(x, \xi_1 + \frac{c^2}{4\xi_1^2})}{dx} \ln \left[\frac{(\sigma_1^2 - \xi_1^2)(\sigma_1^2 - \frac{R_1^4}{\xi_1^2})}{\sigma_1^4} \right] \left(1 - \frac{c^2}{4\xi_1^2} \right) d\xi_1 \\ + \frac{S'_{eb}(x)}{2\pi} \ln \sigma_1 \quad (54)$$

If we define the following quantities

$$q_1 + iq_2 = \frac{1}{\sigma_1^2 - \frac{c^2}{4}} \quad (55)$$

$$q_3 + iq_4 = \frac{\sigma_1}{\sigma_1^2 - \frac{c^2}{4}} \quad (56)$$

$$q_5 + iq_6 = \frac{\sigma_1^2}{\sigma_1^2 - \frac{c^2}{4}} \quad (57)$$

and again restrict attention to the first quadrant of the crossflow plane, equations (38) and (39) provide the following results for the velocity components. For a point at general location but not on the wing surface,

$$\frac{u_2, t}{U_\infty} = \frac{1}{2\pi} \left(\int_{S_{1t}}^{S_1 \ell} \frac{d^2 Z_w(x, \xi + \frac{c^2}{4\xi})}{dx^2} \right) x$$

$$\ln \left\{ \frac{\left[z_1^2 + (y_1 - z_1)^2 \right] \left[z_1^2 + (y_1 + z_1)^2 \right] \left[z_1^2 + (y_1 - \frac{R_1^2}{\xi_1})^2 \right] \left[z_1^2 + (y_1 + \frac{R_1^2}{\xi_1})^2 \right]}{(z_1^2 + y_1^2)^4} \right\} x$$

$$(1 - \frac{c^2}{4\xi_1^2}) d\xi_1$$

$$+ \left(\frac{\lambda^2 - 1}{\lambda^2} \right) a \frac{da}{dx} \begin{pmatrix} -2 & q_1 \\ s_t & \int_{s_t}^s \ell \frac{dZ_w(x, \xi)}{dx} d\xi \end{pmatrix}$$

$$+ \left(\frac{\lambda + 1}{\lambda - 1} \right) \left[-q_5 \int_{\xi_1 t}^{s_1 \ell} \frac{dZ_w(x, \xi_1 + \frac{c^2}{4\xi_1})}{dx} \frac{1}{\xi_1} \frac{(y_1 - \frac{R_1^2}{\xi_1})}{z_1^2 + (y_1^2 - \frac{R_1^2}{\xi_1})^2} d\xi_1 \right]$$

$$- q_6 z_1 \int_{s_1 t}^{s_1 \ell} \frac{dZ_w(x, \xi_1 + \frac{c^2}{4\xi_1})}{dx} \frac{1}{\xi_1} \frac{d\xi_1}{z_1^2 + (y_1 - \frac{R_1^2}{\xi_1})^2}$$

$$+ q_5 \int_{\frac{s_1}{t}}^{\frac{s_1}{\ell}} \frac{dZ_w(x, \xi_1 + \frac{c^2}{4\xi_1})}{dx} \frac{1}{\xi_1} \frac{R_1^2}{y_1 + \frac{R_1^2}{\xi_1}} d\xi_1$$

$$+ q_e z_1 \int_{\frac{s_1}{t}}^{\frac{s_1 \ell}{t}} \frac{dZ_w(x, \xi_1 + \frac{c^2}{4\xi_1})}{dx} \frac{1}{\xi_1} \frac{d\xi_1}{z_1^2 + (y_1 + \frac{R_1^2}{\xi_1})^2}$$

$$+ \frac{c^2}{4} \left[q_3 \int_{\xi_1 t}^{\xi_1 \ell} \frac{dZ_w(x, \xi_1 + \frac{c^2}{4\xi_1})}{dx} \frac{1}{\xi_1^2} \frac{(y_1 - \frac{R_1^2}{\xi_1})}{z_1^2 + (y_1 - \frac{R_1^2}{\xi_1})^2} d\xi_1 \right]$$

(Continued on
next page)

$$+ q_4 z_1 \int_{s_1 t}^{s_1 \ell} \frac{dZ_w(x, \xi_1 + \frac{c^2}{4\xi_1})}{dx} \frac{1}{\xi_1^2} \frac{d\xi_1}{z_1^2 + (y_1 - \frac{R_1^2}{\xi_1})^2}$$

$$+ q_3 \int_{s_1 t}^{s_1 \ell} \frac{dZ_w(x, \xi_1 + \frac{c^2}{4\xi_1})}{dx} \frac{1}{\xi_1^2} \frac{(y_1 + \frac{R_1^2}{\xi_1})}{z_1^2 + (y_1 + \frac{R_1^2}{\xi_1})^2} d\xi_1$$

$$+ q_4 z_1 \int_{s_1 t}^{s_1 \ell} \frac{dZ_w(x, \xi_1 + \frac{c^2}{4\xi_1})}{dx} \frac{1}{\xi_1^2} \frac{d\xi_1}{z_1^2 + (y_1 + \frac{R_1^2}{\xi_1})^2}] \Big)$$

$$- \frac{\lambda^2 - 1}{\lambda^2} a \frac{da}{dx} q_1 \left(-4 \int_{s_1 t}^{s_1 \ell} \frac{dZ_w(x, \xi)}{dx} d\xi + \frac{s_{eb}(x)}{2} \right) + \frac{dZ_w(x, s_\ell)}{dx} \frac{ds_\ell}{dx} \times$$

$$\ln \left\{ \frac{[z_1^2 + (s_{1\ell} - y_1)^2][z_1^2 + (s_{1\ell} + y_1)^2][z_1^2 + (y_1 - \frac{R_1^2}{s_{1\ell}})^2][z_1^2 + (y_1 + \frac{R_1^2}{s_{1\ell}})^2]}{(z_1^2 + y_1^2)^4} \right\}$$

$$- \frac{dZ_w(x, s_t)}{dx} \frac{ds_t}{dx} \times$$

$$\ln \left\{ \frac{[z_1^2 + (y_1 - s_{1t})^2][z_1^2 + (y_1 + s_{1t})^2][z_1^2 + (y_1 - \frac{R_1^2}{s_{1t}})^2][z_1^2 + (y_1 + \frac{R_1^2}{s_{1t}})^2]}{(z_1^2 + y_1^2)^4} \right\}$$

$$+ \frac{s''_{eb}(x)}{2} \ln (z_1^2 + y_1^2) \Big)$$

(58)

$$\begin{aligned}
\frac{v_2, t}{U_\infty} = & \frac{1}{\pi} \left\{ q_5 \int_{s_1 t}^{s_1 l} \frac{dZ_w(x, \xi_1 + \frac{c^2}{4\xi_1})}{dx} \left[\frac{y_1 - \xi_1}{z_1^2 + (y_1 - \xi_1)^2} + \frac{y_1 + \xi_1}{z_1^2 + (y_1 + \xi_1)^2} \right. \right. \\
& \left. \left. + \frac{y_1 - \frac{R_1^2}{\xi_1}}{z_1^2 + (y_1 - \frac{R_1^2}{\xi_1})^2} + \frac{y_1 + \frac{R_1^2}{\xi_1}}{z_1^2 + (y_1 + \frac{R_1^2}{\xi_1})^2} \right] \left(1 - \frac{c^2}{4\xi_1^2} \right) d\xi_1 \right. \\
& \left. + q_6 z_1 \int_{s_1 t}^{s_1 l} \frac{dZ_w(x, \xi_1 + \frac{c^2}{4\xi_1})}{dx} \left[\frac{1}{z_1^2 + (y_1 - \xi_1)^2} + \frac{1}{z_1^2 + (y_1 + \xi_1)^2} \right. \right. \\
& \left. \left. + \frac{1}{z_1^2 + (y_1 - \frac{R_1^2}{\xi_1})^2} + \frac{1}{z_1^2 + (y_1 + \frac{R_1^2}{\xi_1})^2} \right] \left(1 - \frac{c^2}{4\xi_1^2} \right) d\xi_1 \right. \\
& \left. + \frac{q_5 y_1 + q_6 z_1}{z_1^2 + y_1^2} \left(-4 \int_{s_1 t}^{s_1 l} \frac{dZ_w(x, \xi)}{dx} d\xi + \frac{s_{eb}(x)}{2} \right) \right\} \quad (59)
\end{aligned}$$

$$\begin{aligned}
\frac{w_2, t}{U_\infty} = & \frac{1}{\pi} \left\{ -q_6 \int_{s_1 t}^{s_1 l} \frac{dZ_w(x, \xi_1 + \frac{c^2}{4\xi_1})}{dx} \left[\frac{y_1 - \xi_1}{z_1^2 + (y_1 - \xi_1)^2} + \frac{y_1 + \xi_1}{z_1^2 + (y_1 + \xi_1)^2} \right. \right. \\
& \left. \left. + \frac{y_1 - \frac{R_1^2}{\xi_1}}{z_1^2 + (y_1 - \frac{R_1^2}{\xi_1})^2} + \frac{y_1 + \frac{R_1^2}{\xi_1}}{z_1^2 + (y_1 + \frac{R_1^2}{\xi_1})^2} \right] \left(1 - \frac{c^2}{4\xi_1^2} \right) d\xi_1 \right. \\
& \left. + q_5 z_1 \int_{s_1 t}^{s_1 l} \frac{dZ_w(x, \xi_1 + \frac{c^2}{4\xi_1})}{dx} \left[\frac{1}{z_1^2 + (y_1 - \xi_1)^2} + \frac{1}{z_1^2 + (y_1 + \xi_1)^2} \right. \right. \\
& \left. \left. + \frac{1}{z_1^2 + (y_1 - \frac{R_1^2}{\xi_1})^2} + \frac{1}{z_1^2 + (y_1 + \frac{R_1^2}{\xi_1})^2} \right] \left(1 - \frac{c^2}{4\xi_1^2} \right) d\xi_1 \right. \\
& \left. + q_5 y_1 \left(-4 \int_{s_1 t}^{s_1 l} \frac{dZ_w(x, \xi)}{dx} d\xi + \frac{s_{eb}(x)}{2} \right) \right\}
\end{aligned}$$

(Continued on next page)

$$\begin{aligned}
& + \frac{1}{z_1^2 + (y_1 - \frac{R_1^2}{\xi_1})^2} + \frac{1}{z_1^2 + (y_1 + \frac{R_1^2}{\xi_1})^2} \left[\left(1 - \frac{c^2}{4\xi_1^2} \right) d\xi_1 \right] \\
& + \frac{q_5 z_1 - q_6 y_1}{z_1^2 + y_1^2} \left(-4 \int_{s_t}^{s_\ell} \frac{dZ_w(x, \xi)}{dx} d\xi + \frac{s'_{eb}(x)}{2} \right) \quad (60)
\end{aligned}$$

For points on the wing surface, i.e., $z = 0$, $s_t < y < s_\ell$ (or equivalently $z_1 = 0$, $s_{1t} < y_1 < s_{1\ell}$),

$$\begin{aligned}
\frac{u_{2,t}}{U_\infty} = & \frac{1}{2\pi} \left\{ \int_{s_{1t}}^{s_{1\ell}} \frac{\frac{d^2 Z_w(x, \xi_1 + \frac{c^2}{4\xi_1})}{dx^2}}{d\xi_1} \ln \left[\frac{(y_1 + \xi_1)^2 (y_1 + \frac{R_1^2}{\xi_1})^2 (y_1 - \frac{R_1^2}{\xi_1})^2}{y_1^8} \right] \left(1 - \frac{c^2}{4\xi_1^2} \right) d\xi_1 \right. \\
& + \int_{s_{1t}}^{s_{1\ell}} \left(\frac{\frac{d^2 Z_w(x, \xi_1 + \frac{c^2}{4\xi_1})}{dx^2}}{d\xi_1} - \frac{\frac{d^2 Z_w(x, y_1 + \frac{c^2}{4y_1})}{dx^2}}{dy_1} \right) \ln \left[\left(\frac{y_1 - \xi_1}{y_1} \right)^2 \right] \left(1 - \frac{c^2}{4\xi_1^2} \right) d\xi_1 \\
& + \frac{\frac{d^2 Z_w(x, y_1 + \frac{c^2}{4y_1})}{dx^2}}{dy_1} 2 (s_{1\ell} - y_1) \left[\ln \left(\frac{s_{1\ell} - y_1}{y_1} \right) - 1 \right] + (y_1 - s_{1t}) \left[\ln \left(\frac{y_1 - s_{1t}}{y_1} \right) - 1 \right] \\
& - \frac{c^2}{4} \frac{1}{y_1} \left[\left(\frac{s_{1\ell} - y_1}{s_{1\ell}} \right) \ln \left(\frac{s_{1\ell} - y_1}{y_1} \right) + \left(\frac{y_1 - s_{1t}}{s_{1t}} \right) \ln \left(\frac{y_1 - s_{1t}}{y_1} \right) - \ln \left(\frac{s_{1\ell}}{s_{1t}} \right) \right] \\
& + \left(\frac{\lambda^2 - 1}{\lambda^2} \right) a \frac{da}{dx} \left[-2 q_1 \int_{s_t}^{s_\ell} \frac{dZ_w(x, \xi)}{dx} d\xi - q_1 \left(-4 \int_{s_t}^{s_\ell} \frac{dZ_w(x, \xi)}{dx} d\xi + \frac{s'_{eb}(x)}{2} \right) \right]
\end{aligned}$$

(Continued on next page)

$$\begin{aligned}
& + \left(\frac{\lambda + 1}{\lambda - 1} \right) \frac{q_5}{Y_1} \left[- \int_{s_1 t}^{s_1 \ell} \frac{\frac{dZ_w(x, \xi_1 + \frac{c^2}{4\xi_1})}{dx}}{\xi_1 - \frac{R_1^2}{Y_1}} d\xi_1 + \int_{s_1 t}^{s_1 \ell} \frac{\frac{dZ_w(x, \xi_1 + \frac{c^2}{4\xi_1})}{dx}}{\xi_1 + \frac{R_1^2}{Y_1}} d\xi_1 \right] \\
& + \frac{c^2}{4} \frac{q_3}{Y_1} \left[\int_{s_1 t}^{s_1 \ell} \frac{\frac{dZ_w(x, \xi_1 + \frac{c^2}{4\xi_1})}{dx}}{\xi_1 (\xi_1 - \frac{R_1^2}{Y_1})} d\xi_1 + \int_{s_1 t}^{s_1 \ell} \frac{\frac{dZ_w(x, \xi_1 + \frac{c^2}{4\xi_1})}{dx}}{\xi_1 (\xi_1 + \frac{R_1^2}{Y_1})} d\xi_1 \right] \\
& + \frac{dZ_w(x, s_\ell)}{dx} \frac{ds_\ell}{dx} \ln \left[\frac{(s_1 \ell - Y_1)^2 (s_1 \ell + Y_1)^2 (Y_1 - \frac{R_1^2}{s_1 \ell})^2 (Y_1 + \frac{R_1^2}{s_1 \ell})^2}{Y_1^8} \right] \\
& - \frac{dZ_w(x, s_t)}{dx} \frac{ds_t}{dx} \ln \left[\frac{(Y_1 - s_1 t)^2 (Y_1 + s_1 t)^2 (Y_1 - \frac{R_1^2}{s_1 t})^2 (Y_1 + \frac{R_1^2}{s_1 t})^2}{Y_1^8} \right] \\
& + \frac{s''_{eb}(x)}{2} \ln (Y_1^2) \quad \text{(61)}
\end{aligned}$$

$$\begin{aligned}
\frac{v_2, t}{U_\infty} = & \frac{q_s}{\pi} \left[\int_{s_1 t}^{s_1 \ell} \frac{dZ_w(x, \xi_1 + \frac{c^2}{4\xi_1})}{dx} \left(\frac{1}{y_1 + \xi_1} + \frac{1}{y_1 + \frac{R_1^2}{\xi_1}} + \frac{1}{y - \frac{R_1^2}{\xi_1}} \right) \left(1 - \frac{c^2}{4\xi_1^2} \right) d\xi_1 \right. \\
& - \int_{s_1 t}^{s_1 \ell} \frac{\left(\frac{dZ_w(x, \xi_1 + \frac{c^2}{4\xi_1})}{dx} - \frac{dZ_w(x, y_1 + \frac{c^2}{4y_1})}{dx} \right)}{\xi_1 - y_1} \left(1 - \frac{c^2}{4\xi_1^2} \right) d\xi_1 \\
& - \frac{dZ_w(x, y_1 + \frac{c^2}{4y_1})}{dx} \left\{ \ln \left(\frac{s_1 \ell - y_1}{y_1 - s_1 t} \right) + \frac{c^2}{4} \left[\frac{1}{y_1^2} \left[\ln \left(\frac{s_1 \ell}{s_1 t} \right) \right. \right. \right. \\
& \left. \left. \left. - \ln \left(\frac{s_1 \ell - y_1}{y_1 - s_1 t} \right) \right] + \frac{1}{y_1} \left(\frac{s_1 \ell - s_1 t}{s_1 \ell + s_1 t} \right) \right] \right\} \\
& + \left(-4 \int_{s_t}^{s \ell} \frac{dZ_w(x, \xi)}{dx} d\xi + \frac{s_{eb}(x)}{2} \right) \frac{1}{y_1} \quad (62)
\end{aligned}$$

$$\frac{w_2, t}{U_\infty} = \frac{dZ_w(x, y)}{dx} \quad (63)$$

The drag coefficient at zero lift $C_{D_{\alpha=0}}$ of this class of configurations is given by equation (40).

RESULTS AND DISCUSSION

While experimental verification of the theory is considered essential, particularly at this stage of development, there is not available at the present time experimental data for transonic flows about wing-indented body combinations suitable for comparison with theory developed here. Although a parallel experimental program was originally considered for a typical member of the class of configurations described herein, that program has, unfortunately, been delayed. Consequently, experimental verification of the theory, particularly for pressure distribution comparisons which are vital in assessing the validity of the assumptions of the theory within the various regions (body surface, wing surface, wing-body junction, wing leading and trailing edges, etc.) of the near flow field of these configurations will have to be deferred.

In order to illustrate the general behavior of the theoretical results for transonic flows about the slender wing-body combinations considered here, the surface and flow field pressure distributions for several typical members of the classes of configurations described previously are given in figures 4 through 7. For example, in figure 4 pressure distributions are presented for a finite thickness wing-indented circular body combination with a nonzero taper ratio and straight trailing edge in which the equivalent body is a parabolic-arc of thickness ratio $D/\ell = 0.1$, the wing is a truncated delta wing with aspect ratio $AR = 1.7$, and taper ratio $TR = 0.2$ (so that $\beta_{le} = 58^\circ$, $\beta_{te} = 0$), and has parabolic-arc profiles of thickness/chord ratio $t/c_w = 0.04$. The wing root chord is half the body length, i.e., $C_{RT}/\ell = 0.5$, the root chord leading edge is located at $x_{rle}/\ell = 0.25$, and the body base is at $x_{bl}/\ell = 0.86$. The longitudinal pressure distributions given in figure 4 are for the free-stream conditions $M_\infty = 1$, $\alpha = 0^\circ$ and are presented at the two angular positions $\theta = 0^\circ, 90^\circ$ in the crossflow plane and at locations on the body surface and also along lines parallel to the body axis but removed laterally from it by distances of 1, 2, and 4 times the maximum equivalent body diameter D . Thus, the pressure distributions given for $\theta = 0^\circ$ and $r/D = 1, 2$ cut across the wing surface, intersecting the leading edge at the axial positions $x/\ell = 0.410$ and 0.570 , respectively.

The wing-body surface pressure distributions shown in the first plot of figure 4, when compared to the pressure distribution on the equivalent body alone, demonstrate the large effect that the wing has upon the body pressure distribution. Moreover, it clearly shows the rapid variation of the pressure distributions caused by the singularities at the points ($x/l = 0.320, 0.75$) where the wing leading and trailing edges pierce the body surface and also at $x/l = 0.65$ where the leading edge of the wing tip chord is. The discontinuities at the points where the leading and trailing edges intersect the body surface are related to the characteristic logarithmic singularity associated with the two-dimensional thickness problem (i.e., $\phi_{2,t}$) of flow at a sharp edge. The discontinuity at the leading edge of the wing tip chord is due to the discontinuity in slope of the indented body at that point. This discontinuity occurs since in order that the equivalent body area distribution and its derivatives remain smooth, it is necessary for the indented body to have a slope discontinuity at $x/l = 0.65$ to compensate for the one due to the wing. This discontinuity also occurs at the trailing edge of the wing tip chord and would be evident if the trailing edge were swept forward, so that the point ($x = X_{sm_1}$) would be separate and distinct from the axial location where the trailing edge pierces the body surface ($x = X_{rte_1}$). For the case of a straight trailing edge as in figure 4, those points, of course, coincide so that only one singularity is evident. The flow field distributions shown at $r/D = 1, 2$, and 4 illustrate several interesting features. The most prominent is the propagation into the flow field of the singularities which occur in the surface pressure distribution at the three points discussed above. This is a direct consequence of using the transonic equivalence rule to provide flow-field information based upon knowledge of flow properties at the body surface. Also evident in the distributions along the lines $r/D = 1, 2, \theta = 0^\circ$ are the logarithmic singularities at $x/l = 0.410$ and 0.570 , respectively, as those lines cross the wing leading edge. The longitudinal flow field pressure distributions provide insight into the rapidity with which the flow field becomes axisymmetric and equal to that about the equivalent body. At the lateral distance $r/D = 4$, the pressure distributions at $\theta = 0^\circ, 90^\circ$ at points ahead of the leading edge of the wing tip chord ($X_{sm_2}/l = 0.65$) are virtually indistinguishable from that about the equivalent body - except for the exponentially small region of influence of the logarithmic

singularity propagating out from the body surface at the point where the leading edge pierces the body surface. However, within the axial region corresponding to the wing tip chord, $0.65 < x/l < 0.75$, the pressure distribution still shows some effect of the wing, although it is clearly diminishing. This is not surprising and could have been anticipated from the results from the delta wing with zero taper ratio given in figure 4 of reference 7 which also indicate that the effect of the wing on the flow field at lateral distances of several maximum body radii is negligible at all axial locations except those in the near vicinity of the wing maximum span. Knowledge of the region in which the flow about geometrically complex configurations of this type can be considered axisymmetric and equal to that about the equivalent body is quite significant and can provide, for example, useful information for a completely numerical finite difference solution in applying the far-field boundary condition. The drag coefficient for this configuration, which is provided by evaluating numerically the integral in equation (22), is found to be $C_{Dt} = 0.1044$.

Analogous results are given in figure 5 for a lifting flow about this same configuration for the free-stream conditions $M_\infty = 1$. and $\alpha = 2^\circ$. We note again that the singularities discussed with regard to the nonlifting case also appear here. Moreover, due to the nature of lifting flows near a sharp edge, the logarithmic singularities associated with the thickness problem are further reinforced by the inverse square root behavior associated with the two-dimensional lifting problem (i.e., $\phi_{2,\alpha}$) of flow around a sharp edge. The net result is the more rapid variation of pressure evident in those regions. Nevertheless, the flow field distributions again display the strong tendency to return to those generated by the equivalent body alone, as is most apparent in the flow field distributions at $r/D = 4$. At this angle of attack, equations (27), (28), and (29) provide the following results for the aerodynamic coefficients:

$$C_L = 1.7070, \quad C_{Dt} = 0.1342, \quad C_m = -0.8906$$

In order to demonstrate the pressure distribution behavior typical of the wing-body combinations considered here having swept-back trailing edges and non-zero taper ratios, results are given in figure 6 for a finite

thickness wing-indented circular body combination in which the equivalent body is a parabolic-arc of thickness ratio $D/\ell = 0.10$, the wings have parabolic-arc profiles of thickness ratio $t/c_w = 0.04$, planform aspect ratio $AR = 2.8$, taper ratio $TR = 0.4$, root chord $C_{RT}/\ell = 0.3$, with the root chord leading edge at $X_{rle}/\ell = 0.25$ (so that $\beta_{le} = 45^\circ$, $\beta_{te} = 23.75^\circ$). Analogous results are presented in figure 7 for a finite thickness wing-indented elliptic body combination composed of a parabolic-arc body of semimajor to semiminor axes $\lambda = 3$ and a wing essentially identical to the one described above for the circular body except that the trailing edge is swept at the angle $\beta_{te} = 25.05^\circ$. The trailing edge sweep angles of these configurations are such that the axial locations of leading edge of the wing tip chord and the point where the trailing edge pierces the body surface coincide, i.e., $X_{sm_1} = X_{rte_1}$.

In figure 6, we note that the general variation of both surface and flow field pressure distributions are essentially the same as those of the straight trailing edge configuration shown in figure 4 for points ahead of the leading edge of the wing tip chord ($X_{sm_1}/\ell = 0.571$). However, within the axial region containing the wing tip chord ($X_{sm_1} < x < X_{sm_2}$) and coincidentally, the wing trailing edge, the pressure distributions now indicate a much more rapid variation, while still exhibiting the same trend as that shown in figure 4. Apparently the gap between wing and body in the crossflow plane within this region influences the behavior of the surface pressures to a greater degree than in the case when there is no gap, and consequently an unbroken lateral distribution of sources along the wing from body to wing tip. The flow field distributions within the near flow field of this region maintain this rapid variation, with the distributions of C_p at $\theta = 0^\circ$, $r/D = 1, 2$ also exhibiting the characteristic influence of the logarithmic singularities at the points where these lines cross the trailing edge. Nevertheless, beyond the wing tip the flow still displays the characteristic tendency to return to that of the axisymmetric flow about the equivalent body, as is evident in the distribution at $r/D = 4$, a distance which is only slightly beyond the point of maximum span, $r/D = 3.2$.

The surface and flow field pressure distributions shown in figure 7 for the wing-indented elliptic body combination described above are essentially similar in behavior to those in figure 6 for the corresponding

circular body and do not exhibit any new characteristic features. We note that the asymmetry introduced by ellipticity of the cross section alone (excluding the influence of the wing), while being evident at the body surface, rapidly dies out. In reference 6, it was shown that for a smooth elliptic body alone having a semimajor to semiminor axis ratio $\lambda = 3$ the flow field becomes essentially axisymmetric at $r/D = 1$.

Perhaps the most notable feature of the theoretical results presented here (and in ref. 7) for transonic flows about the classes of wing-indented body combinations being considered is the behavior of the pressure distributions caused by the singularities which occur at the following axial locations:

- x_{rle_1} -- leading edge pierces body surface
- x_{rte_1} -- trailing edge pierces body surface
- x_{sm_1} -- leading edge of wing tip chord
- x_{sm_2} -- trailing edge of wing tip chord

Although the singularities at general locations along the leading and trailing edges, for either nonlifting or lifting situations, could be included here, they are not, both since their character and origin are well known and also because they are local phenomena and, consequently, of restricted influence unlike the singularities delineated above.

It is important to realize that the basis of these singularities is essentially geometric in character, with the difficulty arising from either a discontinuity in first (at $x = x_{sm_1}, x_{sm_2}$) or second (at $x = x_{rle_1}, x_{rte_1}$) derivative of the indented body area distribution, which causes, in turn, discontinuities in the surface velocity components. Then, because the transonic equivalence rule is used to provide flow field information based upon knowledge of flow properties on the body surface, these discontinuities are propagated laterally into the flow field making their presence even more evident. A direct method of alleviating this problem, while at the same time providing both a more general and realistic approximation would be to smooth these junction points with monotonically varying fillets. It appears, however, that a simple functional representation of fairing curves of this nature is not possible. Analytic (i.e., cubic), trigonometric, or exponential curves, while

satisfying the end conditions of matching slope and ordinate at two points, fail to be continuously monotonic under boundary conditions typical of the configurations considered here. Thus, a wiggle would result in the faired curve and this is unacceptable. A means of eliminating this problem would be with piecewise continuous spline-fit functions. In any case, by whatever means the smoothing is accomplished, the result would be a more accurate representation of the actual solution in the vicinity of these points.

CONCLUDING REMARKS

Theoretical analysis and development of associated computer programs have been conducted in order to develop calculative techniques for predicting properties of transonic flows about certain classes of slender wing-body combinations. The theoretical analysis is based upon a combination of the transonic equivalence rule and uses either an arbitrarily specified solution or the local linearization method for determining the nonlifting transonic flow about the equivalent body.

Computational programs, which are documented in a general user's manual and included as part of this report, have been developed for finite thickness wing-body combinations in which the bodies are area-rule indented in such a manner that the resultant equivalent bodies remain smooth. The equivalent body profiles are either user-supplied subject to certain continuity and closure restrictions or program-supplied in which case the radius is of the general class $R \sim x/\ell - (x/\ell)^n$ or $1 - x/\ell - (1 - x/\ell)^n$. In addition, the body cross sectional shapes are either (1) circular or (2) elliptic and such that a constant ratio λ of semimajor to semiminor axes is maintained along the entire body length.

A general class of wings is considered which are symmetric in planform about the azimuthal body meridian ($x-z$ plane) and consist of straight leading and trailing edges swept at arbitrary angles. The positions of the leading and trailing edges of the root chord are located at arbitrary locations on the body axis, and the profiles are described by $Z_w \sim \bar{x}/c_w - (\bar{x}/c_w)^m$ or $1 - \bar{x}/c_w - (1 - \bar{x}/c_w)^m$ where \bar{x} is the axial distance from the leading edge and c_w is the local chord.

These programs provide longitudinal pressure distributions for both nonlifting and lifting situations, at arbitrary angular positions in the crossflow plane at points along the body and wing surface and also along lines parallel to the body axis but removed at arbitrarily specified lateral distances from it. In addition to the pressure distributions, the aerodynamic characteristics of lift, drag, and pitching moment are also provided.

The theoretical pressure distributions predicted by these programs for certain members of the class of configurations described above indicate quantitatively the relatively large effects of wing thickness and lift on both the body and flow field pressures, and also serve to point out the singularities inherent to the theory as it is presently constituted. In addition, they demonstrate the large influence that sweeping the trailing edge and introducing a finite tip chord has upon the pressure distributions.

In conclusion, we emphasize that the techniques employed here are quite fundamental and possess great generality so as to allow extension to even more complex configurations. Moreover, since the solutions to the various two-dimensional crossflow problems are independent of Mach number, they can be calculated once and for all once the geometry of the configuration is fixed and then combined with any one of a possible variety of solutions (experimental, numerical, etc.) for the transonic flow about the nonlifting equivalent body. We suggest, furthermore, that experimental work be conducted to determine surface and flow-field pressure distributions on selected wing-body combinations in order to define more clearly the extent to which the theory applies to configurations of this nature and, also, that consideration be given to developing methods to smooth the solutions in the vicinity of the various discontinuities in the area derivatives of the indented body shapes.

Nielsen Engineering & Research, Inc.
Mountain View, California
July 13, 1972

APPENDIX A
COMPUTER PROGRAM USER'S MANUAL

SUMMARY

An operating manual is given for the computer program developed in conjunction with the theoretical work presented in this report. The program computes the transonic surface and flow field pressure distributions and aerodynamic characteristics for various classes of wing-body combinations considered herein. Use is made of the transonic equivalence rule and either the local linearization method or a user-supplied solution for flow about the nonlifting equivalent body.

A description of the general operating procedure of the program is given, together with instructions for the preparation of input data, sample output of test cases, and a listing. The program is written in FORTRAN IV programming language and prepared specifically for use on an IBM 360/67 series computer. Typical running times are approximately 30 to 45 seconds for the equivalent body calculations using the local linearization method and about 2 minutes for the crossflow solution calculations involving approximately 1000 points located typically along the wing, wing-body junction, and flow field.

DESCRIPTION OF PROGRAM

The computer program presented here is applicable to several classes of finite thickness wing-body combinations discussed in the preceding report in which the bodies are area-rule indented along the wing-body junction in such a manner that the total cross-sectional area distribution is identical to that of a smooth body having a specified profile. The programs compute the surface and flow field pressure distributions, for both nonlifting and lifting situations for straight or swept forward trailing edge planforms and for nonlifting situations for swept back trailing edge planforms, at arbitrarily specified angular positions in the crossflow plane, at points along the body and wing surface, and also along lines parallel to the body axis but removed from it at specified lateral distances. In addition, the aerodynamic characteristics of lift, drag, and pitching moment are computed.

Wing and Body Geometry

The wing and body geometries of the configurations programmed are shown schematically in figures 2 and 3. Figure 2 illustrates two members of the class of wing-body combinations which have indented bodies that are circular in cross section, while figure 3 shows the corresponding members of the class having indented bodies with elliptic cross section.

Program-supplied equivalent body profiles.- Unless the user specifies to the contrary, the class of equivalent bodies of revolution of both types of the above configurations consist of profiles described by the equations

$$\frac{R_{eb}}{\ell} = \frac{\tau_{eb} n^{n/(n-1)}}{2(n-1)} \left[\frac{x}{\ell} - \left(\frac{x}{\ell} \right)^n \right] \quad (64)$$

or

$$\frac{R_{eb}}{\ell} = \frac{\tau_{eb} n^{n/(n-1)}}{2(n-1)} \left[1 - \frac{x}{\ell} - \left(1 - \frac{x}{\ell} \right)^n \right] \quad (65)$$

with $n = \text{constant} \geq 2$. In reference 7, the profiles of the elliptic bodies were restricted to parabolic arcs, i.e. equations (64) or (65) with $n = 2$. Thus, this work extends the elliptic body category to include the entire class of equivalent body profiles used for the case of the circular bodies.

User-supplied equivalent body profiles.- At the user's option, an arbitrarily specified equivalent body profile may be substituted in lieu of the above class of profiles. The modifications necessary to the program are detailed in the PROGRAM INPUT section. The restrictions on these profiles depend, in part, on the method used to calculate the solution for the nonlifting flow about the equivalent body, i.e. u_B . If the local linearization method, as presently constituted, is used to calculate u_B (see eqs. (5), (6), and (7)), then it is necessary that the profiles be closed, have sharp tips, and have continuous derivatives through the fourth. On the other hand, if the solution for u_B is user-supplied, then the requirement from the other portions of

APPENDIX A

the solution, i.e. $\phi_{2,\alpha}$, $\phi_{2,t}$, and $\phi_{2,B}$, is that the equivalent body profiles have continuous derivatives through the second.

Indented-body profiles.— The ordinates of the indented body profiles are fixed once the equivalent body profile and wing profile are specified. For circular bodies with straight/sweptforward trailing edge planforms, the indented body radius R_b is found through a Newton-Raphson iteration procedure on the expression

$$\pi R_{eb}^2 = \pi R_b^2 + 4 \int_{R_b}^s z_w(x, \xi) d\xi \quad (66)$$

while the derivatives dR_b/dx and d^2R_b/dx^2 are calculated by using an appropriate five-point difference formula. For sweptback trailing edge planforms, the above method applies up to $x = X_{rte_1}$. For $X_{rte_1} < x < X_{sm_2}$, R_b is found without iteration from the expression

$$\pi R_{eb}^2 = \pi R_b^2 + 4 \int_{s_t}^{s_l} z_w(x, \xi) d\xi \quad (67)$$

Analogously, for elliptic bodies with straight/sweptforward trailing edges the semimajor axis a of the indented elliptic cross section is found by iteration on

$$\pi R_{eb}^2 = \frac{\pi a^2}{\lambda} + 4 \int_a^s z_w(x, \xi) d\xi \quad (68)$$

with the derivatives da/dx and d^2a/dx^2 being evaluated numerically by using the appropriate five-point difference formula. For sweptback trailing edge planforms with $X_{rte_1} < x < X_{sm_2}$, a is found directly from the expression

$$\pi R_{eb}^2 = \frac{\pi a^2}{\lambda} + 4 \int_{s_t}^{s_l} z_w(x, \xi) d\xi \quad (69)$$

APPENDIX A

The general class of wings considered for both types of body shapes described above have wing planforms that consist of symmetric straight leading and trailing edges, swept at arbitrary angles β_{le} and β_{te} , respectively, to the y axis. Both β_{le} and β_{te} , are measured positive clockwise; thus, for β_{te} less than, equal to, or greater than zero, the trailing edge is correspondingly sweptforward, straight, or sweptback. The position of the leading edge of the wing root chord x_{rle} and its length C_{Rt} are arbitrary. The wing profiles are represented by expressions of the form

$$\frac{z_w}{c_w} = \frac{\tau_w^{m/(m-1)}}{2(m-1)} \left(\frac{\bar{x}}{c_w} - \left(\frac{\bar{x}}{c_w} \right)^m \right) \quad (70)$$

or

$$\frac{z_w}{c_w} = \frac{\tau_w^{m/(m-1)}}{2(m-1)} \left(1 - \frac{\bar{x}}{c_w} - \left(1 - \frac{\bar{x}}{c_w} \right)^m \right) \quad (71)$$

where c_w is the local chord, \bar{x} the distance from the leading edge, m is a constant ≥ 2 , and τ_w is the wing thickness-to-chord ratio. The wings are assumed to maintain a constant thickness-to-chord ratio across the span, with the consequence that the wing profiles at all spanwise locations are geometrically similar so that

$$\frac{\tau_w}{2} = \frac{(z_w(x,y))_{\max}}{c_w(y)} = \frac{(z_w(x,o))_{\max}}{C_{Rt}} \quad (72)$$

General

The coordinate system used in the program is a body-fixed Cartesian system centered at the body nose with the x axis directed rearward and aligned with the longitudinal axis of the body, the y axis directed to the right facing forward, and the z axis directed vertically upward, as shown in figure 1. Because the transonic equivalence rule allows the perturbation potential ϕ to be expressed in the form

$$\phi = \phi_{2,\alpha} + \phi_{2,t} - \phi_{2,B} + \psi_B \quad (73)$$

where each of the components has the meaning indicated in figure 1, and since $\phi_{2,\alpha}$, $\phi_{2,t}$, and $\phi_{2,B}$ satisfy the two-dimensional Laplace equation

$$(\phi_{2,i})_{yy} + (\phi_{2,i})_{zz} = 0 \quad (74)$$

they are independent of Mach number. Consequently, once the geometry of the configuration is fixed they can be calculated once and for all, stored, and used, for example, in a comparative study of a certain wing-body combination as the Mach number is varied systematically throughout the transonic range. An option for doing this is available and is discussed in the PROGRAM INPUT section. The only portion of the solution dependent upon M_∞ is ψ_B and this term represents the solution to the full transonic equation (1) for flow about the nonlifting equivalent body.

Local linearization solution of u_B . - If the local linearization method is used to determine the solution for ψ_B , or more conveniently, $u_B = (\psi_B)_x$, then according to whether M_∞ is near one, below the lower critical, or above the upper critical, equation (5), (6), or (7) must be integrated. Since these are all first order ordinary nonlinear differential equations, appropriate initial conditions are required. These are given at the point x_s , which is the positive root of the equation

$$S''_{eb}(x) = 0 \quad (75)$$

that is closest to the origin. The values of u_B/U_∞ at this point are, for accelerating transonic flows with $M_\infty \approx 1$ (eq. (5))

$$\frac{u_B}{U_\infty} = \frac{1 - M_\infty^2}{M_\infty^2(\gamma + 1)} + \frac{1}{4\pi} \int_0^x \frac{S''_{eb}(\xi) - S''_{eb}(\tilde{\xi})}{x - \xi} d\xi \quad (76)$$

for purely subsonic flow (eq. (6))

$$\frac{u_B}{U_\infty} = \frac{1}{4\pi} \int_0^l \frac{s''_{eb}(x) - s''_{eb}(\xi)}{|x - \xi|} d\xi \quad (77)$$

and for purely subsonic flow (eq. (7))

$$\frac{u_B}{U_\infty} = \frac{1}{2\pi} \int_0^x \frac{s''_{eb}(x) - s''_{eb}(\xi)}{x - \xi} d\xi \quad (78)$$

The integrations start at x_s , proceed to a specified point near the nose, and upon reaching that point, return to x_s , restart the integration procedure, and then continue toward the tail. In each of these programs, the differential equations are integrated by using Hamming's modified predictor-corrector method described in the Scientific Subroutine Package (SSP) available from the IBM Corporation. The integrals involved in those differential equations are evaluated by using Simpson's rule.

User-supplied solution for u_B .— At the user's option, an arbitrarily-specified solution for u_B can be used in lieu of the local linearization solution. This solution can involve mixed transonic flows with imbedded shocks and can be determined in any of a variety of ways (numerical, experimental, etc.). Details regarding the manner of inputting this information to the program are discussed in the PROGRAM INPUT section.

Crossflow Potentials and Aerodynamic Characteristics

This section assembles for user convenience, the crossflow potentials and aerodynamic characteristics of all of the configurations considered in this report.

Straight/Sweptforward trailing-edge planforms.— For the classes of finite thickness wing-circular body combinations considered herein which have straight/sweptforward trailing edge planforms, (see fig. 2(a)), the following results are provided for $w_{2,a}$, $w_{2,t}$, and $w_{2,B}$ at the indicated axial locations:

APPENDIX A

$$\frac{w_2, \alpha}{U_\infty} = \frac{i\alpha R_{eb}^2}{\sigma} \quad (0 < x < x_{rle_1}) \quad (79)$$

$$\frac{w_2, \alpha}{U_\infty} = -i\alpha \left\{ \left[\left(\sigma + \frac{R_b^2}{\sigma} \right)^2 - \left(s_\ell + \frac{R_b^2}{s_\ell} \right)^2 \right]^{1/2} - \sigma \right\} \quad (x_{rle_1} < x < x_{sm_2}) \quad (80)$$

$$\frac{w_2, t}{U_\infty} = \frac{s'_{eb}(x)}{2\pi} \ln \sigma \begin{cases} 0 < x < x_{rle_1} \\ x_{rte_1} < x < \ell \end{cases} \quad (81)$$

$$\frac{w_2, t}{U_\infty} = \frac{1}{\pi} \int_{R_b}^s \frac{dZ_w(x, \xi)}{dx} \ln \left[\frac{(\sigma^2 - \xi^2)(\sigma^2 - \frac{R_b^4}{\xi^2})}{\sigma^4} \right] d\xi + \frac{1}{2\pi} \left[s'_{eb}(x) + 4Z_w(x, R_b) \frac{dR_b}{dx} \right] \ln \sigma \quad (x_{rle_1} < x < x_{rte_1}) \quad (82)$$

$$\frac{w_2, B}{U_\infty} = \frac{s'_{eb}(x)}{2\pi} \ln \sigma \quad (0 < x < \ell) \quad (83)$$

where s in equation (82) denotes either the leading ($s = s_\ell$) or trailing ($s = s_t$) edge, depending upon the axial location. We note that for all of the configurations considered in this report, the solution for $w_{2,B}$ is given by equation (83).

The aerodynamic characteristics of this class of configurations are given as follows. The drag coefficient at zero lift is found through a numerical integration of the expression

$$C_{D_{\alpha=0}} = C_{D_{eb}} = \frac{1}{S_m} \int_0^{X_b} C_{p_{eb}} \frac{ds_{eb}(x)}{dx} dx \quad (84)$$

where $C_{D_{eb}}$ is the drag coefficient of the equivalent body alone, S_m is the maximum area of the equivalent body, and $C_{p_{eb}}$ is the pressure coefficient on the surface of the nonlifting equivalent body and is equal to

$$C_{p_{eb}} = -2 \frac{u_B}{U_\infty} - \left(\frac{dR_{eb}(x)}{dx} \right)^2 \quad (85)$$

Because of the symmetry of these configurations no lateral forces or moments exist at $\alpha = 0$. For the lifting situation, the coefficients of lift, drag, and pitching moment are given by

$$C_L = \frac{2\pi\alpha}{S_m} \left(s_\ell^2 + \frac{R_b^4}{s_\ell^2} - R_{eb}^2 \right) \Big|_{x = X_{sm_2}} \quad (86)$$

$$C_{D_t} = C_{D_{\alpha=0}} + \frac{\alpha}{2} C_L \quad (87)$$

$$C_m = \frac{2\pi\alpha}{S_m \cdot \ell} \left[-x \left(s_\ell^2 + \frac{R_b^4}{s_\ell^2} - R_{eb}^2 \right) \right]_{x = X_{sm_2}} + \int_0^{X_{rle_1}} R_{eb}^2 d\xi$$

$$+ \int_{X_{rle_1}}^{X_{sm_2}} \left(s_\ell^2 + \frac{R_b^4}{s_\ell^2} - R_{eb}^2 \right) d\xi \quad (88)$$

where X_{sm_2} and X_{rle_1} are the axial locations, respectively, of the trailing edge of the wing tip-chord and the point where the wing leading

APPENDIX A

edge pierces the body surface. The integrals involved in evaluating the pitching moment are calculated by using Simpson's rule.

The corresponding results for the wing-elliptic body combinations (see fig. 3(a)) are for $w_{2,\alpha}$, $w_{2,t}$:

$$\frac{w_{2,\alpha}}{U_\infty} = i\alpha \left\{ \sigma_1 - \frac{R_1^2}{\sigma_1} - \sigma \right\} \quad (0 < x < x_{rle_1}) \quad (89)$$

$$\frac{w_{2,\alpha}}{U_\infty} = -i\alpha \left\{ \left[\left(\sigma_1 + \frac{R_1^2}{\sigma_1} \right)^2 - \left(s_1 + \frac{R_1^2}{s_1} \right)^2 \right]^{1/2} - \sigma \right\} \quad (x_{rle_1} < x < x_{sm_2}) \quad (90)$$

$$\frac{w_{2,t}}{U_\infty} = \frac{s'_{eb}(x)}{2\pi} \ln \sigma_1 \quad \begin{cases} 0 < x < x_{rle_1} \\ x_{rte_1} < x < l \end{cases} \quad (91)$$

$$\frac{w_{2,t}}{U_\infty} = \frac{1}{\pi} \int_{R_1}^{s_1} \frac{dZ_w(x, \xi_1 + \frac{c^2}{4\xi_1})}{dx} \ln \left[\frac{(\sigma_1^2 - \xi_1)(\sigma_1^2 - \frac{R_1^4}{\xi_1^2})}{\sigma_1^4} \right] \left(1 - \frac{c^2}{4\xi_1^2} \right) d\xi_1 + \left(\frac{s'_{eb}(x)}{2\pi} + 2Z_w(x, a) \frac{da}{dx} \right) \ln \sigma_1 \quad (x_{rle_1} < x < x_{rte_1}) \quad (92)$$

where s_1 in equation (92) denotes either the leading ($s_1 = s_{1l}$) or trailing ($s_1 = s_{1t}$) edge in the transformed σ_1 plane.

The aerodynamic characteristics of these elliptic body configurations are given, for nonlifting flows, by

$$C_{D_{a=0}} = C_{D_{eb}} - \frac{1}{S_m} \left(\frac{s'_{eb}(x)}{2\pi} \right)^2 2 \left[\frac{2}{\lambda} \ln \left(\frac{a(\lambda + 1)}{2\lambda} \right) K \left(\frac{\sqrt{\lambda^4 - 1}}{\lambda^2} \right) - \pi \ln R_{eb} \right] \quad (93)$$

where $C_{D_{eb}}$ is given by equation (84) and $K(\cdot)$ is the complete elliptic integral of the first kind; and for lifting flows by

$$C_L = \frac{2\pi\alpha}{S_m} \left\{ \left(\frac{s_\ell + \sqrt{s_\ell^2 - c^2}}{2} \right)^2 \left[1 + \frac{2c^2}{(s_\ell + \sqrt{s_\ell^2 - c^2})^2} \right. \right. \\ \left. \left. + \left(\frac{a+b}{(s_\ell + \sqrt{s_\ell^2 - c^2})} \right)^4 \right] - R_{eb}^2 \right\} \Big|_{x=X_{sm_2}} \quad (94)$$

$$C_{D_t} = C_{D_{\alpha=0}} + \frac{\alpha}{2} C_L \quad (95)$$

$$C_m = \frac{2\pi\alpha}{S_m \cdot \ell} \left\{ -x \left\{ \left(\frac{s_\ell + \sqrt{s_\ell^2 - c^2}}{2} \right)^2 \left[1 + \frac{2c^2}{(s_\ell + \sqrt{s_\ell^2 - c^2})^2} \right. \right. \right. \\ \left. \left. \left. + \left(\frac{a+b}{s_\ell + \sqrt{s_\ell^2 - c^2}} \right)^4 \right] - R_{eb}^2 \right\} \Big|_{x=X_{sm_2}} + \lambda \int_0^{X_{r\ell e_1}} R_{eb}^2(x) dx \right. \\ \left. + \int_{X_{r\ell e_1}}^{X_{sm_2}} \left\{ \left(\frac{s_\ell + \sqrt{s_\ell^2 - c^2}}{2} \right)^2 \left[1 + \frac{2c^2}{(s_\ell + \sqrt{s_\ell^2 - c^2})^2} + \left(\frac{a+b}{s_\ell + \sqrt{s_\ell^2 - c^2}} \right)^4 \right] - R_{eb}^2 \right\} dx \right) \quad (96)$$

where the integrals involved in evaluating the pitching moment are calculated by using Simpson's rule.

Sweptback trailing edge planforms.- For the classes of finite thickness wing-circular body combinations having sweptback trailing edge planforms considered here (see fig. 2(b)), the following results for $w_{2,t}$ are provided:

APPENDIX A

$$\frac{w_2, t}{U_\infty} = \frac{s'_{eb}(x)}{2\pi} \ln \sigma \begin{cases} 0 < x < x_{rle_1} \\ x_{sm_2} < x < l \end{cases} \quad (97)$$

$$\frac{w_2, t}{U_\infty} = \frac{1}{\pi} \int_{R_b}^s \frac{dZ_w(x, \xi)}{dx} \ln \left[\frac{(\sigma^2 - \xi^2)(\sigma^2 - \frac{R_b^4}{\xi^2})}{\sigma^4} \right] d\xi$$

$$+ \frac{1}{2\pi} \left[s'_{eb}(x) + 4Z_w(x, R_b) \frac{dR_b}{dx} \right] \ln \sigma \quad (x_{rle_1} < x < x_{rte_1}) \quad (98)$$

$$\frac{w_2, t}{U_\infty} = \frac{1}{\pi} \int_{s_t}^s \frac{dZ_w(x, \xi)}{dx} \ln \left[\frac{(\sigma^2 - \xi^2)(\sigma^2 - \frac{R_b^4}{\xi^2})}{\sigma^4} \right] d\xi + \frac{s'_{eb}(x)}{2\pi} \ln \sigma \quad (x_{rte_1} < x < x_{sm_2}) \quad (99)$$

and the drag coefficient at zero lift is given by

$$C_{D_{a=0}} = C_{D_{eb}} \quad (100)$$

where $C_{D_{eb}}$ is given by equation (84).

The corresponding results for the wing-elliptic body combinations are

$$\frac{w_2, t}{U_\infty} = \frac{s'_{eb}(x)}{2\pi} \ln \sigma_1 \begin{cases} 0 < x < x_{rle_1} \\ x_{sm_2} < x < l \end{cases} \quad (101)$$

$$\frac{w_2, t}{U_\infty} = \frac{1}{\pi} \int_{R_1}^{s_1} \frac{dZ_w(x, \xi_1 + \frac{c^2}{4\xi_1})}{dx} \ln \left[\frac{(\sigma_1^2 - \xi_1^2)(\sigma_1^2 - \frac{R_1^4}{\xi_1^2})}{\sigma_1^4} \right] \left(1 - \frac{c^2}{4\xi_1^2} \right) d\xi_1$$

$$+ \left(\frac{s'_{eb}(x)}{2\pi} + 2Z_w(x, a) \frac{da}{dx} \right) \ln \sigma_1 \quad (x_{rle_1} < x < x_{rte_1}) \quad (102)$$

$$\frac{w_2, t}{U_\infty} = \frac{1}{\pi} \int_{R_1}^{S_1 \ell} \frac{dz_w(x, \xi_1 + \frac{c^2}{4\xi_1})}{dx} \ln \left[\frac{(\sigma_1^2 - \xi_1^2)(\sigma_1^2 - \frac{R_1^4}{\xi_1^2})}{\sigma_1^4} \right] \left(1 - \frac{c^2}{4\xi_1^2} \right) d\xi_1$$

$$+ \frac{s'_{eb}(x)}{2\pi} \ln \sigma_1 \quad (X_{rte_1} < x < X_{sm_2}) \quad (103)$$

with the drag coefficient at zero lift $C_{D_{\alpha=0}}$ given by equation (93).

Operating Procedure

The basic characteristics and general operating procedure of the computer program developed herein are straightforward and can be outlined as follows. After reading the input data (which is detailed in a subsequent section) and checking it for obvious errors, the program proceeds to calculate certain required geometrical and flow-field constants. Then, if the user selects the equivalent body profile to be of the class described by equations (64) or (65), the program proceeds to calculate the exponent n from information regarding the point of maximum thickness (see equations (12), (14)). The point x_s is next found by solving equation (75). If however, the equivalent body profile is user supplied, the calculation of n and x_s are omitted. Next, the axial locations X_{rle_1} and X_{rte_1} , which represent, respectively, the points where the wing leading and trailing edges pierce the body surface, are calculated. The exponent m describing the wing ordinates (see eqs. (70), (71)) is then calculated in a manner similar to that used to determine n . The calculation of n , x_s , X_{rle_1} , X_{rte_1} , and m are all performed in an iterative fashion by using the standard Newton-Raphson iteration scheme.

With the calculation of the above parameters complete, the program prints a number of geometrical and flow-field characteristics for the case at hand. If the solution of u_B is user-supplied, the program begins at a point close to the nose ($x/\ell = 0.005$) and proceeds toward the tail. If the local linearization method is used to determine u_B , then the appropriate initial value (eqs. (76), (77), or (78)) for the local linearization equation at hand (eqs. (5), (6), or (7)) is

APPENDIX A

calculated at $x = x_s$ and the numerical integration begun. In the case of purely sub- or supersonic (eqs. (6), (7)) flow, it is convenient to redefine the dependent variables (see eqs. (80) through (88), ref. 6) and integrate a simplified differential equation. For the $M_\infty \approx 1$ case, it is more advantageous to integrate equation (5) as it stands. Because of the special character of that equation at $x = x_s$, it is necessary to use a Taylor series for u_B/U_∞ in the neighborhood of that point in order to avoid a singularity in the numerical integration. Consequently, for that case in addition to u_B/U_∞ several derivatives are also required and are calculated by the program. Details are given in reference 6. The numerical integrations then continue toward the nose and stop at a point ($x/\ell = 0.005$) close to it. The integrations are not carried directly to the nose because, although this is possible for the purely supersonic case, the local linearization method predicts a logarithmic singularity at $x = 0$ for a sharp-tipped body, much like that indicated by linearized theory. With the integration to the nose complete, the program returns to x_s , restarts the numerical integration, and continues toward the tail. As these calculations progress (using either a user-supplied or local linearization solution for u_B), the surface and flow-field pressure distributions are calculated from equations (2) and (3) and the output printed at specified axial locations. Until the point $x = X_{rlle_1}$ is reached, the appropriate crossflow solutions for determining these pressure distributions are those for the smooth body alone (see eqs. (79), (81), (83), (89), (91), and (101)). Beyond X_{rlle_1} , for the case of nonlifting flows, the crossflow solutions are calculated from equation (82), (83), or (92) and (83) for $X_{rlle_1} < x < X_{rte_1}$. Beyond X_{rte_1} , for planforms with straight/sweptforward trailing edges, the crossflow solutions revert to those for the smooth body alone; while for planforms with sweptback trailing edges, the appropriate crossflow solutions for $X_{rte_1} < x < X_{sm_2}$ are given by equations (99), (83), or (103), (83) and beyond X_{sm_2} the solutions revert to those for the smooth body alone. The calculations continue until the body base is reached, i.e. $x = X_b$; the calculation then returns to the mainline program, prints the value of the drag coefficient, and reads the input data for the next case. For lifting flows about planforms with straight/sweptforward trailing edges, the calculations proceed in a similar fashion to that of the nonlifting case (with the additional

output of surface and flow-field pressure distributions at the angular locations $\pm \theta$ rather than just $+ \theta$) until the axial location of the trailing edge of the wing tip chord is reached, i.e. $x = X_{SM_2}$. Beyond that point, for reasons given in reference 7, no further pressure distributions are given. However, the calculation of flow about the equivalent body, i.e. u_B , continues to the body base in order that the drag coefficient at zero lift $C_{D\alpha=0}$ can be determined. When $x = X_b$, the calculation returns to the mainline program, determines the coefficients of lift, drag, and pitching moment from equation (86), (87), and (88), or (94), (95), and (96), prints these values, and then proceeds to read the input data for the next case.

PROGRAM INPUT

The variables that are input to the program are described in the following list:

Dictionary of Input Variables

AL	ratio of semimajor to semiminor axis (a/b) of elliptic cross section; program default value AL = 1
ALPHA	angle of attack, in degrees; program default value, ALPHA = 0
AMACH	free-stream Mach number
ANGLE	sweep angle, in degrees, of wing leading edge (measured positive clockwise from y axis and restricted to values $0 < \text{ANGLE} < 90$, see figures 2, 3)
CRT	wing root chord normalized by complete body length, c_{R_t}/l
ICOPY	integer index for program option for using previously-stored values of crossflow solutions; equal to 0 or 1; program default value, ICOPY = 0
MAREA	integer index for program option for using user-supplied or program-supplied subroutines for equivalent body area and derivatives, equal to 0 or 1; program default value, MAREA = 0
MOPT	integer index for program option for using user-supplied distribution for u_B or program-supplied local linearization solution; equal to 1, 2, 3, or 4.

APPENDIX A

NTHETA	integer indicating number of angular positions in crossflow plane at which output is desired; $1 \leq NTHETA \leq 5$
NXEB	integer indicating number of table entries of the user-supplied distribution of u_B ; $NXEB \leq 201$
RF(I)	six-dimensional vector representing values of r/D (the radial distance in the crossflow plane normalized by the maximum equivalent body diameter D) at which flow-field pressure distributions are to be calculated
SSMAX	maximum wing semispan normalized by complete body length, s_{max}/ℓ
TAUB	thickness ratio of equivalent body, D/ℓ
TAUW	thickness-to-chord ratio of wing (see eq. (10))
THETA(I)	NTHETA-dimensional vector representing values of the angle θ (in degrees) in the crossflow plane; $0 \leq THETA(I) \leq 90$
TR	wing planform taper ratio, c_{tip}/c_{R_t} ; $0 \leq TR \leq 1$
XEB(I)	NXEB-dimensional vector representing values of the axial locations (normalized by the complete body length) where values for the user-supplied distribution u_B are given
XLBASE	axial location of body base normalized by the complete body length, x_b/ℓ
XLOUTP	interval size, as fraction of complete body length, between output stations for pressure distribution print-out
XRLE	axial location of leading edge of wing root chord normalized by complete body length, x_{rle}/ℓ
XMTB	axial location of position of maximum thickness of equivalent body of revolution normalized by complete body length (see eqs. (12), (14))
XMTW	location, as fraction of distance from wing leading edge to local chord length (\bar{x}/c_w), of position of wing maximum thickness (see eqs. (8), (9))
XS2EB	user-supplied value of the axial location, normalized by the complete body length, where the user-supplied equivalent body profile satisfies $S''_{eb}(x) = 0$; only necessary as input when user supplies equivalent body profile and also uses local linearization method to calculate u_B

UEB(I) NXEB-dimensional vector representing values of u_B/u_∞ for the user-supplied distribution of u_B .

Input Format and Options

All of the input variables are entered into the program under a NAMELIST format (the one exception being the vectors UEB(I), XEB(I) which represent the ordinates and abscissas, respectively, of the user-supplied velocity distribution u_B and the format of these quantities is discussed below). The name of the NAMELIST data block is TRANIN.

Default values.- The following input variables have default values that are indicated below and unless the user wishes to change them, it is not necessary to enter them in the input data block

<u>Variable Name</u>	<u>Default Value</u>
AL	1.
ALPHA	0.
RF(I), I=1,2,3, 4,5,6	1.,2.,3.,4.,5.,6.,
NTHETA	2
THETA(I), I=1,2	0.,90.
MAREA	0
ICOPY	0
XLOUTP	.01

It is important to realize that the above variables assume their default values each time the program is run. If the user wishes any of the above variables to be different from its default value, this must be specified in the data statement for each run. All other input variables, once specified, remain unchanged by the program; thus, it is unnecessary to respecify them in subsequent runs if their values are to remain constant.

Local lineariztation option.- To use the local linearization method to determine u_B , it is necessary to specify in the input data the appropriate value for the integer index MOPT. Depending on the free stream Mach number, the proper value of MOPT to use the local linearization method is

APPENDIX A

<u>Free Stream Mach No.</u>	<u>MOPT</u>
$M_\infty \approx 1$ (near sonic flow)	1
$M_\infty \leq M_{cr,l}$ (below lower critical)	2
$M_{cr,u} \leq M_\infty$ (above upper critical)	3

User-supplied u_B option. - If the user wishes to supply the solution for u_B , then the program will bypass the local linearization calculations by specifying MOPT = 4. The solution for u_B is read into the program in the form of a tabular input of values of $u_B/U_\infty - vs - x/\ell$ immediately after the NAMELIST input block. Provision has been made for inputting ordinate and abscissa values up to a maximum number of 201 each (UEB(201), XEB(201)), i.e. values at each half percent of the body length if equally spaced. It is assumed that a sufficient number entries are made that linear interpolation in the table is appropriate.

User-supplied equivalent body profile. - If a class of equivalent body profiles not included in equation (64) or (65) is desired, then the user must set the integer index MAREA = 1, remove the following function subroutines from the program,

- FUNCTION SEBPI(DZ)
- FUNCTION S1EBPI(DZ)
- FUNCTION S2EBPI(DZ)
- FUNCTION S3EBPI(DZ)
- FUNCTION S4EBPI(DZ)

and replace them with his own. The above subroutines which are non-dimensionalized by normalizing them with respect to the body length, are defined in the following fashion.

$$\frac{S_{eb}(x/\ell)}{4\pi\ell^2} = SEBPI(x/\ell)$$

$$\frac{S'_{eb}(x/\ell)}{4\pi\ell^2} = \frac{1}{4\pi\ell^2} \frac{dS_{eb}(x/\ell)}{d(x/\ell)} = S1EBPI(x/\ell)$$

$$\frac{S''_{eb}(x/\ell)}{4\pi\ell^2} = \frac{d^2S_{eb}(x/\ell)}{4\pi\ell^2 d(x/\ell)^2} = S2EBPI(x/\ell)$$

$$\frac{S'''_{eb}(x/\ell)}{4\pi\ell^2} = \frac{1}{4\pi\ell^2} \frac{d^3S_{eb}(x/\ell)}{d(x/\ell)^3} = S3EBPI(x/\ell)$$

$$\frac{S^{IV}_{eb}(x/\ell)}{4\pi\ell^2} = \frac{1}{4\pi\ell^2} \frac{d^4S_{eb}(x/\ell)}{d(x/\ell)^4} = S4EBPI(x/\ell)$$

We note again the requirements that if the local linearization method is to be used with these subroutines, then the functions must be such that the complete profiles are closed, sharp-tipped, and have continuous area derivatives through the fourth. In addition, the user must supply the point $x/\ell = XS2EB$, i.e. the point closest to the origin where

$$S''_{eb}(x/\ell) = 0$$

If, however, the user supplies both the equivalent body profiles and the distribution of $u_B/U_\infty - vs - x/\ell$, then it is only necessary that the equivalent body area derivatives be continuous through the second. Also, for this case, it is unnecessary to specify $XS2EB$. These requirements are summarized below when user-specifying the equivalent body profile:

Value of MOPT

MOPT = 1, 2, 3

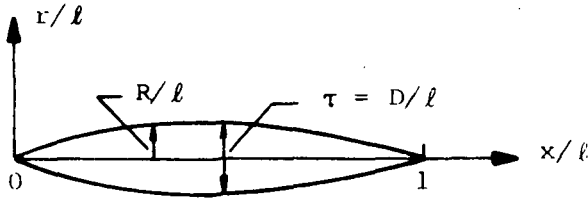
MOPT = 4

Requirements

- ① $S_{eb}, S'_{eb}, S''_{eb}, S'''_{eb}, S^{IV}_{eb}$ continuous for $0 < x < \ell$
- ② User must input value of $x/\ell = XS2EB$ where $S''_{eb}(XS2EB) = 0$
- ③ Set index MAREA = 1 in input
- ① $S_{eb}, S'_{eb}, S''_{eb}$ continuous for $0 < x < \ell$
- ② Set index MAREA = 1 in input

APPENDIX A

An illustrative example of a user-supplied equivalent body profile and the corresponding area and derivative subroutines to be used with, say, the local linearization method (MOPT = 1, 2, or 3) can be given as follows. Consider an equivalent body profile formed by the top half of the sinusoidal curve given by



$$\frac{R_{eb}(x/\ell)}{\ell} = \frac{\tau_{eb}}{2} \sin \left(\pi \left(\frac{x}{\ell} \right) \right) \quad \text{with say } \tau = .1$$

so that

$$\frac{S_{eb}(x/\ell)}{4\pi\ell^2} = \frac{\tau_{eb}^2}{16} (1 - \cos (2\pi(x/\ell)))$$

$$\frac{S'_{eb}(x/\ell)}{4\pi\ell^2} = \frac{\pi\tau_{eb}^2}{8} \sin (2\pi(x/\ell))$$

$$\frac{S''_{eb}(x/\ell)}{4\pi\ell^2} = \frac{\pi^2\tau_{eb}^2}{4} \cos (2\pi(x/\ell))$$

$$\frac{S'''_{eb}(x/\ell)}{4\pi\ell^2} = - \frac{\pi^3\tau_{eb}^2}{2} \sin (2\pi(x/\ell))$$

$$\frac{S^{IV}_{eb}(x/\ell)}{4\pi\ell^2} = - \pi^4\tau_{eb}^2 \cos (2\pi(x/\ell))$$

The function subroutines for $SEBPI(x/\ell)$ and $SLEBPI(x/\ell)$ with $\tau = .1$ are given by

```

FUNCTION SEBPI(DZ)
TAU = .1
PI = 3.1415927
SEBPI = TAU*TAU*(1. - COS(2.*PI*DZ))/16.

```

```

RETURN
END
FUNCTION S1EBPI(DZ)
TAU = .1
PI = 3.1415927
S1EBPI = PI*TAU*TAU*SIN (2.*PI*DZ)/8.
RETURN
END

```

The FUNCTION subroutines S2EBPI, S3EBPI, and S4EBPI are given in analogous fashion. The point where

$$S''_{eb}(x/\ell) = 0$$

is given by

$$XS2EB = 0.25$$

and must be included in the NAMELIST input data block.

Repetitive calculation storage option.- If the user wishes to undertake a systematic study of a wing-body configuration of the classes considered herein in which the geometry of the configuration is frozen and the Mach number and/or angle of attack are varied, a provision is included in the program whereby the velocity components associated with the crossflow solution for W_2,t - which is independent of M_∞ and α , and is by far the most time consuming crossflow potential to calculate - is stored at the user-specified output locations for later use. These velocity components are then provided for the remainder of the cases to be run rather than recalculated unnecessarily.

In order to activate the repetitive calculation option and make use of previously-stored results from a base run, it is necessary to set the integer index ICOPY = 1. The default value for ICOPY is ICOPY = 0 and this default value instructs the program to perform the crossflow calculations at the user-indicated axial locations and then automatically store these results in anticipation of use with the next case. If it is not desired to use those stored results for the next run, (i.e. ICOPY = 0 for the next case) the program simply replaces the previously-stored results with the ones being currently calculated.

APPENDIX A

Because for lifting situations, the crossflow calculations only proceed to $x/\ell = X_{SM_2}$ (as opposed to the $\alpha = 0$ case, which carries the calculation to $x/\ell = X_b$) unless all of the cases in the study are for $\alpha \neq 0$, the initial or base run which stores the crossflow results should be made for $\alpha = 0$.

Finally, when using the storage option, it is necessary, because of the different starting conditions involved, to use the same method for calculating u_B , i.e. (1) local linearization or (2) user-supplied distribution of u_B .

Data Format

The data format is most easily demonstrated by an example. Consider the case of a wing-elliptic body combination composed of a parabolic-arc equivalent body of thickness ratio 1/10, the ratio of semimajor to semiminor axis of the elliptic cross section is 3, the body base is at 85 percent of the complete body length, the wing profiles are parabolic arcs having a thickness/chord ratio of 0.04, the wing root chord is 40 percent of the complete body length with the leading edge of the wing root chord located at $x/\ell = 0.3$, the leading edge swept at 45 degrees, a taper ratio of 0.3, and a wing semispan being 28 percent of the complete body length (this implies the trailing edge is straight). The pressure distributions are required to be output at every 2 percent of the complete body length at angular locations $\theta = 0^\circ, 45^\circ, 90^\circ$, at radial distances $r/D = 1, 1.5, 2, 2.5, 3$, and 3.5 in the crossflow plane, at sonic free-stream conditions and 2 degrees angle of attack, by using the local linearization method to determine the flow about the equivalent body.

Thus, the input data cards would read (note that with a NAMELIST format, input variable sequencing is arbitrary):

CARD NO. 1

COLUMN NO.	2	9	80
	& TRANIN	AL=3., AMACH=1., MOPT=1., TAUB=.1., TAUW=.04, XMTB=.5,	

CARD NO. 2

COLUMN NO.	2	80
	XMTW=.5, XRLE=.3, CRT=.4, ANGLE=45., TR=.3, SSMAX=.28, NTHETA=3,	

APPENDIX A

CARD NO. 3

COLUMN NO.	2	80
$\text{THETA}(1)=0., \text{THETA}(2)=40., \text{THETA}(3)=90., \text{RF}(1)=1., \text{RF}(2)=1.5,$		

CARD NO. 4

COLUMN NO.	2	80
$\text{RF}(3)=2., \text{RF}(4)=2.5, \text{RF}(5)=3., \text{RF}(6)=3.5, \text{ALPHA}=2., \text{XLOUTP}=.02,$		

CARD NO. 5

COLUMN NO.	2	80
&END		

If for this case the user wished to supply his own distribution of u_B/U_∞ - vs. $-x/\ell$, this would have been done by specifying MOPT = 4 and also the integer NXEB representing the number (say, for example, 101) of values of u_B/U_∞ being entered (i.e. NXEB = 101) in the NAMELIST input data block. Next, all of the NXEB (101, in this example) values of $u_B/U_\infty = UEB(I)$ would be read in under the card format 8F10.0, with each successive value of u_B/U_∞ occupying a space of 10 columns (including decimal point) with 8 values per card. Finally, the NXEB values (101, in this example) of the corresponding axial locations $x/\ell = XEB(I)$ of the above values of u_B/U_∞ would be read in under the same format. Thus,

Card format for UEB(I): Format (8F10.0), decimal point required

COLUMN NO.	10	20		70	80
Data for	UEB(1)	UEB(2)		UEB(8)	
: etc.					

COLUMN NO.	10	20	30	40	50
Data for	UEB(97)	UEB(98)	UEB(99)	UEB(100)	UEB(101)

Card format for XEB(I): Format (8F10.0), decimal point required

COLUMN NO.	10	20		70	80
Data for	XEB(1)	XEB(2)		XEB(8)	
: etc.					

APPENDIX A

COLUMN NO.	10	20	30	40	50
Data for	XEB(97)	XEB(98)	XEB(99)	XEB(100)	XEB(101)

MESSAGES PRINTED BY THE PROGRAMS

This section lists the messages printed by the programs and indicates what to do when they are encountered. The first group of messages (1 to 15) are concerned with errors in input quantities and are self-explanatory.

- (1) INTERVAL SIZE FOR PRESSURE DISTRIBUTION PRINT-OUT MUST BE GREATER THAN 0 AND LESS THAN 1

This message indicates that the condition $0 < XLOUTP/\ell < 1$ has been violated.

- (2) XMTB MUST BE GREATER THAN 0 AND LESS THAN 1

This message indicates that the condition $0 < (x/\ell)_{R_{max}} < 1$ has been violated.

- (3) EQUIVALENT BODY THICKNESS RATIO MUST BE GREATER THAN ZERO.

This message indicates that the condition $D/\ell > 0$ has been violated.

- (4) XMTW MUST BE GREATER THAN 0 AND LESS THAN 1

This message indicates that the condition $0 < \left(\frac{x}{c_w}\right)_{Z_{max}} < 1$ has been violated.

- (5) WING THICKNESS/CHORD RATIO MUST BE GREATER THAN ZERO

This message indicates that the condition $Z_{max}/c_w > 0$ has been violated.

- (6) XRLE MUST BE GREATER THAN 0 AND LESS THAN 1

This message indicates that the condition $0 < x_{rl_e}/\ell < 1$ has been violated.

- (7) CRT MUST BE GREATER THAN 0 AND LESS THAN 1

This message indicates that the condition $0 < c_{R_t}/\ell < 1$ has been violated.

(8) XRL_E MUST BE LESS THAN XRT_E

This message indicates that the condition $x_{rle} < x_{rte}$ has been violated.

(9) ANGLE MUST BE BETWEEN 0 DEGREES AND 90 DEGREES

This message indicates that the condition $0 < \text{ANGLE} < 90$ has been violated.

(10) AXIAL LOCATION OF BODY BASE MUST BE AT OR BEHIND POINT WHERE WING TRAILING EDGE PIERCES BODY SURFACE

This message indicates that the condition $x_{rle_1} < x_b$ has been violated.

(11) AXIAL LOCATION OF BODY BASE MUST BE AT OR BEHIND TRAILING EDGE OF WING TIP CHORD

This message indicates that the condition $x_{sm_2} < x_b$ has been violated.

(12) RATIO OF MAJOR TO MINOR AXIS MUST BE GREATER THAN 0

This message indicates that the condition $\lambda (=a/b) > 0$ has been violated.

(13) TAPER RATIO MUST BE BETWEEN 0 AND 1

This message indicates that the condition $0 \leq TR \leq 1$ has been violated.

The following error messages, numbers (14) through (18) should not occur in the present programs. If they do, they are probably caused by an error in reproducing the source decks.

(14) EXECUTION TERMINATED BECAUSE EXPONENT N CANNOT BE DETERMINED TO WITHIN .01 PERCENT IN 20 ITERATIONS

This message is printed by the circular body programs when the exponent n describing the equivalent body ordinates (see eqs. (11) to (14)) cannot be found accurately from information regarding the point of maximum radius (eqs. (12) or (16)) by using a Newton-Raphson procedure 20 times.

APPENDIX A

- (15) EXECUTION TERMINATED BECAUSE POINT WHERE WING LEADING EDGE PIERCES BODY CANNOT BE FOUND TO WITHIN .01 PERCENT IN 20 ITERATIONS

This message is printed when the point x_{rle_1}/l cannot be found accurately by using a Newton-Raphson iteration procedure 20 times.

- (16) EXECUTION TERMINATED BECAUSE POINT WHERE WING TRAILING EDGE PIERCES BODY CANNOT BE FOUND TO WITHIN .01 PERCENT IN 20 ITERATIONS

This message is printed when the point x_{rte_1}/l cannot be found accurately by using a Newton-Raphson iteration procedure 20 times.

- (17) EXECUTION TERMINATED BECAUSE $SEB''(X)=0$ POINT CANNOT BE DETERMINED TO WITHIN SUFFICIENT ACCURACY IN 10 ITERATIONS

This message is printed by the circular body programs when the point x_s/l cannot be found accurately by using a Newton-Raphson iteration procedure 10 times.

- (18) INTEGRATION TERMINATED BECAUSE ACCUMULATED ERRORS HAVE CAUSED INTEGRATION SUBROUTINE TO BISECT ORIGINAL STEP SIZE (.001) 10 TIMES

This message is printed when the integration subroutine used (Hammings modified predictor-corrector scheme as described in the Scientific Subroutine Package from IBM Corporation) cannot achieve the integration accuracy (DPRMT(4)) desired even though the original step size (DPRMT(3) = 0.001) has been bisected 10 times.

- (19) PROGRAM TERMINATED BECAUSE INDENTED BODY RADIUS HAS BECOME LESS THAN ZERO AT $x/l =$

This message is printed by the program when the cross-sectional area of the wing is larger than that of the equivalent body, so that the indented body radius is less than zero. A wing with smaller thickness/chord ratio or smaller span must be used.

- (20) PROGRAM TERMINATED BECAUSE INDENTED BODY MAJOR AXIS HAS BECOME LESS THAN ZERO AT $x/l =$

This message is printed by the program for the same reason as message (20).

- (21) CALCULATION TERMINATED BECAUSE FLOW ABOUT EQUIVALENT BODY HAS
BECOME SUPERSONIC AT $x/\ell = .$ INPUT MACH NUMBER GREATER THAN
LOWER CRITICAL

This message is printed when using the local linearization method for purely subsonic flow to calculate u_B and indicates that the free stream Mach number is greater than the lower critical. There exists a region of supersonic flow and the local linearization method does not apply.

- (22) CALCULATION TERMINATED BECAUSE FLOW ABOUT EQUIVALENT BODY HAS
BECOME SUBSONIC AT $x/\ell =$

This message is printed using the local linearization method for purely supersonic flow to calculate u_B and it indicates that a region of subsonic flow has been encountered. This always occurs near the tail of the equivalent bodies considered here and the phenomenon is discussed fully in reference 6. However, if this region occurs at or near the nose, the local linearization method does not apply. In this case, the following error message is also printed,

INPUT MACH NUMBER LESS THAN UPPER CRITICAL

indicating that the condition $M_{cr,u} < M_\infty$ has been violated.

- (23) START OF SUPERSONIC CALCULATION

SUPERSONIC CALCULATION STARTS AT $x/\ell =$

This message is printed when using the local linearization method for $M_\infty \approx 1$ flows to calculate u_B and indicates where transfer is made from the parabolic (eq. (5)) to the hyperbolic (eq. (7)) differential equation. See reference 6 for details.

- (24) START OF SUBSONIC CALCULATION

SUBSONIC CALCULATION STARTS AT $x/\ell =$

This message is printed when using the local linearization method for $M_\infty \approx 1$ flows to calculate u_B and indicates where transfer is made from the hyperbolic (eq. (7)) to the elliptic (eq. (6)) differential equation. See reference 6 for details.

APPENDIX A

NUMERICAL EXAMPLES.

General Description of the Output

The output format of the program developed is as follows. On the top of the first page, a heading is printed describing the Mach number range, the general class of body (circular or elliptic) and wing being considered, and the theory used. Next, the wing-body geometry and flow field characteristics are printed. Then, if the local linearization method is being used, the program prints the fact that the integrations are starting at $x = x_s$ and proceeding to the nose. If the user supplies the distribution of u_B , this is omitted. A heading of independent and dependent variables is printed next which contains, from left to right, the axial location x/ℓ at which output is to be given, the actual body radius R_b/ℓ (or actual semimajor axis a/ℓ in the case of elliptic bodies) at that axial location, the angles θ (in degrees) in the crossflow plane at which output is desired, the surface pressure coefficient C_p (body), and six flow-field pressure coefficients $C_p(r/D =)$ at the indicated distances r/D in the crossflow plane. For the case when the user supplies the u_B distribution, the calculation begins at a point close to the nose and proceeds toward the body base with the values of the above quantities being printed out in the indicated tabular form at specified axial locations. When the local linearization method is used to determine u_B , the calculation begins at $x = x_s$ and proceeds to a point close to the nose, with the quantities described being printed at the specified axial locations, then, when the point close to the nose is reached, the program returns to $x = x_s$, prints the fact that the integration is restarting at that point and proceeding to the tail, prints the independent and dependent variable heading described above, and proceeds with the calculation to the body base. If it should happen at some point that the radial distance in the crossflow plane at which output is desired is less than the body radius (i.e. the point is inside the body), or if an output point falls on the wing leading or trailing edge, the pressure coefficient at that point is set equal to $1.E + 6$ and the program continues. Also, because of the discontinuity in the second derivative of the indented body d^2R_b/dx^2 (or d^2a/dx^2) at the points $x/\ell = x_{rle_1}$ and $x/\ell = x_{rte_1}$

APPENDIX A

and the discontinuity in the slope of the wing span at the points $x/l = x_{sm_1}$, and $x/l = x_{sm_2}$, output is not printed within a band ($\Delta x/l = 0.005$) of those points. When the calculations are successfully completed, the pertinent aerodynamic coefficients are calculated and printed and the program then proceeds to read the data for the next case.

Sample Cases

In order to provide checks on the programs, sample test cases have been run for each program and the results are provided in figures 8 through 12. In each case, the input data is provided together with the corresponding output.

Finally, we note that in order to improve their accuracy, changes have been made in the subroutines, as given in reference 6, which compute the derivatives of the indented circular and elliptic body area distributions. Consequently, the test case results that appear in reference 6 will differ slightly from the results which the current program will produce for those same wing-body geometries.

APPENDIX B

APPENDIX B

APPENDIX B

APPENDIX B

APPENDIX B

۱۱

120014

THE JOURNAL OF CLIMATE

APPENDIX B


```

FUNCTION UEBODY(X)
  DIMENSION A6(7,1),A6(2,1)
  COMMON /BLK19/ XE,B,XER,ITEST
  IF (ITEST.EQ.0) GO TO 10
  IF (X.EQ.B) RETURN
  10 IF (X.EQ.1) X=1.3*12
    IF (X.EQ.2) X=1.2*2
    1 CAPTURE
      2 UBODY=UE(j-1)*(1+UEB(j-1))/((XE(j)-XE(j-1))+(XE(j-1)-XE(j)))
      XE=j-1
      MEDIUM
      10 IF (X.EQ.1) -1.01*0.0 TU 11
        MEDIUM
        11 UE=0.001
          12 IF (UE.EQ.0) GO TO 12
            K=2
            GU TU 12
            11 IF (UE.EQ.0) ((UE-1.2)-UE6(1))/((XE(2)-XE(1))+(XE(1)-XE(2)))
              XE=1
              MEDIUM
              12 IF (UE.EQ.0) UEB(j)=UEB(i)*UEB(i-1)/XE(MEDIUM)
              13 IF (X.EQ.1) RETURN
              END
            END

SUBROUTINE RCTLU(X,Y,U2)
  DIMENSION U(11),DZ11
  COMMON /BLK19/ DM,DK,DI,DMU,U2M,U7S,MU1,U2A0,DY,DV2,DTAU2
  COMMON /BLK18/ AL,AL12,AL1,AL2,AL3,AL4,MUPT,MELLPT
  COMMON /BLK17/ MN
  COMMON /BLK16/ UH,M,DEF
  DAESEPU1(X)
  DAESEPU2(X)
  DAESEPU3(X)
  DAESEPU4(X)
  IF (MOPT.EQ.1) GO TO 11
  IF (MOPT.EQ.2) GO TO 12
  IF (MOPT.EQ.3) GO TO 13
  1 IF (X.EQ.0.5) DZ11=0.5
  2 IF (X.EQ.1.0) DZ11=1.0
  3 IF (X.EQ.1.5) DZ11=1.5
  4 IF (X.EQ.2.0) DZ11=2.0
  5 IF (X.EQ.2.5) DZ11=2.5
  6 IF (X.EQ.3.0) DZ11=3.0
  7 IF (X.EQ.3.5) DZ11=3.5
  8 IF (X.EQ.4.0) DZ11=4.0
  9 IF (X.EQ.4.5) DZ11=4.5
  10 IF (X.EQ.5.0) DZ11=5.0
  11 IF (X.EQ.5.5) DZ11=5.5
  12 IF (X.EQ.6.0) DZ11=6.0
  13 IF (X.EQ.6.5) DZ11=6.5
  14 IF (X.EQ.7.0) DZ11=7.0
  15 IF (X.EQ.7.5) DZ11=7.5
  16 IF (X.EQ.8.0) DZ11=8.0
  17 IF (X.EQ.8.5) DZ11=8.5
  18 IF (X.EQ.9.0) DZ11=9.0
  19 IF (X.EQ.9.5) DZ11=9.5
  20 IF (X.EQ.10.0) DZ11=10.0
  21 IF (X.EQ.10.5) DZ11=10.5
  22 IF (X.EQ.11.0) DZ11=11.0
  23 IF (X.EQ.11.5) DZ11=11.5
  24 IF (X.EQ.12.0) DZ11=12.0
  25 IF (X.EQ.12.5) DZ11=12.5
  26 IF (X.EQ.13.0) DZ11=13.0
  27 IF (X.EQ.13.5) DZ11=13.5
  28 IF (X.EQ.14.0) DZ11=14.0
  29 IF (X.EQ.14.5) DZ11=14.5
  30 IF (X.EQ.15.0) DZ11=15.0
  31 IF (X.EQ.15.5) DZ11=15.5
  32 IF (X.EQ.16.0) DZ11=16.0
  33 IF (X.EQ.16.5) DZ11=16.5
  34 IF (X.EQ.17.0) DZ11=17.0
  35 IF (X.EQ.17.5) DZ11=17.5
  36 IF (X.EQ.18.0) DZ11=18.0
  37 IF (X.EQ.18.5) DZ11=18.5
  38 IF (X.EQ.19.0) DZ11=19.0
  39 IF (X.EQ.19.5) DZ11=19.5
  40 IF (X.EQ.20.0) DZ11=20.0
  41 IF (X.EQ.20.5) DZ11=20.5
  42 IF (X.EQ.21.0) DZ11=21.0
  43 IF (X.EQ.21.5) DZ11=21.5
  44 IF (X.EQ.22.0) DZ11=22.0
  45 IF (X.EQ.22.5) DZ11=22.5
  46 IF (X.EQ.23.0) DZ11=23.0
  47 IF (X.EQ.23.5) DZ11=23.5
  48 IF (X.EQ.24.0) DZ11=24.0
  49 IF (X.EQ.24.5) DZ11=24.5
  50 IF (X.EQ.25.0) DZ11=25.0
  51 IF (X.EQ.25.5) DZ11=25.5
  52 IF (X.EQ.26.0) DZ11=26.0
  53 IF (X.EQ.26.5) DZ11=26.5
  54 IF (X.EQ.27.0) DZ11=27.0
  55 IF (X.EQ.27.5) DZ11=27.5
  56 IF (X.EQ.28.0) DZ11=28.0
  57 IF (X.EQ.28.5) DZ11=28.5
  58 IF (X.EQ.29.0) DZ11=29.0
  59 IF (X.EQ.29.5) DZ11=29.5
  60 IF (X.EQ.30.0) DZ11=30.0
  61 IF (X.EQ.30.5) DZ11=30.5
  62 IF (X.EQ.31.0) DZ11=31.0
  63 IF (X.EQ.31.5) DZ11=31.5
  64 IF (X.EQ.32.0) DZ11=32.0
  65 IF (X.EQ.32.5) DZ11=32.5
  66 IF (X.EQ.33.0) DZ11=33.0
  67 IF (X.EQ.33.5) DZ11=33.5
  68 IF (X.EQ.34.0) DZ11=34.0
  69 IF (X.EQ.34.5) DZ11=34.5
  70 IF (X.EQ.35.0) DZ11=35.0
  71 IF (X.EQ.35.5) DZ11=35.5
  72 IF (X.EQ.36.0) DZ11=36.0
  73 IF (X.EQ.36.5) DZ11=36.5
  74 IF (X.EQ.37.0) DZ11=37.0
  75 IF (X.EQ.37.5) DZ11=37.5
  76 IF (X.EQ.38.0) DZ11=38.0
  77 IF (X.EQ.38.5) DZ11=38.5
  78 IF (X.EQ.39.0) DZ11=39.0
  79 IF (X.EQ.39.5) DZ11=39.5
  80 IF (X.EQ.40.0) DZ11=40.0
  81 IF (X.EQ.40.5) DZ11=40.5
  82 IF (X.EQ.41.0) DZ11=41.0
  83 IF (X.EQ.41.5) DZ11=41.5
  84 IF (X.EQ.42.0) DZ11=42.0
  85 IF (X.EQ.42.5) DZ11=42.5
  86 IF (X.EQ.43.0) DZ11=43.0
  87 IF (X.EQ.43.5) DZ11=43.5
  88 IF (X.EQ.44.0) DZ11=44.0
  89 IF (X.EQ.44.5) DZ11=44.5
  90 IF (X.EQ.45.0) DZ11=45.0
  91 IF (X.EQ.45.5) DZ11=45.5
  92 IF (X.EQ.46.0) DZ11=46.0
  93 IF (X.EQ.46.5) DZ11=46.5
  94 IF (X.EQ.47.0) DZ11=47.0
  95 IF (X.EQ.47.5) DZ11=47.5
  96 IF (X.EQ.48.0) DZ11=48.0
  97 IF (X.EQ.48.5) DZ11=48.5
  98 IF (X.EQ.49.0) DZ11=49.0
  99 IF (X.EQ.49.5) DZ11=49.5
  100 IF (X.EQ.50.0) DZ11=50.0
  101 IF (X.EQ.50.5) DZ11=50.5
  102 IF (X.EQ.51.0) DZ11=51.0
  103 IF (X.EQ.51.5) DZ11=51.5
  104 IF (X.EQ.52.0) DZ11=52.0
  105 IF (X.EQ.52.5) DZ11=52.5
  106 IF (X.EQ.53.0) DZ11=53.0
  107 IF (X.EQ.53.5) DZ11=53.5
  108 IF (X.EQ.54.0) DZ11=54.0
  109 IF (X.EQ.54.5) DZ11=54.5
  110 IF (X.EQ.55.0) DZ11=55.0
  111 IF (X.EQ.55.5) DZ11=55.5
  112 IF (X.EQ.56.0) DZ11=56.0
  113 IF (X.EQ.56.5) DZ11=56.5
  114 IF (X.EQ.57.0) DZ11=57.0
  115 IF (X.EQ.57.5) DZ11=57.5
  116 IF (X.EQ.58.0) DZ11=58.0
  117 IF (X.EQ.58.5) DZ11=58.5
  118 IF (X.EQ.59.0) DZ11=59.0
  119 IF (X.EQ.59.5) DZ11=59.5
  120 IF (X.EQ.60.0) DZ11=60.0
  121 IF (X.EQ.60.5) DZ11=60.5
  122 IF (X.EQ.61.0) DZ11=61.0
  123 IF (X.EQ.61.5) DZ11=61.5
  124 IF (X.EQ.62.0) DZ11=62.0
  125 IF (X.EQ.62.5) DZ11=62.5
  126 IF (X.EQ.63.0) DZ11=63.0
  127 IF (X.EQ.63.5) DZ11=63.5
  128 IF (X.EQ.64.0) DZ11=64.0
  129 IF (X.EQ.64.5) DZ11=64.5
  130 IF (X.EQ.65.0) DZ11=65.0
  131 IF (X.EQ.65.5) DZ11=65.5
  132 IF (X.EQ.66.0) DZ11=66.0
  133 IF (X.EQ.66.5) DZ11=66.5
  134 IF (X.EQ.67.0) DZ11=67.0
  135 IF (X.EQ.67.5) DZ11=67.5
  136 IF (X.EQ.68.0) DZ11=68.0
  137 IF (X.EQ.68.5) DZ11=68.5
  138 IF (X.EQ.69.0) DZ11=69.0
  139 IF (X.EQ.69.5) DZ11=69.5
  140 IF (X.EQ.70.0) DZ11=70.0
  141 IF (X.EQ.70.5) DZ11=70.5
  142 IF (X.EQ.71.0) DZ11=71.0
  143 IF (X.EQ.71.5) DZ11=71.5
  144 IF (X.EQ.72.0) DZ11=72.0
  145 IF (X.EQ.72.5) DZ11=72.5
  146 IF (X.EQ.73.0) DZ11=73.0
  147 IF (X.EQ.73.5) DZ11=73.5
  148 IF (X.EQ.74.0) DZ11=74.0
  149 IF (X.EQ.74.5) DZ11=74.5
  150 IF (X.EQ.75.0) DZ11=75.0
  151 IF (X.EQ.75.5) DZ11=75.5
  152 IF (X.EQ.76.0) DZ11=76.0
  153 IF (X.EQ.76.5) DZ11=76.5
  154 IF (X.EQ.77.0) DZ11=77.0
  155 IF (X.EQ.77.5) DZ11=77.5
  156 IF (X.EQ.78.0) DZ11=78.0
  157 IF (X.EQ.78.5) DZ11=78.5
  158 IF (X.EQ.79.0) DZ11=79.0
  159 IF (X.EQ.79.5) DZ11=79.5
  160 IF (X.EQ.80.0) DZ11=80.0
  161 IF (X.EQ.80.5) DZ11=80.5
  162 IF (X.EQ.81.0) DZ11=81.0
  163 IF (X.EQ.81.5) DZ11=81.5
  164 IF (X.EQ.82.0) DZ11=82.0
  165 IF (X.EQ.82.5) DZ11=82.5
  166 IF (X.EQ.83.0) DZ11=83.0
  167 IF (X.EQ.83.5) DZ11=83.5
  168 IF (X.EQ.84.0) DZ11=84.0
  169 IF (X.EQ.84.5) DZ11=84.5
  170 IF (X.EQ.85.0) DZ11=85.0
  171 IF (X.EQ.85.5) DZ11=85.5
  172 IF (X.EQ.86.0) DZ11=86.0
  173 IF (X.EQ.86.5) DZ11=86.5
  174 IF (X.EQ.87.0) DZ11=87.0
  175 IF (X.EQ.87.5) DZ11=87.5
  176 IF (X.EQ.88.0) DZ11=88.0
  177 IF (X.EQ.88.5) DZ11=88.5
  178 IF (X.EQ.89.0) DZ11=89.0
  179 IF (X.EQ.89.5) DZ11=89.5
  180 IF (X.EQ.90.0) DZ11=90.0
  181 IF (X.EQ.90.5) DZ11=90.5
  182 IF (X.EQ.91.0) DZ11=91.0
  183 IF (X.EQ.91.5) DZ11=91.5
  184 IF (X.EQ.92.0) DZ11=92.0
  185 IF (X.EQ.92.5) DZ11=92.5
  186 IF (X.EQ.93.0) DZ11=93.0
  187 IF (X.EQ.93.5) DZ11=93.5
  188 IF (X.EQ.94.0) DZ11=94.0
  189 IF (X.EQ.94.5) DZ11=94.5
  190 IF (X.EQ.95.0) DZ11=95.0
  191 IF (X.EQ.95.5) DZ11=95.5
  192 IF (X.EQ.96.0) DZ11=96.0
  193 IF (X.EQ.96.5) DZ11=96.5
  194 IF (X.EQ.97.0) DZ11=97.0
  195 IF (X.EQ.97.5) DZ11=97.5
  196 IF (X.EQ.98.0) DZ11=98.0
  197 IF (X.EQ.98.5) DZ11=98.5
  198 IF (X.EQ.99.0) DZ11=99.0
  199 IF (X.EQ.99.5) DZ11=99.5
  200 IF (X.EQ.100.0) DZ11=100.0
  201 IF (X.EQ.100.5) DZ11=100.5
  202 IF (X.EQ.101.0) DZ11=101.0
  203 IF (X.EQ.101.5) DZ11=101.5
  204 IF (X.EQ.102.0) DZ11=102.0
  205 IF (X.EQ.102.5) DZ11=102.5
  206 IF (X.EQ.103.0) DZ11=103.0
  207 IF (X.EQ.103.5) DZ11=103.5
  208 IF (X.EQ.104.0) DZ11=104.0
  209 IF (X.EQ.104.5) DZ11=104.5
  210 IF (X.EQ.105.0) DZ11=105.0
  211 IF (X.EQ.105.5) DZ11=105.5
  212 IF (X.EQ.106.0) DZ11=106.0
  213 IF (X.EQ.106.5) DZ11=106.5
  214 IF (X.EQ.107.0) DZ11=107.0
  215 IF (X.EQ.107.5) DZ11=107.5
  216 IF (X.EQ.108.0) DZ11=108.0
  217 IF (X.EQ.108.5) DZ11=108.5
  218 IF (X.EQ.109.0) DZ11=109.0
  219 IF (X.EQ.109.5) DZ11=109.5
  220 IF (X.EQ.110.0) DZ11=110.0
  221 IF (X.EQ.110.5) DZ11=110.5
  222 IF (X.EQ.111.0) DZ11=111.0
  223 IF (X.EQ.111.5) DZ11=111.5
  224 IF (X.EQ.112.0) DZ11=112.0
  225 IF (X.EQ.112.5) DZ11=112.5
  226 IF (X.EQ.113.0) DZ11=113.0
  227 IF (X.EQ.113.5) DZ11=113.5
  228 IF (X.EQ.114.0) DZ11=114.0
  229 IF (X.EQ.114.5) DZ11=114.5
  230 IF (X.EQ.115.0) DZ11=115.0
  231 IF (X.EQ.115.5) DZ11=115.5
  232 IF (X.EQ.116.0) DZ11=116.0
  233 IF (X.EQ.116.5) DZ11=116.5
  234 IF (X.EQ.117.0) DZ11=117.0
  235 IF (X.EQ.117.5) DZ11=117.5
  236 IF (X.EQ.118.0) DZ11=118.0
  237 IF (X.EQ.118.5) DZ11=118.5
  238 IF (X.EQ.119.0) DZ11=119.0
  239 IF (X.EQ.119.5) DZ11=119.5
  240 IF (X.EQ.120.0) DZ11=120.0
  241 IF (X.EQ.120.5) DZ11=120.5
  242 IF (X.EQ.121.0) DZ11=121.0
  243 IF (X.EQ.121.5) DZ11=121.5
  244 IF (X.EQ.122.0) DZ11=122.0
  245 IF (X.EQ.122.5) DZ11=122.5
  246 IF (X.EQ.123.0) DZ11=123.0
  247 IF (X.EQ.123.5) DZ11=123.5
  248 IF (X.EQ.124.0) DZ11=124.0
  249 IF (X.EQ.124.5) DZ11=124.5
  250 IF (X.EQ.125.0) DZ11=125.0
  251 IF (X.EQ.125.5) DZ11=125.5
  252 IF (X.EQ.126.0) DZ11=126.0
  253 IF (X.EQ.126.5) DZ11=126.5
  254 IF (X.EQ.127.0) DZ11=127.0
  255 IF (X.EQ.127.5) DZ11=127.5
  256 IF (X.EQ.128.0) DZ11=128.0
  257 IF (X.EQ.128.5) DZ11=128.5
  258 IF (X.EQ.129.0) DZ11=129.0
  259 IF (X.EQ.129.5) DZ11=129.5
  260 IF (X.EQ.130.0) DZ11=130.0
  261 IF (X.EQ.130.5) DZ11=130.5
  262 IF (X.EQ.131.0) DZ11=131.0
  263 IF (X.EQ.131.5) DZ11=131.5
  264 IF (X.EQ.132.0) DZ11=132.0
  265 IF (X.EQ.132.5) DZ11=132.5
  266 IF (X.EQ.133.0) DZ11=133.0
  267 IF (X.EQ.133.5) DZ11=133.5
  268 IF (X.EQ.134.0) DZ11=134.0
  269 IF (X.EQ.134.5) DZ11=134.5
  270 IF (X.EQ.135.0) DZ11=135.0
  271 IF (X.EQ.135.5) DZ11=135.5
  272 IF (X.EQ.136.0) DZ11=136.0
  273 IF (X.EQ.136.5) DZ11=136.5
  274 IF (X.EQ.137.0) DZ11=137.0
  275 IF (X.EQ.137.5) DZ11=137.5
  276 IF (X.EQ.138.0) DZ11=138.0
  277 IF (X.EQ.138.5) DZ11=138.5
  278 IF (X.EQ.139.0) DZ11=139.0
  279 IF (X.EQ.139.5) DZ11=139.5
  280 IF (X.EQ.140.0) DZ11=140.0
  281 IF (X.EQ.140.5) DZ11=140.5
  282 IF (X.EQ.141.0) DZ11=141.0
  283 IF (X.EQ.141.5) DZ11=141.5
  284 IF (X.EQ.142.0) DZ11=142.0
  285 IF (X.EQ.142.5) DZ11=142.5
  286 IF (X.EQ.143.0) DZ11=143.0
  287 IF (X.EQ.143.5) DZ11=143.5
  288 IF (X.EQ.144.0) DZ11=144.0
  289 IF (X.EQ.144.5) DZ11=144.5
  290 IF (X.EQ.145.0) DZ11=145.0
  291 IF (X.EQ.145.5) DZ11=145.5
  292 IF (X.EQ.146.0) DZ11=146.0
  293 IF (X.EQ.146.5) DZ11=146.5
  294 IF (X.EQ.147.0) DZ11=147.0
  295 IF (X.EQ.147.5) DZ11=147.5
  296 IF (X.EQ.148.0) DZ11=148.0
  297 IF (X.EQ.148.5) DZ11=148.5
  298 IF (X.EQ.149.0) DZ11=149.0
  299 IF (X.EQ.149.5) DZ11=149.5
  300 IF (X.EQ.150.0) DZ11=150.0
  301 IF (X.EQ.150.5) DZ11=150.5
  302 IF (X.EQ.151.0) DZ11=151.0
  303 IF (X.EQ.151.5) DZ11=151.5
  304 IF (X.EQ.152.0) DZ11=152.0
  305 IF (X.EQ.152.5) DZ11=152.5
  306 IF (X.EQ.153.0) DZ11=153.0
  307 IF (X.EQ.153.5) DZ11=153.5
  308 IF (X.EQ.154.0) DZ11=154.0
  309 IF (X.EQ.154.5) DZ11=154.5
  310 IF (X.EQ.155.0) DZ11=155.0
  311 IF (X.EQ.155.5) DZ11=155.5
  312 IF (X.EQ.156.0) DZ11=156.0
  313 IF (X.EQ.156.5) DZ11=156.5
  314 IF (X.EQ.157.0) DZ11=157.0
  315 IF (X.EQ.157.5) DZ11=157.5
  316 IF (X.EQ.158.0) DZ11=158.0
  317 IF (X.EQ.158.5) DZ11=158.5
  318 IF (X.EQ.159.0) DZ11=159.0
  319 IF (X.EQ.159.5) DZ11=159.5
  320 IF (X.EQ.160.0) DZ11=160.0
  321 IF (X.EQ.160.5) DZ11=160.5
  322 IF (X.EQ.161.0) DZ11=161.0
  323 IF (X.EQ.161.5) DZ11=161.5
  324 IF (X.EQ.162.0) DZ11=162.0
  325 IF (X.EQ.162.5) DZ11=162.5
  326 IF (X.EQ.163.0) DZ11=163.0
  327 IF (X.EQ.163.5) DZ11=163.5
  328 IF (X.EQ.164.0) DZ11=164.0
  329 IF (X.EQ.164.5) DZ11=164.5
  330 IF (X.EQ.165.0) DZ11=165.0
  331 IF (X.EQ.165.5) DZ11=165.5
  332 IF (X.EQ.166.0) DZ11=166.0
  333 IF (X.EQ.166.5) DZ11=166.5
  334 IF (X.EQ.167.0) DZ11=167.0
  335 IF (X.EQ.167.5) DZ11=167.5
  336 IF (X.EQ.168.0) DZ11=168.0
  337 IF (X.EQ.168.5) DZ11=168.5
  338 IF (X.EQ.169.0) DZ11=169.0
  339 IF (X.EQ.169.5) DZ11=169.5
  340 IF (X.EQ.170.0) DZ11=170.0
  341 IF (X.EQ.170.5) DZ11=170.5
  342 IF (X.EQ.171.0) DZ11=171.0
  343 IF (X.EQ.171.5) DZ11=171.5
  344 IF (X.EQ.172.0) DZ11=172.0
  345 IF (X.EQ.172.5) DZ11=172.5
  346 IF (X.EQ.173.0) DZ11=173.0
  347 IF (X.EQ.173.5) DZ11=173.5
  348 IF (X.EQ.174.0) DZ11=174.0
  349 IF (X.EQ.174.5) DZ11=174.5
  350 IF (X.EQ.175.0) DZ11=175.0
  351 IF (X.EQ.175.5) DZ11=175.5
  352 IF (X.EQ.176.0) DZ11=176.0
  353 IF (X.EQ.176.5) DZ11=176.5
  354 IF (X.EQ.177.0) DZ11=177.0
  355 IF (X.EQ.177.5) DZ11=177.5
  356 IF (X.EQ.178.0) DZ11=178.0
  357 IF (X.EQ.178.5) DZ11=178.5
  358 IF (X.EQ.179.0) DZ11=179.0
  359 IF (X.EQ.179.5) DZ11=179.5
  360 IF (X.EQ.180.0) DZ11=180.0
  361 IF (X.EQ.180.5) DZ11=180.5
  362 IF (X.EQ.181.0) DZ11=181.0
  363 IF (X.EQ.181.5) DZ11=181.5
  364 IF (X.EQ.182.0) DZ11=182.0
  365 IF (X.EQ.182.5) DZ11=182.5
  366 IF (X.EQ.183.0) DZ11=183.0
  367 IF (X.EQ.183.5) DZ11=183.5
  368 IF (X.EQ.184.0) DZ11=184.0
  369 IF (X.EQ.184.5) DZ11=184.5
  370 IF (X.EQ.185.0) DZ11=185.0
  371 IF (X.EQ.185.5) DZ11=185.5
  372 IF (X.EQ.186.0) DZ11=186.0
  373 IF (X.EQ.186.5) DZ11=186.5
  374 IF (X.EQ.187.0) DZ11=187.0
  375 IF (X.EQ.187.5) DZ11=187.5
  376 IF (X.EQ.188.0) DZ11=188.0
  377 IF (X.EQ.188.5) DZ11=188.5
  378 IF (X.EQ.189.0) DZ11=189.0
  379 IF (X.EQ.189.5) DZ11=189.5
  380 IF (X.EQ.190.0) DZ11=190.0
  381 IF (X.EQ.190.5) DZ11=190.5
  382 IF (X.EQ.191.0) DZ11=191.0
  383 IF (X.EQ.191.5) DZ11=191.5
  384 IF (X.EQ.192.0) DZ11=192.0
  385 IF (X.EQ.192.5) DZ11=192.5
  386 IF (X.EQ.193.0) DZ11=193.0
  387 IF (X.EQ.193.5) DZ11=193.5
  388 IF (X.EQ.194.0) DZ11=194.0
  389 IF (X.EQ.194.5) DZ11=194.5
  390 IF (X.EQ.195.0) DZ11=195.0
  391 IF (X.EQ.195.5) DZ11=195.5
  392 IF (X.EQ.196.0) DZ11=196.0
  393 IF (X.EQ.196.5) DZ11=196.5
  394 IF (X.EQ.197.0) DZ11=197.0
  395 IF (X.EQ.197.5) DZ11=197.5
  396 IF (X.EQ.198.0) DZ11=198.0
  397 IF (X.EQ.198.5) DZ11=198.5
  398 IF (X.EQ.199.0) DZ11=199.0
  399 IF (X.EQ.199.5) DZ11=199.5
  400 IF (X.EQ.200.0) DZ11=200.0
  401 IF (X.EQ.200.5) DZ11=200.5
  402 IF (X.EQ.201.0) DZ11=201.0
  403 IF (X.EQ.201.5) DZ11=201.5
  404 IF (X.EQ.202.0) DZ11=202.0
  405 IF (X.EQ.202.5) DZ11=202.5
  406 IF (X.EQ.203.0) DZ11=203.0
  407 IF (X.EQ.203.5) DZ11=203.5
  408 IF (X.EQ.204.0) DZ11=204.0
  409 IF (X.EQ.204.5) DZ11=204.5
  410 IF (X.EQ.205.0) DZ11=205.0
  411 IF (X.EQ.205.5) DZ11=205.5
  412 IF (X.EQ.206.0) DZ11=206.0
  413 IF (X.EQ.206.5) DZ11=206.5
  414 IF (X.EQ.207.0) DZ11=207.0
  415 IF (X.EQ.207.5) DZ11=207.5
  416 IF (X.EQ.208.0) DZ11=208.0
  417 IF (X.EQ.208.5) DZ11=208.5
  418 IF (X.EQ.209.0) DZ11=209.0
  419 IF (X.EQ.209.5) DZ11=209.5
  420 IF (X.EQ.210.0) DZ11=210.0
  421 IF (X.EQ.210.5) DZ11=210.5
  422 IF (X.EQ.211.0) DZ11=211.0
  423 IF (X.EQ.211.5) DZ11=211.5
  424 IF (X.EQ.212.0) DZ11=212.0
  4
```

APPENDIX B

APPENDIX B

```

FUNCTION FUNK5001 FUNK1001
COMMON /BLK13/ COMMON /BLK13/ Y12345678910111213141516171819202122232425262728293031323334353637383940414243444546474849505152535455565758596061626364656667686970717273747576777879808182838485868788899091929394959697989910010110210310410510610710810911011111211311411511611711811912012112212312412512612712812913013113213313413513613713813914014114214314414514614714814915015115215315415515615715815916016116216316416516616716816917017117217317417517617717817918018118218318418518618718818919019119219319419519619719819920020120220320420520620720820921021121221321421521621721821922022122222322422522622722822923023123223323423523623723823924024124224324424524624724824925025125225325425525625725825926026126226326426526626726826927027127227327427527627727827928028128228328428528628728828929029129229329429529629729829930030130230330430530630730830931031131231331431531631731831932032132232332432532632732832933033133233333433533633733833934034134234334434534634734834935035135235335435535635735835936036136236336436536636736836937037137237337437537637737837938038138238338438538638738838939039139239339439539639739839940040140240340440540640740840941041141241341441541641741841942042142242342442542642742842943043143243343443543643743843944044144244344444544644744844945045145245345445545645745845945045145245345445545645745845946046146246346446546646746846947047147247347447547647747847948048148248348448548648748848949049149249349449549649749849950050150250350450550650750850951051151251351451551651751851951051151251351451551651751851952052152252352452552652752852952052152252352452552652752852953053153253353453553653753853953053153253353453553653753853954054154254354454554654754854954054154254354454554654754854955055155255355455555655755855955055155255355455555655755855956056156256356456556656756856956056156256356456556656756856957057157257357457557657757857957057157257357457557657757857958058158258358458558658758858958058158258358458558658758858959059159259359459559659759859959059159259359459559659759859960060160260360460560660760860960060160260360460560660760860961061161261361461561661761861961061161261361461561661761861962062162262362462562662762862962062162262362462562662762862963063163263363463563663763863963063163263363463563663763863964064164264364464564664764864964064164264364464564664764864965065165265365465565665765865965065165265365465565665765865966066166266366466566666766866966066166266366466566666766866967067167267367467567667767867967067167267367467567667767867968068168268368468568668768868968068168268368468568668768868969069169269369469569669769869969069169269369469569669769869970070170270370470570670770870970070170270370470570670770870971071171271371471571671771871971071171271371471571671771871972072172272372472572672772872972072172272372472572672772872973073173273373473573673773873973073173273373473573673773873974074174274374474574674774874974074174274374474574674774874975075175275375475575675775875975075175275375475575675775875976076176276376476576676776876976076176276376476576676776876977077177277377477577677777877977077177277377477577677777877978078178278378478578678778878978078178278378478578678778878979079179279379479579679779879979079179279379479579679779879980080180280380480580680780880980080180280380480580680780880981081181281381481581681781881981081181281381481581681781881982082182282382482582682782882982082182282382482582682782882983083183283383483583683783883983083183283383483583683783883984084184284384484584684784884984084184284384484584684784884985085185285385485585685785885985085185285385485585685785885986086186286386486586686786886986086186286386486586686786886987087187287387487587687787887987087187287387487587687787887988088188288388488588688788888988088188288388488588688788888989089189289389489589689789889989089189289389489589689789889990090190290390490590690790890990090190290390490590690790890991091191291391491591691791891991091191291391491591691791891992092192292392492592692792892992092192292392492592692792892993093193293393493593693793893993093193293393493593693793893994094194294394494594694794894994094194294394494594694794894995095195295395495595695795895995095195295395495595695795895996096196296396496596696796896996096196296396496596696796896997097197297397497597697797897997097197297397497597697797897998098198298398498598698798898998098198298398498598698798898999099199299399499599699799899
```


APPENDIX B

REFERENCES

1. Steger, J. L. and Lomax, H.: Generalized Relaxation Methods Applied to Problems in Transonic Flow. Proc. 2nd Int. Conf. on Numerical Methods in Fluid Dynamics, Sept. 1970; Lecture Notes in Physics, 1971, pp. 193-197.
2. Garabedian, P. R. and Korn, D. G.: Numerical Design of Transonic Airfoils. Numerical Solution of Partial Differential Equations - II, Bert Hubbard, ed., Academic Press, Inc., 1971, pp. 253-271.
3. Murman, E. M. and Cole, J. D.: Calculation of Plane Steady Transonic Flows. AIAA J., Vol. 9, No. 1, Jan. 1971, pp. 114-121.
4. Murman, E. M. and Krupp, J. A.: The Numerical Calculation of Steady Transonic Flows Past Thin Lifting Airfoils and Slender Bodies. AIAA Paper No. 71-566, Presented at AIAA 4th Fluid and Plasma Dynamics Conf., Palo Alto, Calif., June 21-23, 1971
5. Bailey, F. R.: Numerical Calculation of Transonic Flow About Slender Bodies of Revolution. NASA TN D-6582, Dec. 1971.
6. Spreiter, J. R. and Stahara, S. S.: Calculative Techniques for Transonic Flows About Certain Classes of Airfoils and Slender Bodies. NASA CR-1722, 1971.
7. Stahara, S. S. and Spreiter, J. R.: Calculative Techniques for Transonic Flows About Certain Classes of Wing-Body Combinations. NEAR TR 36, Nov. 1971. NASA CR-2103, 1972.
8. Heaslet, M. A. and Spreiter, J. R.: Three-Dimensional Transonic Flow Theory Applied to Slender Wings and Bodies. NACA Rep. 1318, 1957.
9. Adams, M. C. and Sears, W. R.: Slender-Body Theory - Review and Extensions. J. Aero. Sci., Vol. 20, No. 2, 1953, pp. 85-98.
10. Stocker, P. M.: Supersonic Flow Past Bodies of Revolution with Thin Wings of Small Aspect Ratio. Aero. Quart., Vol. III, May 1951, pp. 61-79.

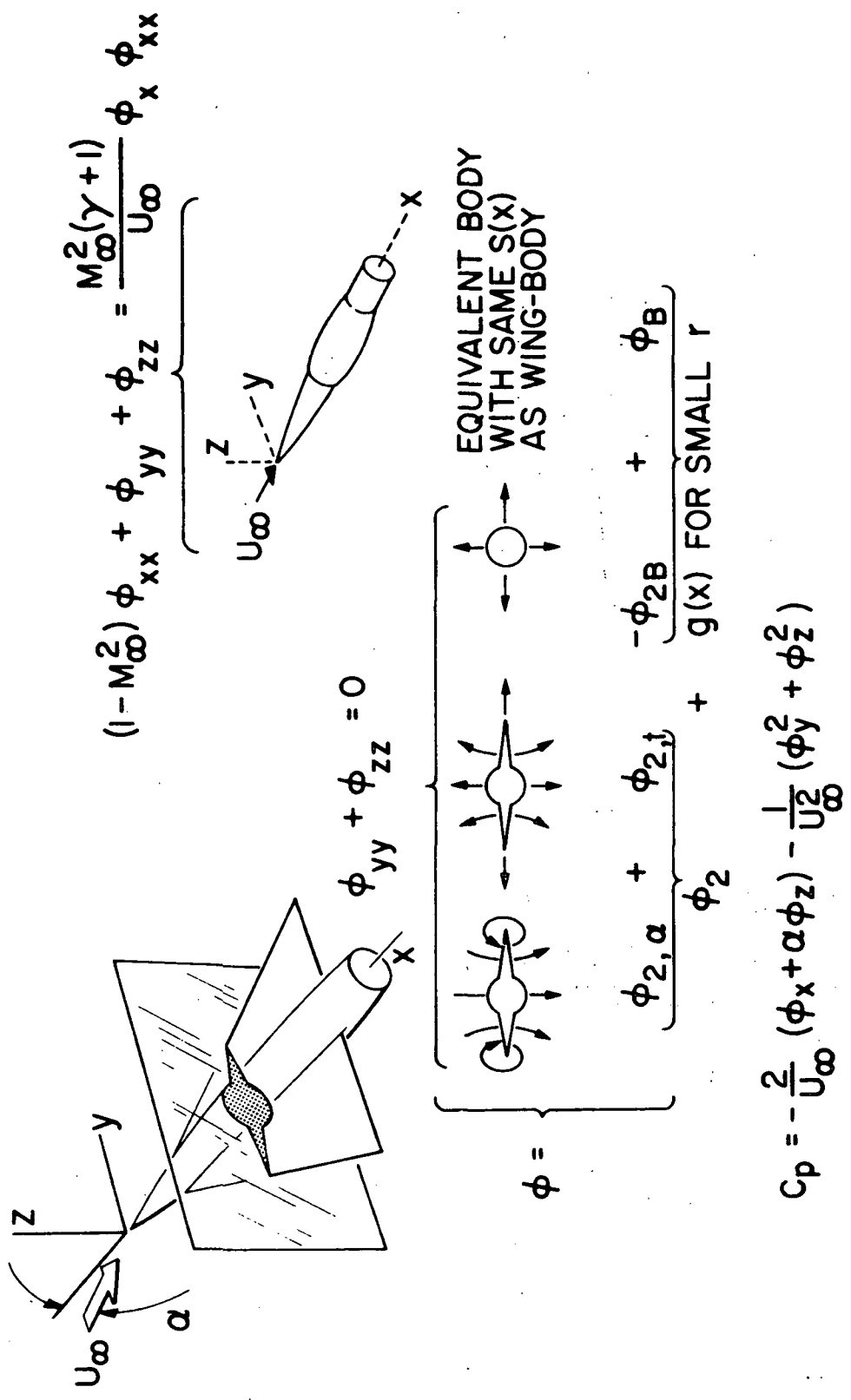
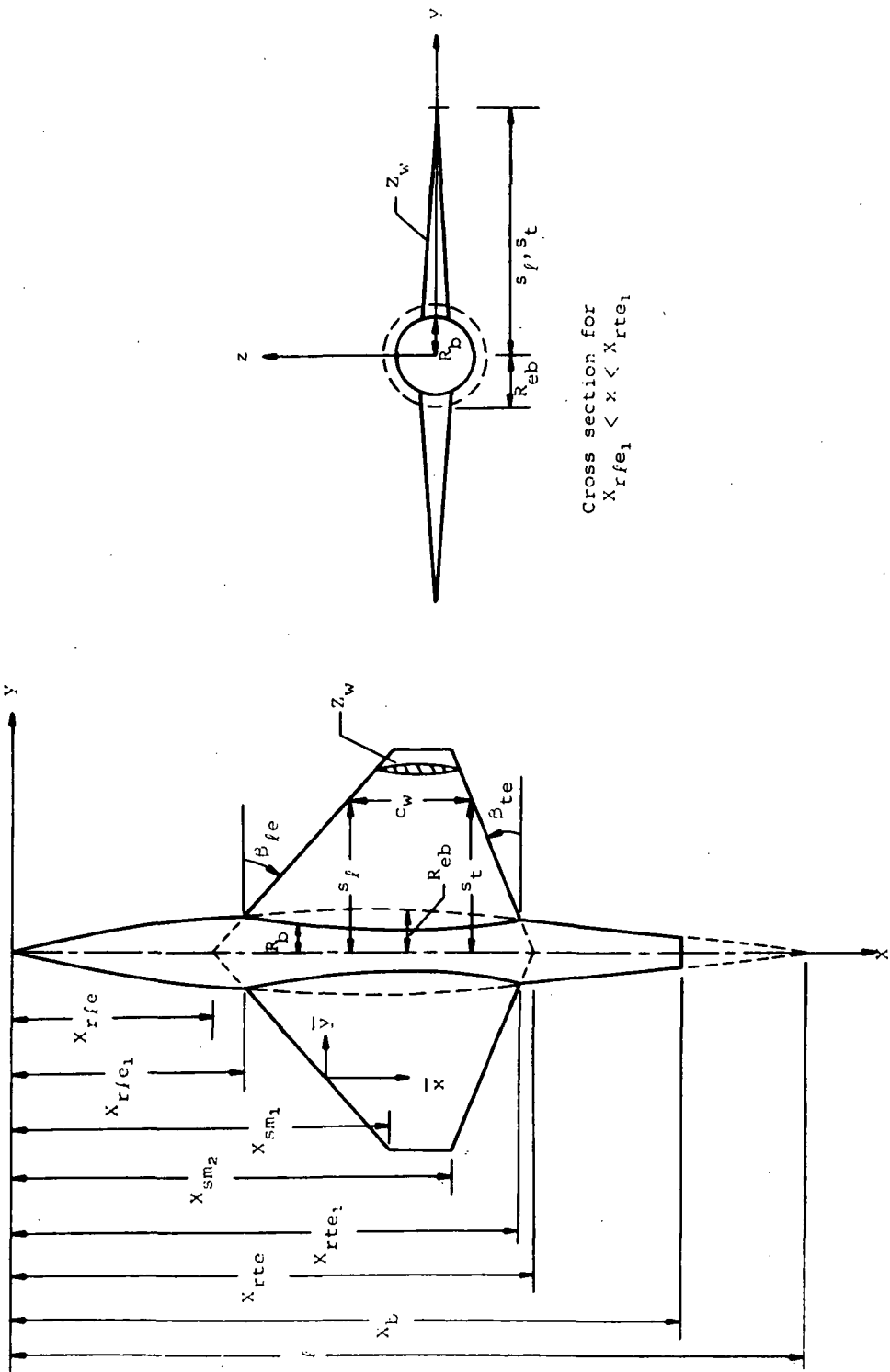


Figure 1.— Transonic equivalence rule for slender wing-body combinations.



Cross section for
 $x_{rfce_1} < x < x_{rte_1}$

Figure 2(a). General configuration of finite thickness wing-inertial circular body combinations with straight/sweptforward trailing edge planforms ($\beta_{te} \leq 0$).

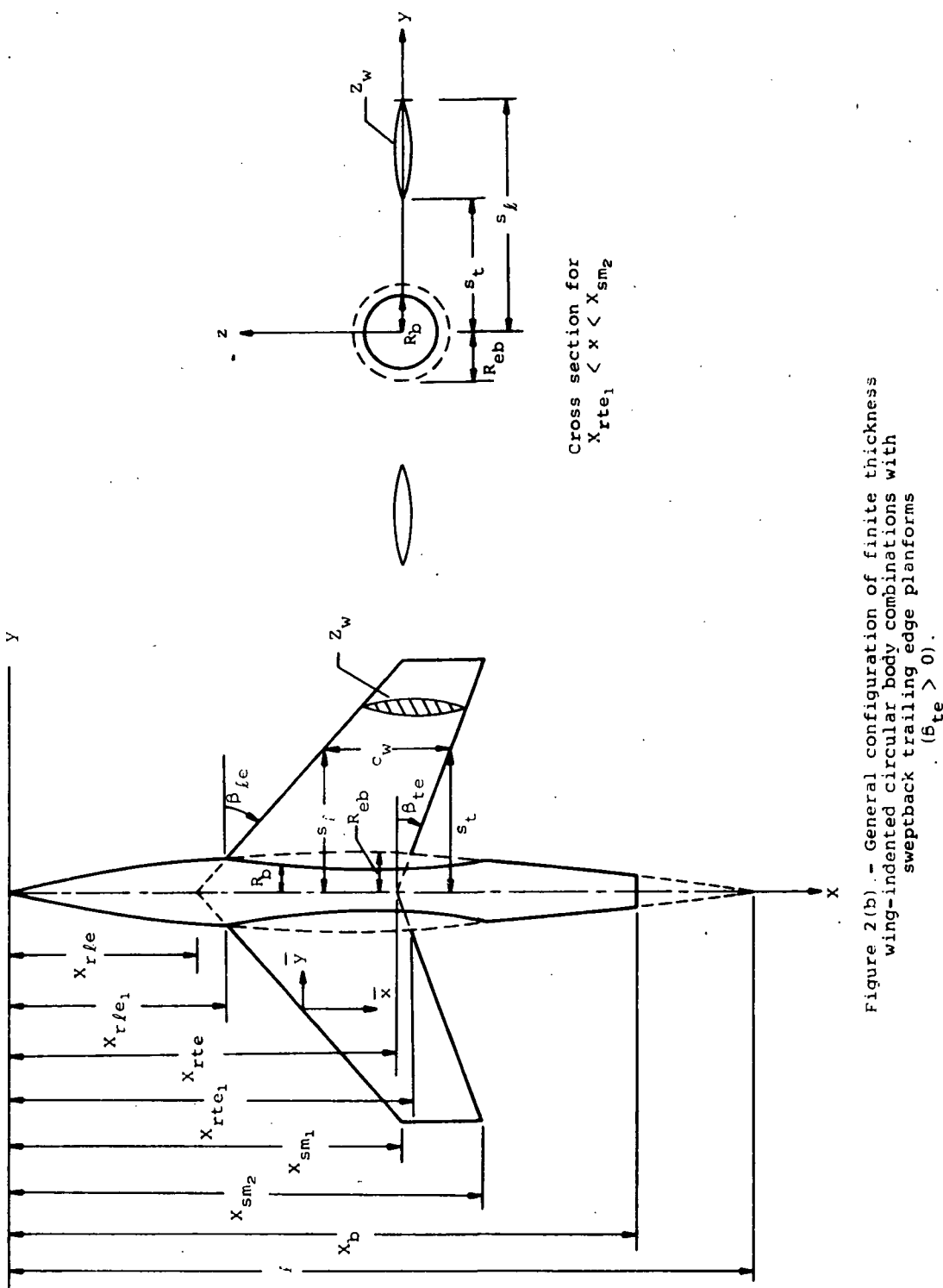


Figure 2(b) - General configuration of finite thickness wing-indented circular body combinations with sweptback trailing edge planforms. ($\beta_{te} > 0$).

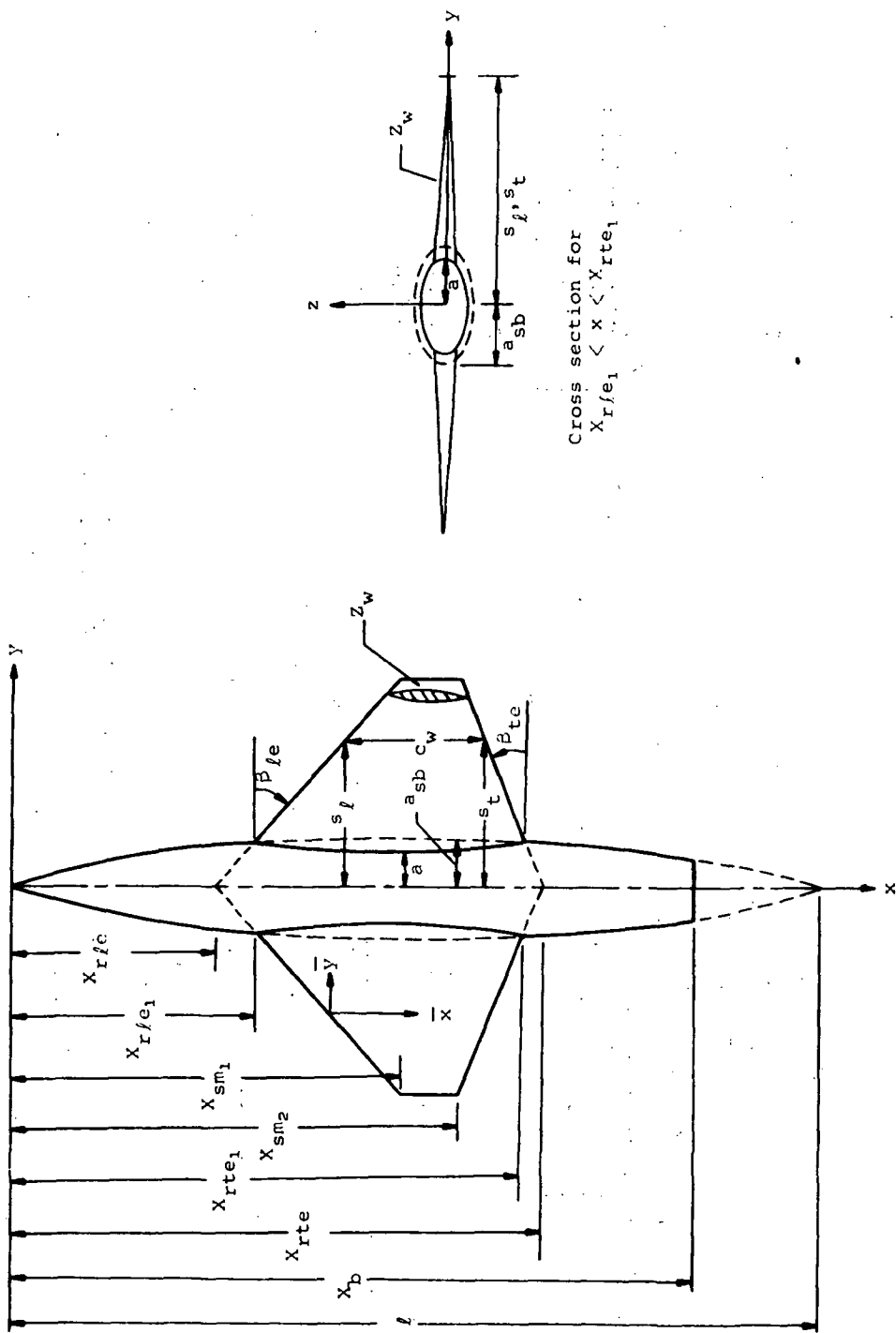


Figure 3(a). - General configuration of finite thickness wing-indented elliptic body combinations with straight/sweptforward trailing edge planforms ($\beta_{te} \leq 0$).

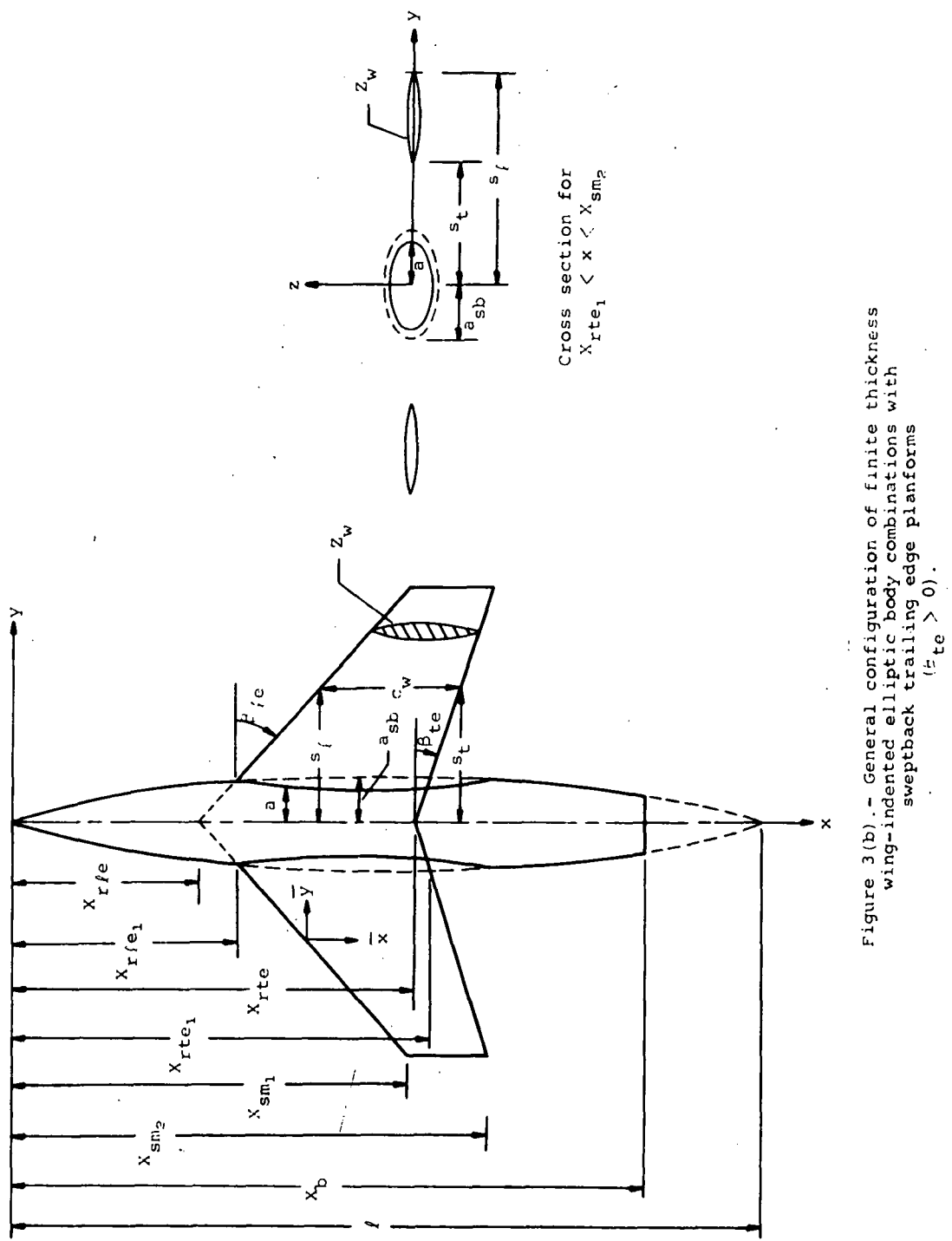


Figure 3(b).—General configuration of finite thickness wing-indented elliptic body combinations with sweptback trailing edge planforms ($r_{te} > 0$).

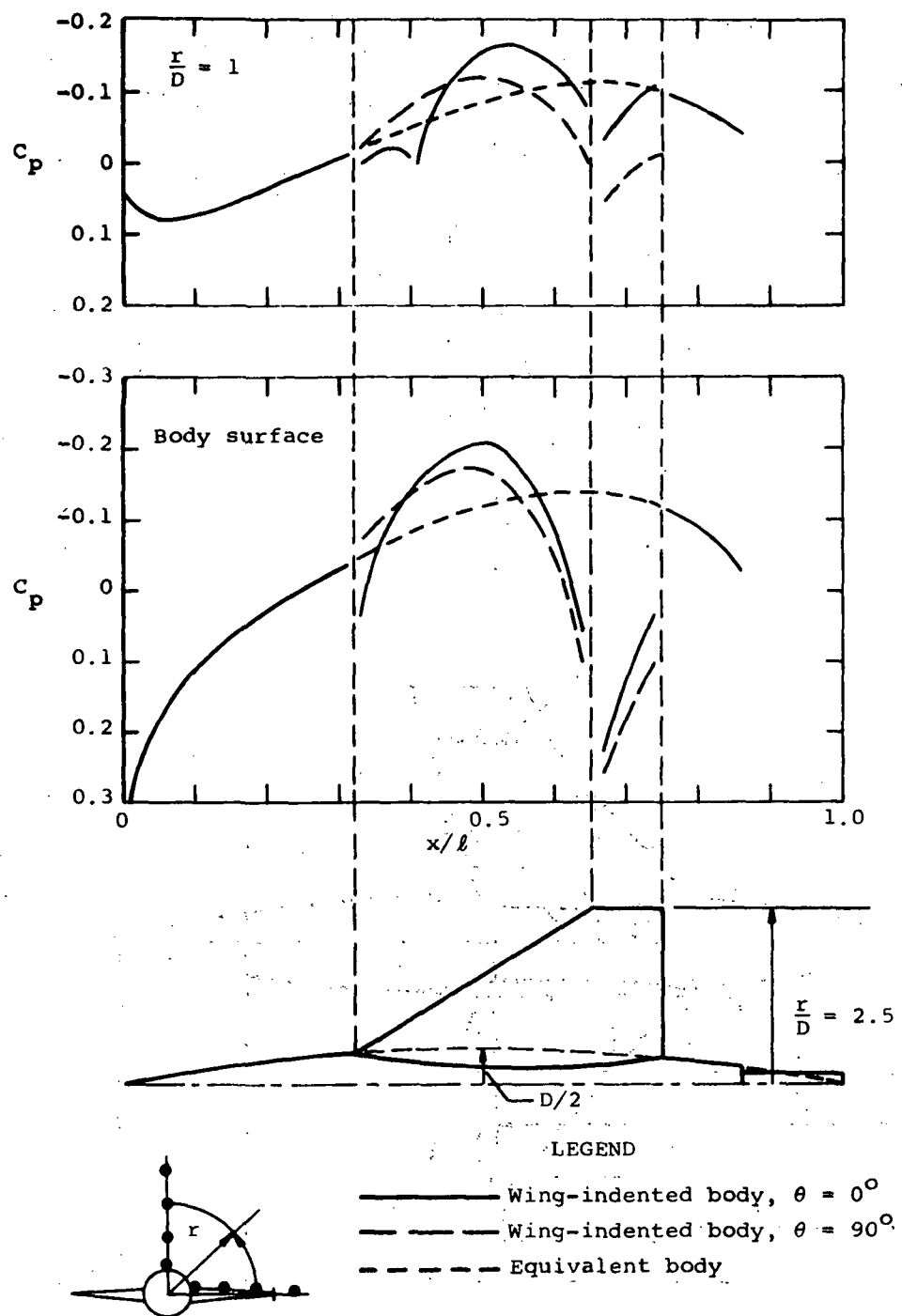


Figure 4.- Theoretical surface and flow field pressure distributions at $M_\infty = 1$ for a nonlifting parabolic-arc profile wing-indented parabolic-arc body combination; equivalent body thickness ratio $D/\ell = 0.1$, wing aspect ratio $AR = 1.7$, thickness/chord ratio $t/c_w = 0.04$, planform taper ratio $TR = 0.2$, and with $x_{rlc}/\ell = 0.25$, $C_{R_T} = 0.50$, $x_b/\ell = 0.86$.

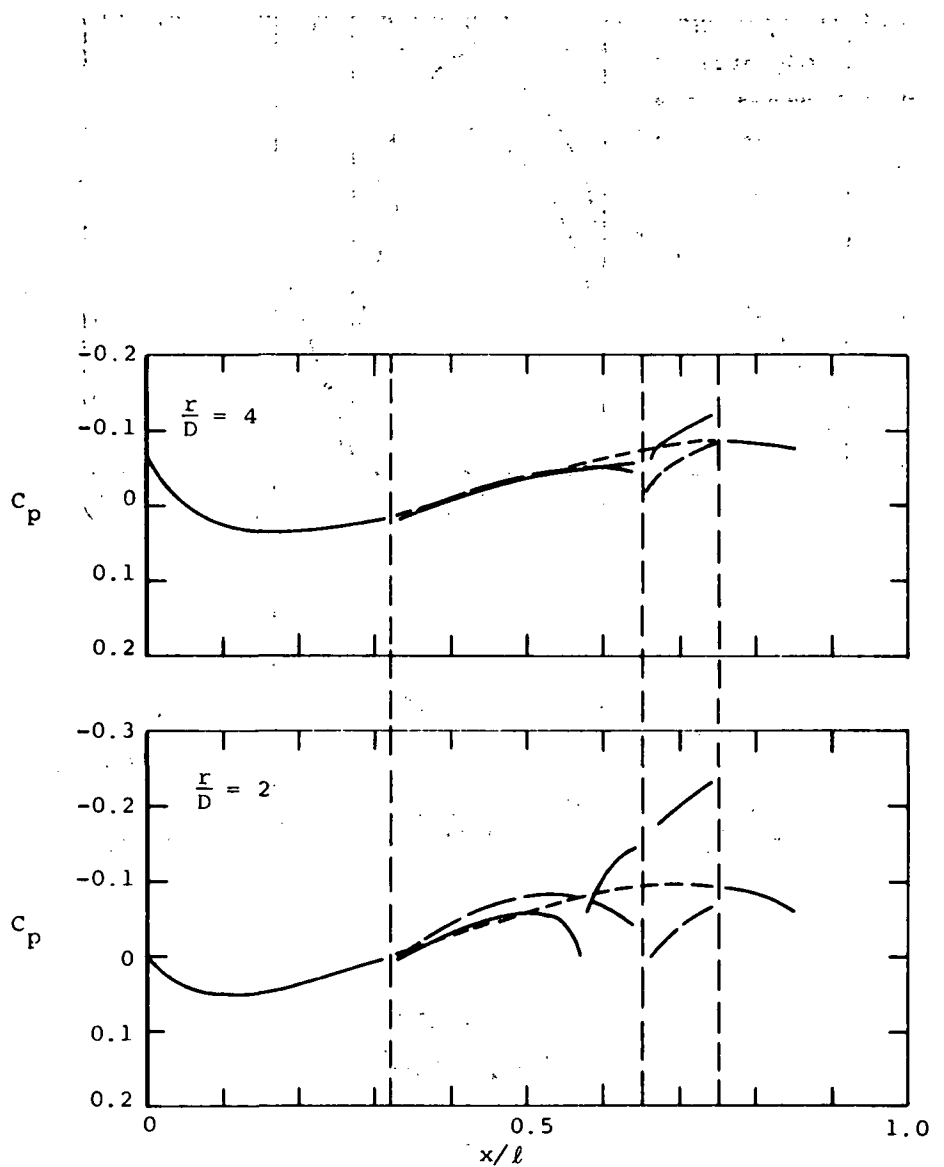


Figure 4.- Concluded

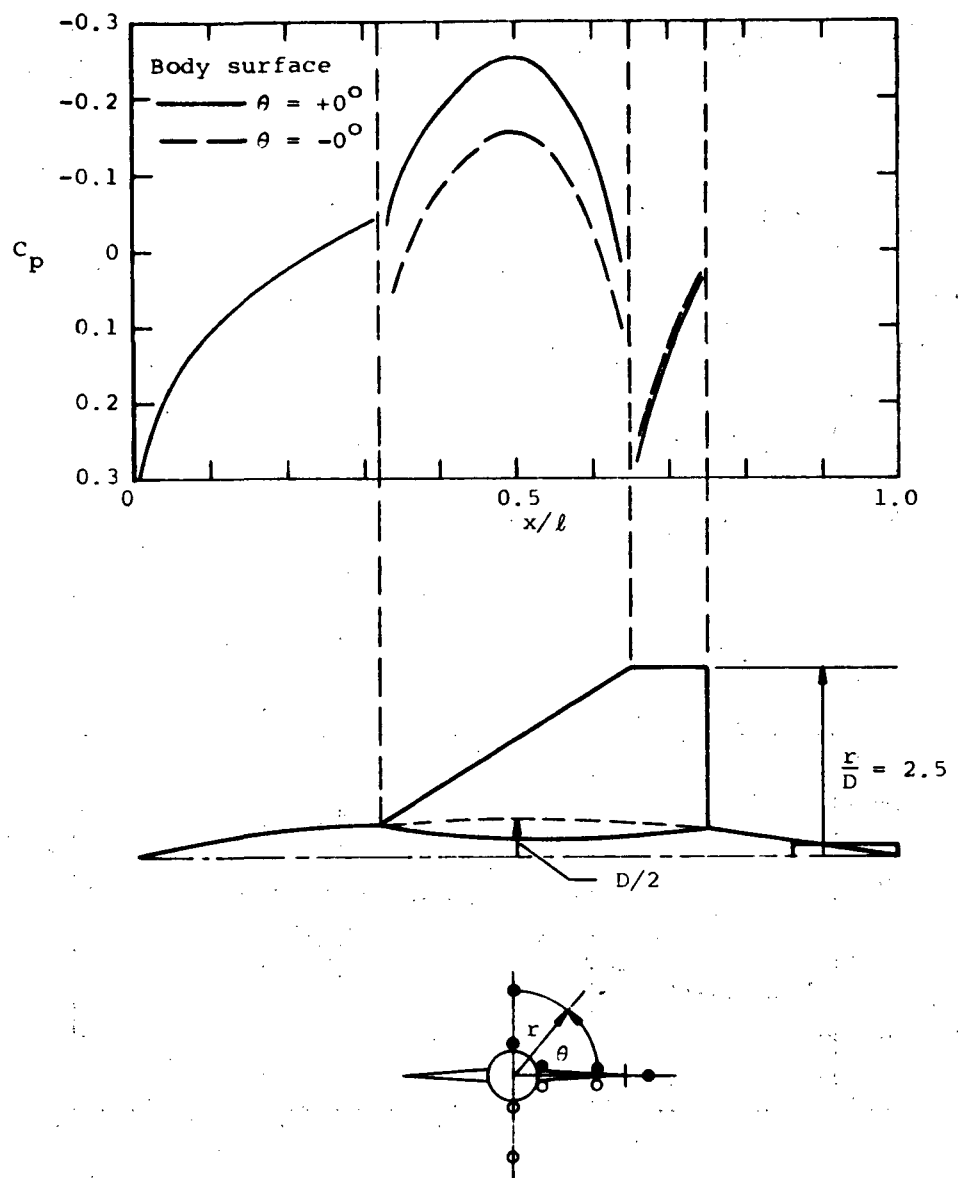


Figure 5.- Theoretical surface and flow field pressure distributions and loadings at $M_{\infty} = 1$ and $\alpha = 2^\circ$ for a parabolic-arc profile wing--indented parabolic-arc body combination; equivalent body thickness ratio $D/l = 0.1$, wing aspect ratio $AR = 1.7$, thickness/chord ratio $t/c_w = 0.04$, planform taper ratio $TR = 0.2$, and with $x_{rel}/l = 0.25$, $C_{R_{T/l}} = 0.5$, $x_b/l = 0.86$.

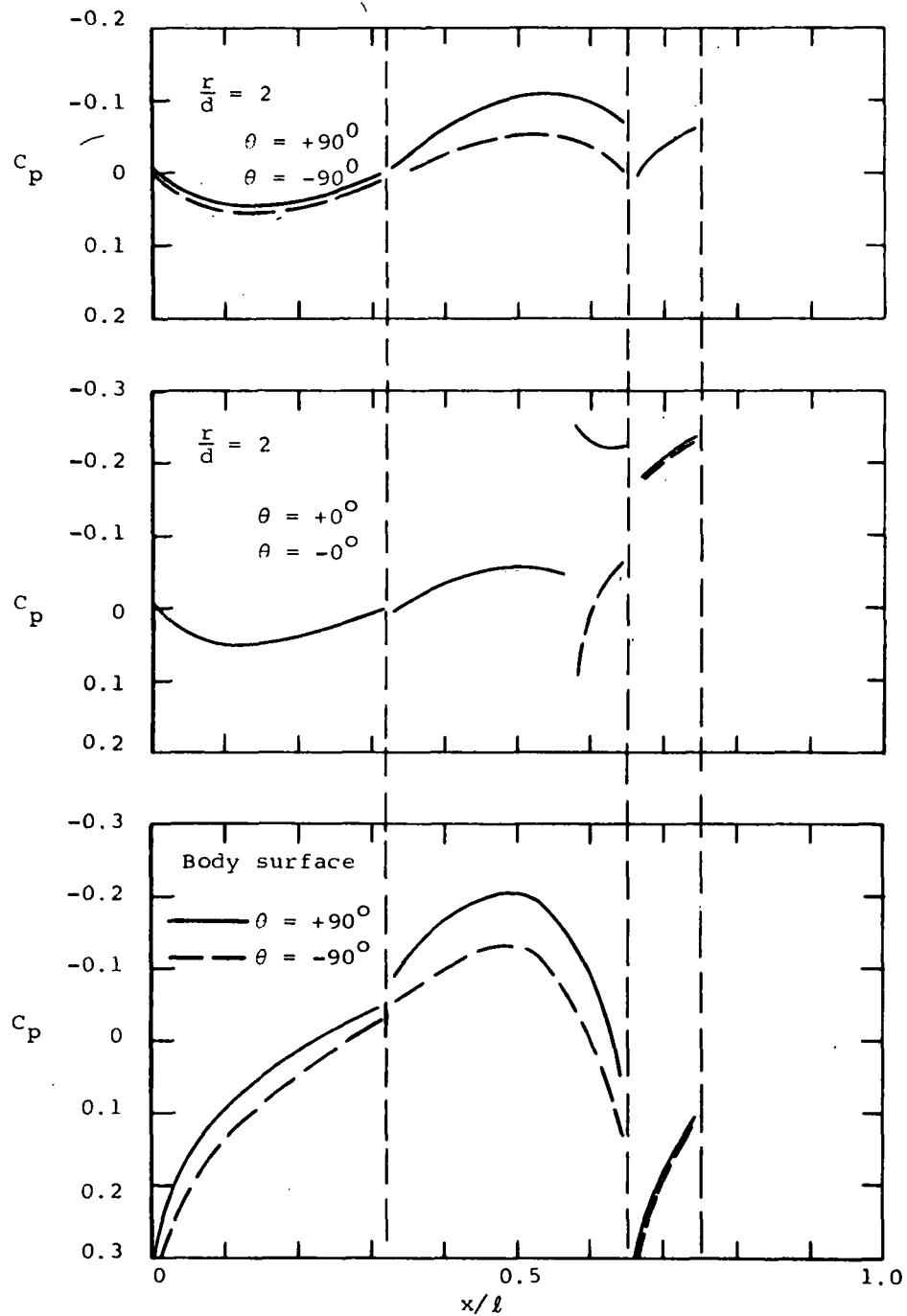


Figure 5.- Continued.

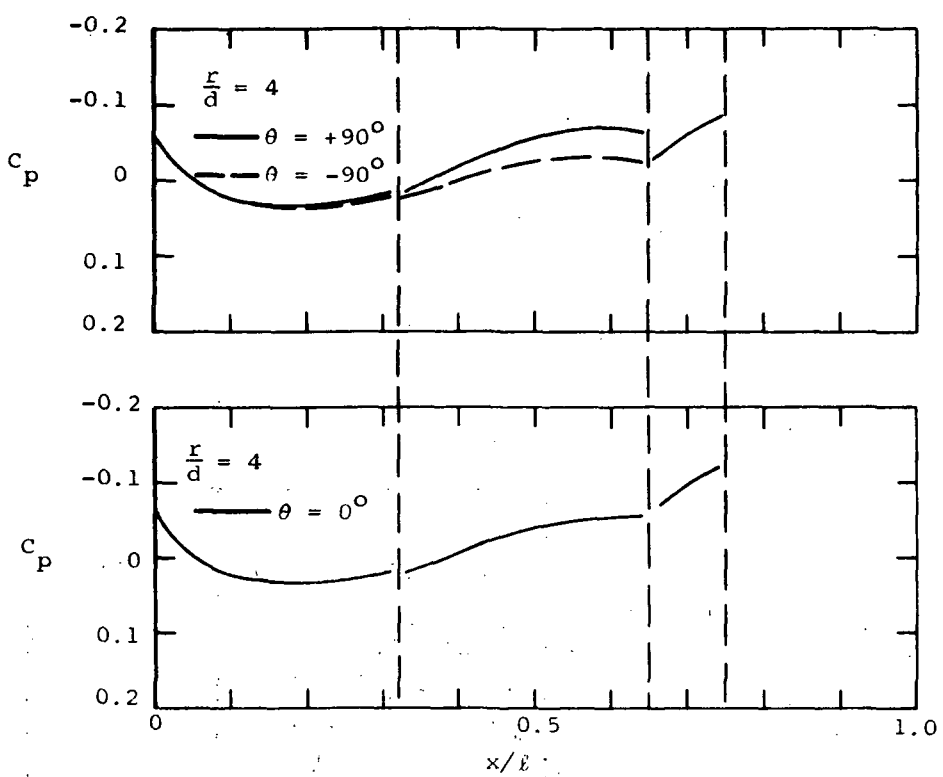


Figure 5.- Concluded.

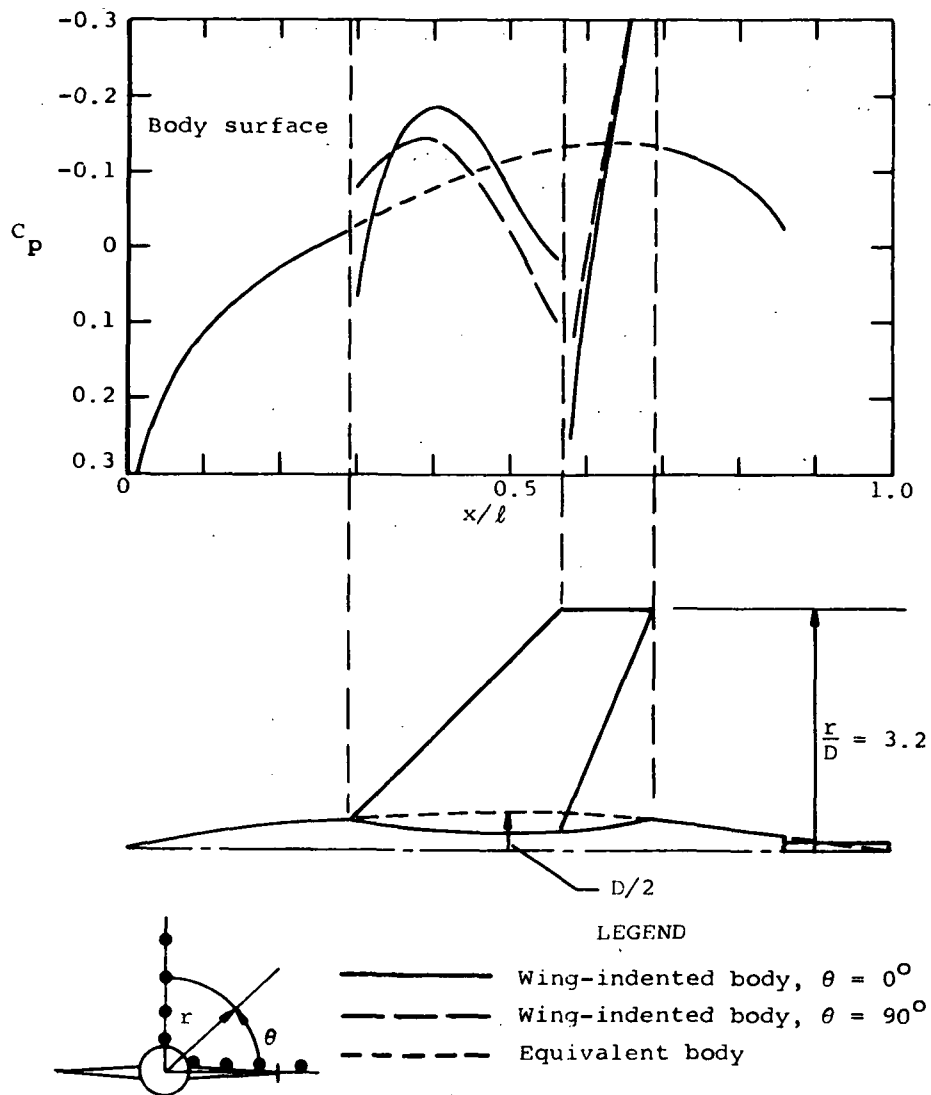


Figure 6.- Theoretical surface and flow field pressure distributions at $M_\infty = 1$ for a nonlifting parabolic-arc profile wing-indented parabolic-arc body combination; equivalent body thickness ratio $D/\ell = 0.1$, wing aspect ratio $AR = 2.8$, thickness ratio $t/c_w = 0.04$, planform taper ratio $TR = 0.4$, and with $x_{ref/\ell} = 0.25$, $C_{T_R} = 0.3$, $x_b/\ell = 0.86$.

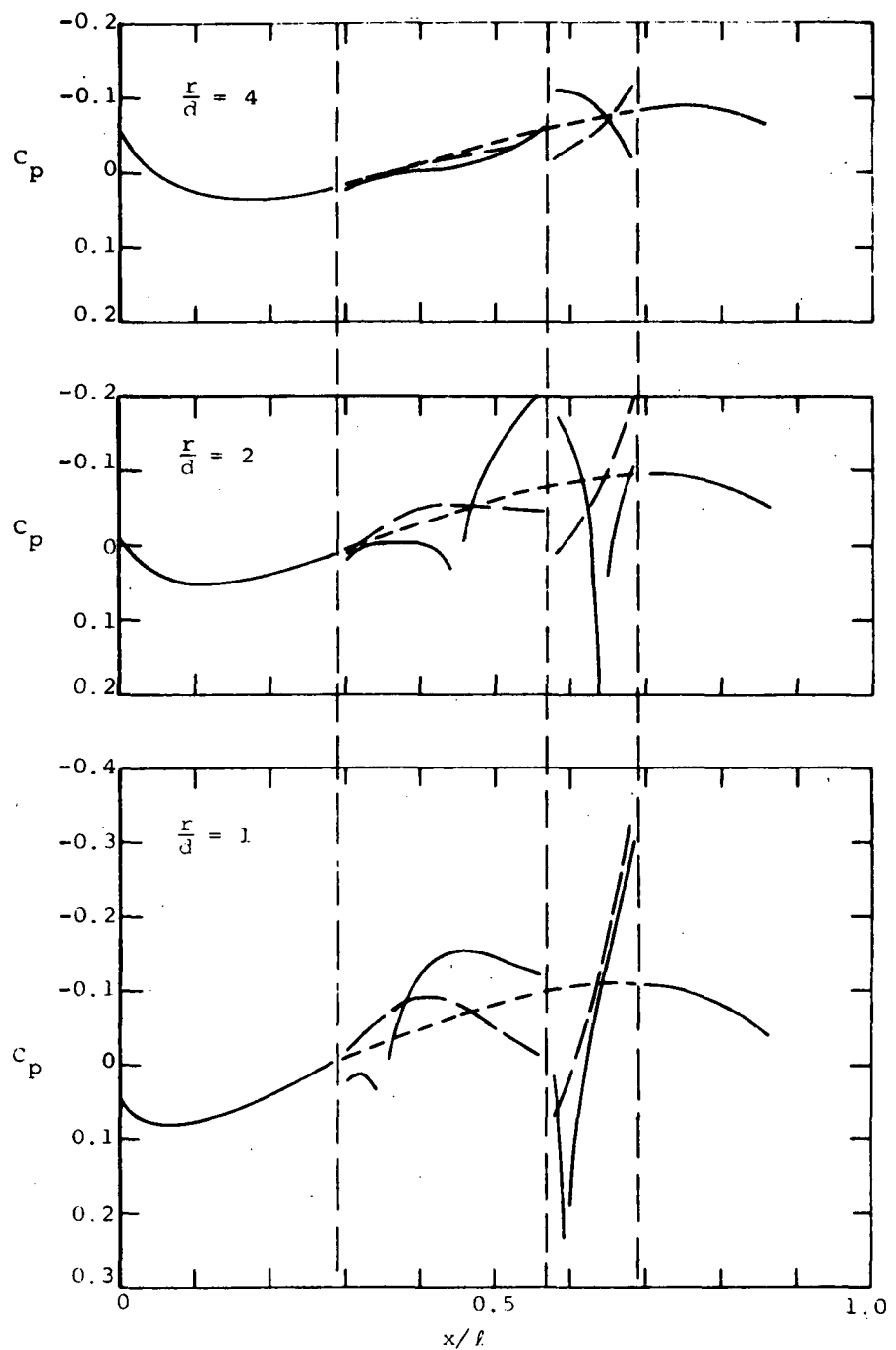


Figure 6.- Concluded.

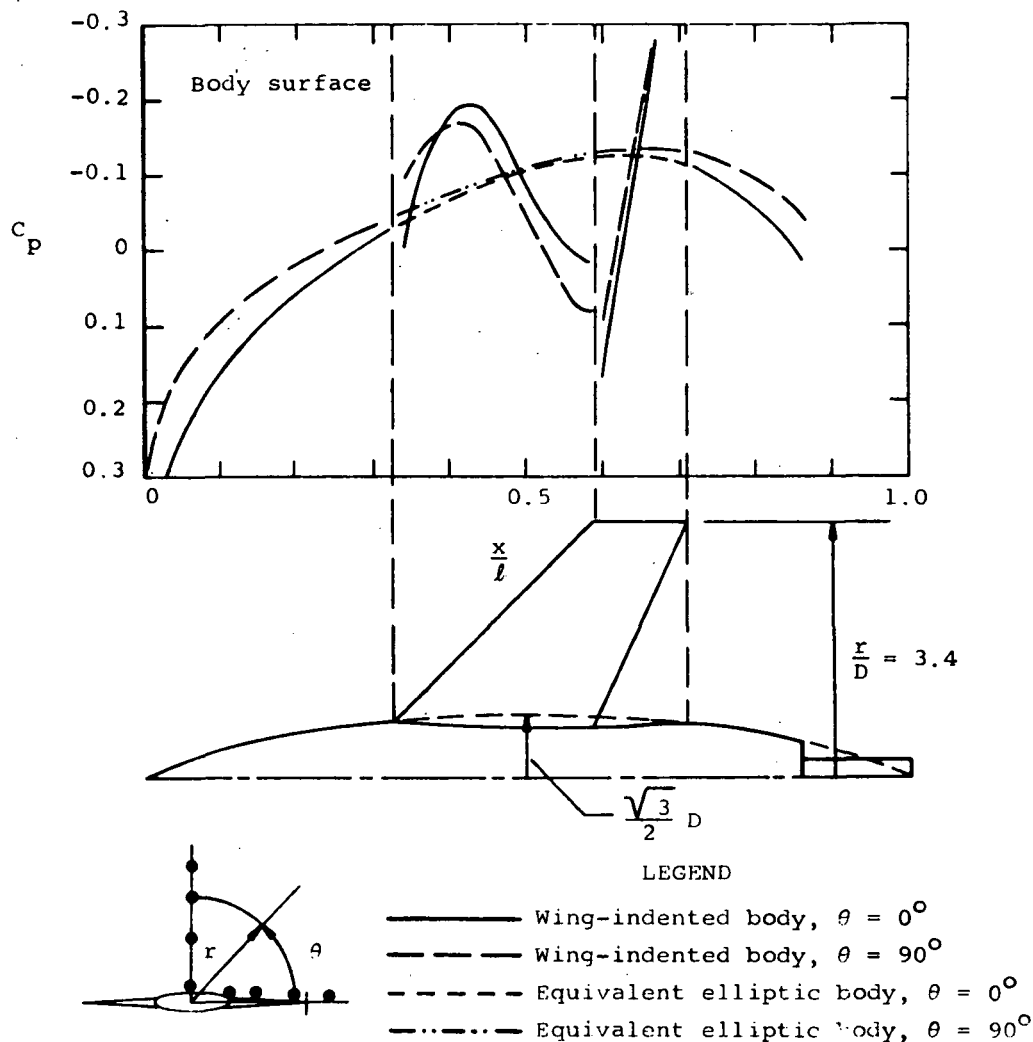


Figure 7.- Theoretical surface and flow field pressure distributions at $M_\infty = 1$ for a nonlifting parabolic-arc profile wing--indented parabolic-arc body combination; having a body of elliptical cross section with $\lambda = 3$; equivalent body thickness ratio $D/\ell = 0.1$, wing aspect ratio $AR = 2.8$, thickness ratio $t/c_w = 0.04$, planform taper ratio $TR = 0.4$, and with $x_{rlc}/\ell = 0.25$, $C_{R_{T/\ell}} = 0.3$, $x_b/\ell = 0.86$.

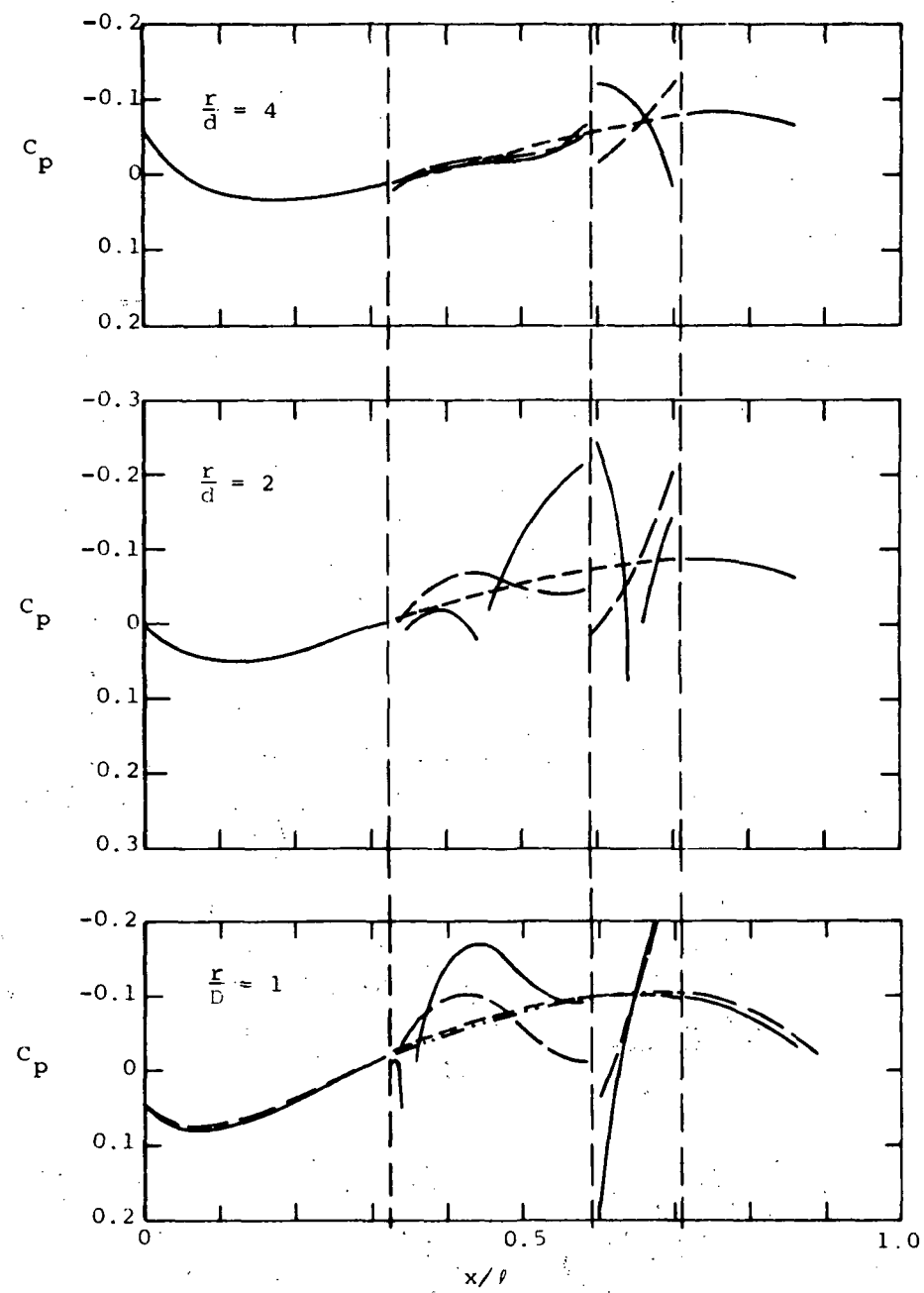


Figure 7.- Concluded.

*TRANIN AMACH=1., MOPT=1, TAUB=.1, TAUM=.04, XMTB=.5, XMTW=.5, ANGLE=58.,
 SSMAX=.25, XRLE=.25, TR=.2, CRT=.5, XLOBASE=.86, XLOUTP=.05, 6END

(a) Input.

CALCULATION OF SURFACE AND FLOW FIELD PRESSURE DISTRIBUTIONS
 FOR FLOW AT FREE STREAM MACH NUMBERS AT OR NEAR ONE, BELOW
 THE LOWER CRITICAL, OR ABOVE THE UPPER CRITICAL ASPECT A FINITE
 THICKNESS WING-INDENTED CIRCULAR BODY COMBINATION WITH THE
 EQUIVALENT BODY OF REVOLUTION EITHER USER-SPECIFIED OR HAVING
 ORDINATES R PROPORTIONAL TO $X/L - (X/L)^{1/n}$ OR $1-X/L - (1-X/L)^{1/n}$,
 THE WING HAVING A CONSTANT THICKNESS/CHORD RATIO, TAPER RATIO
 BETWEEN 0 AND 1, AND WITH ORDINATES Z PROPORTIONAL TO $XBAR/C$
 $-(XBAR/C)^{1/m}$ OR $1-XBAR/C - (1-XBAR/C)^{1/m}$ BY USING THE TRANSONIC
 EQUIVALENCE RULE AND THE LOCAL LINEARIZATION METHOD

WING-BODY COMBINATION GEOMETRY AND FLOW FIELD CHARACTERISTICS

EQUIVALENT BODY THICKNESS RATIO = 0.1000E 00
 EQUIVALENT BODY MAXIMUM THICKNESS AT X/L = 0.5000E 00
 EXPONENT N FOR EQUIVALENT BODY ORDINATES = 0.2000E 01
 SEB** (X) = 0 AT X/L = C.21132E 00
 WING MAX. THICKNESS AT XBAR/C = C.5000E 00
 WING THICKNESS/CHORD RATIO = C.4000E-01
 EXPONENT M FOR WING UORDINATES = C.2000E 01
 LEADING EDGE OF WING ROOT CHORD AT X/L = C.2500E 00
 TRAILING EDGE OF WING ROOT CHORD AT X/L = C.7500E 00
 PLANFORM TAPER RATIO = C.2000E 00
 LEADING EDGE PIERCES BODY AT X/L = C.3196E 00
 TRAILING EDGE PIERCES BODY AT X/L = C.7500E 00
 BODY BASE AT X/L = C.8600E 00
 LEADING EDGE SWEET ANGLE (DEG) = C.5800E 02
 TRAILING EDGE SWEET ANGLE (DEG) = C.00000
 LOCATION OF WINGTIP LEADING EDGE AT X/L = C.6500E 00
 LOCATION OF WINGTIP TRAILING EDGE AT X/L = C.7500E 00
 NORMALIZED MAX. SEMISPAN SSMAX/L = C.2500E 00
 ANGLE OF ATTACK ALPHAO (DEG) = C.00000
 RATIO OF SPECIFIC HEATS = C.1400E 01
 FREE STREAM MACH NUMBER = C.1000E 01

START OF INTEGRATION FROM SEB** (X) = 0 TO NCSE

X/L	RBODY/L	THETA(DEG)	CP(BODY)	CP(R/D= 1.00)CP(R/D= 2.00)CP(R/D= 3.00)CP(R/D= 4.00)CP(R/D= 5.00)CP(R/D= 6.00)						
0.2113	0.0333	0.0000	2.1307E-02	3.3159E-02	3.4270E-02	3.4476E-02	3.4548E-02	3.4582E-02	3.4600E-02	
0.2113	0.0333	9.0000E 01	2.1307E-02	3.3159E-02	3.4270E-02	3.4476E-02	3.4548E-02	3.4582E-02	3.4600E-02	
0.2003	C.0320	0.0000	2.8813E-02	3.8171E-02	3.7124E-02	3.6069E-02	3.5247E-02	3.4587E-02	3.4039E-02	
0.2003	C.0320	9.0000E 01	2.8813E-02	3.8171E-02	3.7124E-02	3.6069E-02	3.5247E-02	3.4587E-02	3.4039E-02	
0.1503	0.0255	0.0000	6.6692E-02	5.9471E-02	4.7472E-02	4.0071E-02	3.4755E-02	3.0613E-02	2.7221E-02	
0.1503	0.0255	9.0000E 01	6.6692E-02	5.9471E-02	4.7472E-02	4.0071E-02	3.4755E-02	3.0613E-02	2.7221E-02	
0.1003	0.0181	0.0000	1.1374E-01	7.5672E-02	5.0874E-02	3.6118E-02	2.56C7E-02	1.7441E-02	1.0765E-02	
0.1003	0.0181	9.0000E 01	1.1374E-01	7.5672E-02	5.0874E-02	3.6118E-02	2.56C7E-02	1.7441E-02	1.0765E-02	
0.0503	0.0056	0.0000	1.8138E-01	7.9464E-02	4.0133E-02	1.7036E-02	6.3612E-04	-1.2090E-02	-2.2490E-02	
0.0503	0.0056	9.0000E 01	1.8138E-01	7.9464E-02	4.0133E-02	1.7036E-02	6.3612E-04	-1.2090E-02	-2.2490E-02	
0.0043	0.0049	0.0000	3.7747E-01	4.61C7E-02	-7.9117E-03	-3.9512E-02	-6.1932E-02	-7.9323E-02	-9.3533E-02	
0.0043	0.0049	9.0000E 01	3.7747E-01	4.61C7E-02	-7.9117E-03	-3.9512E-02	-6.1932E-02	-7.9323E-02	-9.3533E-02	

START OF INTEGRATION FROM SEB** (X) = 0 TO TAIL

X/L	RBODY/L	THETA(DEG)	CP(BODY)	CP(R/D= 1.00)CP(R/D= 2.00)CP(R/D= 3.00)CP(R/D= 4.00)CP(R/D= 5.00)CP(R/D= 6.00)						
0.2113	0.0333	0.0000	2.1307E-02	3.3159E-02	3.4270E-02	3.4476E-02	3.4548E-02	3.4582E-02	3.4600E-02	
0.2113	0.0333	9.0000E 01	2.1307E-02	3.3159E-02	3.4270E-02	3.4476E-02	3.4548E-02	3.4582E-02	3.4600E-02	
0.2503	C.0375	0.0000	-3.4545E-03	1.4950E-02	2.3030E-02	2.7311E-02	3.0278E-02	3.2559E-02	3.4413E-02	
0.2503	C.0375	9.0000E 01	-3.4545E-03	1.4950E-02	2.3030E-02	2.7311E-02	3.0278E-02	3.2559E-02	3.4413E-02	
0.3003	J.0420	0.0000	-3.1658E-02	-8.32C7E-03	6.9848E-03	1.5600E-02	2.1656E-02	2.6337E-02	3.0154E-02	
0.3003	J.0420	9.0000E 01	-3.1658E-02	-8.32C7E-03	6.9848E-03	1.5600E-02	2.1656E-02	2.6337E-02	3.0154E-02	
0.3503	J.0453	0.0000	-4.2756E-02	-1.1470E-02	-4.4772E-03	5.0147E-03	1.2459E-02	1.8439E-02	2.3466E-02	
0.3503	J.0453	9.0000E 01	-4.2756E-02	-4.9736E-02	-1.1314E-02	1.9768E-03	1.0749E-02	1.7344E-02	2.2646E-02	

Figure 8.- Sample input/output for a wing-body combination having a circular body and with $TB \neq 0$, $\beta_{te} \leq 0$, $a = 0$.

0.4003	0.0463	0.0000	-1.3545E-01	-9.0759E-03	-2.9387E-02	-1.6439E-02	-5.84C1E-03	2.7547E-03	9.9210E-03
0.4003	0.0463	9.0000E 01	-1.3421E-01	-7.9245E-02	-4.0477E-02	-2.1309E-02	-8.5757E-C3	1.0043E-03	8.7054E-03
0.4503	0.0452	0.0000	-1.8585E-01	-1.0661E-01	-4.7339E-02	-3.4247E-02	-2.2217E-02	-1.2275E-02	-3.9321E-C3
0.4503	0.0452	9.0000E 01	-1.6115E-01	-1.0676E-01	-6.3579E-02	-4.1061E-02	-2.0016E-02	-1.4701E-02	-5.6153E-03
0.5003	0.0421	0.0000	-2.0276E-01	-1.5242E-01	-5.6059E-C2	-4.7548E-02	-3.5858E-02	-2.59C2E-02	-1.7476E-02
0.5003	0.0421	9.0000E 01	-1.6633E-01	-1.1840E-01	-7.8063E-02	-5.5503E-02	-4.0206E-02	-2.8662E-02	-1.9387E-02

START OF SUPERSONIC CALCULATION

SUPERSONIC CALCULATION STARTS AT X/L = 0.54232E 00

X/L	RBODY/L	THETA(DEG)	CPIBCDY)	CP(R/D= 1.00)CP(R/D= 2.00)CP(R/D= 3.00)CP(R/D= 4.00)CP(R/D= 5.00)CP(R/D= 6.00)					
0.5503	0.0374	0.0000	-1.7406E-01	-1.6090E-01	-4.4047E-02	-5.5216E-02	-4.5729E-02	-3.7216E-02	-2.9953E-02
0.5503	0.0374	9.0000E 01	-1.3590E-01	-1.0833E-01	-8.0084E-02	-6.1958E-02	-4.9152E-02	-3.9346E-02	-3.1418E-02
0.6003	0.0319	0.0000	-7.6846E-02	-1.1388E-01	-1.0586E-01	-5.6845E-02	-5.0777E-C2	-4.4920E-02	-3.9556E-C2
0.6003	0.0319	9.0000E 01	-4.4981E-02	-6.8740E-02	-6.4622E-02	-5.6721E-02	-4.9885E-02	-4.4233E-02	-3.9450E-02
0.7003	0.0300	0.0000	1.3714E-01	-6.9617E-02	-2.0376E-01	-1.3049E-01	-9.9491E-02	-8.6103E-02	-7.8081E-02
0.7003	0.0300	9.0000E 01	1.8803E-01	2.0855E-02	-3.4187E-02	-5.4919E-02	-6.0142E-02	-6.1365E-02	-6.1009E-02
0.8003	0.0320	0.0000	-8.8124E-02	-7.8922E-02	-8.0057E-02	-8.1227E-02	-8.21C2E-02	-8.2804E-02	-8.3386E-02
0.8003	0.0320	9.0000E 01	-8.8124E-02	-7.8922E-02	-8.0057E-02	-8.1227E-02	-8.21C2E-02	-8.2904E-02	-8.3386E-02
0.8503	0.0255	0.0000	-3.9535E-C2	-4.7040E-02	-5.9191E-02	-6.6680E-02	-7.2057E-C2	-7.6247E-02	-7.9679E-02
0.8503	0.0255	9.0000E 01	-3.9535E-02	-4.7040E-02	-5.9191E-02	-6.6680E-02	-7.2057E-02	-7.6247E-02	-7.9679E-02

DRAG COEFFICIENT = 0.10440E 00

(b) Output.

Figure 8.- Concluded.

STRANIN AMACH=1., MOPT=1, TAUB=.1, TAUW=.04, XMTB=.5, XMTW=.5, ANGLE=58.,
 SSMAX=.25, XRLE=.25, TR=.2, CRT=.5, XLBASE=.86, XLOUTP=.05, ALPHA=2., &END

(a) Input.

CALCULATION OF SURFACE AND FLOW FIELD PRESSURE DISTRIBUTIONS
 FOR FLOW AT FREE STREAM MACH NUMBERS AT OR NEAR CRITICAL, BELOW
 THE LOWER CRITICAL, OR ABOVE THE UPPER CRITICAL ALONG A FINITE
 THICKNESS WING-INDENTED CIRCULAR BODY COMBINATION WITH THE
 EQUIVALENT BODY OF REVOLUTION EITHER USER-SPECIFIED OR HAVING
 ORDINATES X PROPORTIONAL TO $X/L - (X/L)^{M+1}$ OR $1 - X/L - (1 - X/L)^{M+1}$,
 THE WING HAVING A CONSTANT THICKNESS/CHORD RATIO, TAPER RATIO
 $(XBAR/C)^{P+1}$ OR $1 - XBAR/C - (1 - XBAR/C)^{P+1}$ BY USING THE TRANSONIC
 EQUIVALENCE RULE AND THE LOCAL LINEARIZATION METHOD

WING-BODY COMBINATION GEOMETRY AND FLOW FIELD CHARACTERISTICS

EQUIVALENT BODY THICKNESS RATIO = C.1000E 00
 EQUIVALENT BODY MAXIMUM THICKNESS AT X/L = 0.5000E 00
 EXPONENT K FOR EQUIVALENT BODY ORDINATES = C.2000E 01
 SEB** (X) = 0 AT X/L = C.21132E 00
 WING MAX. THICKNESS AT XBAR/C = C.5000E 00
 WING THICKNESS/CHORD RATIO = C.4000E-01
 EXPONENT M FOR WING ordinates = C.2000E 01
 LEADING EDGE OF WING ROOT CHORD AT X/L = C.2500E 00
 TRAILING EDGE OF WING ROOT CHORD AT X/L = C.7500E 00
 PLANEFORM TAPER RATIO = C.2000E 00
 LEADING EDGE PIERCES BODY AT X/L = C.31960E 00
 TRAILING EDGE PIERCES BODY AT X/L = C.7500E 00
 BODY BASE AT X/L = C.8600E 00
 LEADING EDGE SWEEP ANGLE (DEG) = C.5800E 02
 TRAILING EDGE SWEEP ANGLE (DEG) = C.0000
 LOCATION OF WINGTIP LEADING EDGE AT X/L = C.6500E 00
 LOCATION OF WINGTIP TRAILING EDGE AT X/L = C.7500E 00
 NORMALIZED MAX. SEMISPAN SSMAX/L = C.2500E 00
 ANGLE OF ATTACK ALPHA (DEG) = C.2000E 01
 RATIO OF SPECIFIC HEATS = C.1400E 01
 FREE STREAM MACH NUMBER = C.1000E 01

START OF INTEGRATION FROM SEB** (X) = C TO NOSE

X/L	RBODY/L	THETA(DEG)	CP(BCEY)	CP(R/D= 1.00)CP(R/D= 2.00)CP(R/D= 3.00)CP(R/D= 4.00)CP(R/D= 5.00)CP(R/D= 6.00)						
0.2113	0.0333	0.0000	1.7652E-02	3.2874E-02	3.4202E-02	3.4446E-02	3.4531E-02	3.4571E-02	3.4592E-02	
0.2113	0.0333	9.0000E 01	6.4031E-03	2.5652E-02	3.0344E-02	3.1830E-02	3.2554E-02	3.2982E-02	3.3265E-02	
0.2113	-9.0000E 01	3.7645E-02	4.1178E-02	3.8331E-02	3.7182E-02	3.6576E-02	3.6202E-02	3.5949E-02		
0.2003	0.0320	0.0000	2.5157E-02	3.7938E-02	3.7060E-02	3.0041E-02	3.5231E-02	3.4577E-02	3.4032E-02	
0.2003	0.0320	9.0000E 01	1.3279E-02	3.0690E-02	3.3198E-02	3.2826E-02	3.3256E-02	3.2991E-02	3.2706E-02	
0.2003	-9.0000E 01	4.6768E-02	4.6177E-02	4.1173E-02	3.8768E-02	3.7269E-02	3.6204E-02	3.5385E-02		
0.1503	0.0255	0.0000	6.3037E-02	5.9307E-02	4.7432E-02	4.0053E-02	3.4745E-02	3.0607E-02	2.7216E-02	
0.1503	0.0255	9.0000E 01	4.8381E-02	4.3034E-02	4.3790E-02	3.7600E-02	3.2897E-02	2.9124E-02	2.5979E-02	
0.1503	-9.0000E 01	8.7441E-02	6.6545E-02	5.1233E-02	4.2577E-02	3.6634E-02	3.2115E-02	2.8472E-02		
0.1003	0.0181	0.0000	1.1008E-01	7.5591E-02	5.0554E-02	3.6105E-02	2.5623E-02	1.7438E-02	1.0762E-02	
0.1003	0.0181	9.0000E 01	9.2611E-02	6.9771E-02	4.7879E-02	3.4114E-02	2.4122E-02	1.6236E-02	9.7557E-03	
0.1003	-9.0000E 01	1.3728E-01	8.1728E-02	5.3476E-02	3.9139E-02	2.7122E-02	1.8653E-02	1.1774E-02		
0.0503	0.0095	0.0000	1.7773E-01	7.9442E-02	4.0126E-02	1.7035E-02	6.3473E-04	-1.2091E-02	-2.2491E-02	
0.0503	0.0095	9.0000E 01	1.5746E-01	7.5897E-02	3.8340E-02	1.5846E-02	-2.6243E-04	-1.2809E-02	-2.3090E-02	
0.0503	-9.0000E 01	2.0771E-01	8.3076E-02	4.1938E-02	1.4240E-02	1.5375E-03	-1.1369E-02	-2.1850E-02		
0.0043	0.0009	0.0000	3.7394E-01	4.6177E-02	-7.1117E-03	-3.4512E-02	-6.1932E-02	-7.4932E-02	-9.3533E-02	
0.0043	0.0009	9.0000E 01	3.5100E-01	4.5750E-02	-8.0920E-03	-3.6316E-02	-6.2022E-02	-7.9395E-02	-9.3552E-02	
0.0043	-9.0000E 01	4.8637E-01	4.6465E-02	-7.7331E-03	-3.4939E-02	-6.1843E-02	-7.9252E-02	-9.3473E-02		

START OF INTEGRATION FROM SEB** (X) = C TO TAIL

X/L	RBODY/L	THETA(DEG)	CP(BCEY)	CP(R/D= 1.00)CP(R/D= 2.00)CP(R/D= 3.00)CP(R/D= 4.00)CP(R/D= 5.00)CP(R/D= 6.00)						
0.2113	0.0333	0.0000	1.7652E-02	3.2874E-02	3.4202E-02	3.4446E-02	3.4531E-02	3.4571E-02	3.4592E-02	
0.2113	0.0333	9.0000E 01	4.4031E-03	2.5652E-02	3.0344E-02	3.1830E-02	3.2554E-02	3.2982E-02	3.3265E-02	
0.2113	-9.0000E 01	3.7645E-02	4.1178E-02	3.8331E-02	3.7182E-02	3.6576E-02	3.6202E-02	3.5949E-02		
0.2503	0.0375	0.0000	-1.1049E-03	1.4623E-02	-2.2742E-02	2.4727E-02	3.0257E-02	3.2545E-02	3.4404E-02	
0.2503	0.0375	9.0000E 01	-1.6141E-02	7.9276E-03	1.4435E-02	2.4746E-02	2.8343E-02	3.1005E-02	3.3116E-02	
0.2503	-9.0000E 01	1.1708E-02	2.2771E-02	2.6953E-02	2.9952E-02	3.2257E-02	3.4140E-02	3.5730E-02		

Figure 9.- Sample input/output for a wing-body combination having a circular body and with $TR \neq 0$, $\beta_{le} \leq 0$, $\alpha \neq 0$.

0.3003	0.0420	0.0000	-3.5314E-02	-8.7891E-03	6.8748E-03	1.9552E-02	2.1629E-02	2.6320E-02	3.0142E-02
0.3003	0.0420	9.0000E 01	-4.1592E-02	-1.5454E-02	3.6267E-03	1.3319E-02	1.9932E-02	2.4951E-02	2.8997E-02
0.3003	0.0420	-9.0000E 01	-1.5288E-02	-1.3121E-03	1.0553E-02	1.7975E-02	2.3434E-02	2.7757E-02	3.1336E-02
0.3503	0.0453	0.01UPPER1	-1.0355E-01	-1.2315E-02	-4.0357E-03	4.4651E-03	1.2420E-02	1.6414E-02	2.3389E-02
0.3503	0.0453	0.01LOWER1	2.0472E-02	-1.2315E-02	-4.0357E-03	4.4945E-03	1.2420E-02	1.6414E-02	2.3389E-02
0.3503	0.0453	9.0000E 01	-1.1550E-01	-5.8221E-02	-2.2168E-02	-5.5204E-03	5.0506E-03	1.2755E-02	1.8608E-02
0.3503	0.0453	-9.0000E 01	-1.5025E-02	-2.0265E-02	-1.7150E-04	9.6057E-03	1.6523E-02	2.1981E-02	2.6516E-02
0.4003	0.0463	0.01UPPER1	-1.0853E-01	-1.7800E-02	-2.9744E-02	-1.6557E-02	-5.9150E-03	2.7077E-03	5.8886E-03
0.4003	0.0463	0.01LOWER1	-7.9930E-02	-1.7800E-02	-2.9744E-02	-1.6557E-02	-5.9150E-03	2.7077E-03	5.8886E-03
0.4003	0.0463	9.0000E 01	-1.0554E-01	-1.0647E-01	-5.8079E-02	-3.3811E-02	1.8194E-02	-6.7745E-03	2.1792E-03
0.4003	0.0463	-9.0000E 01	-1.0004E-01	-5.0703E-02	-2.2359E-02	-8.5742E-03	1.1681E-03	8.8714E-03	1.5269E-02
0.4503	0.0452	0.01UPPER1	-2.3600E-01	-1.8094E-01	-4.8127E-02	-3.4507E-02	-2.2351E-02	-1.2358E-02	-3.9884E-03
0.4503	0.0452	0.01LOWER1	-1.3318E-01	-3.3905E-02	-4.8127E-02	-3.4507E-02	-2.2351E-02	-1.2358E-02	-3.9884E-03
0.4503	0.0452	9.0000E 01	-1.4957E-01	-1.3825E-01	-8.5776E-02	-5.7394E-02	-3.8717E-02	-2.5058E-02	-1.4341E-02
0.4503	0.0452	-9.0000E 01	-1.2414E-01	-7.3650E-02	-4.0675E-02	-2.4400E-02	-1.3094E-02	-4.1977E-03	3.2137E-03
0.5003	0.0421	0.01UPPER1	-2.5131E-01	-2.1180E-01	-5.7976E-02	-4.7998E-02	-3.6079E-02	-2.6035E-02	-1.7565E-02
0.5003	0.0421	0.01LOWER1	-1.5177E-01	-9.2198E-02	-5.7976E-02	-4.7998E-02	-3.6079E-02	-2.6035E-02	-1.7565E-02
0.5003	0.0421	9.0000E 01	-2.0258E-01	-1.5245E-01	-1.0375E-01	-7.4991E-02	-5.5641E-02	-4.1356E-02	-3.0135E-02
0.5003	0.0421	-9.0000E 01	-1.2763E-01	-8.2973E-02	-5.1443E-02	-3.5490E-02	-2.4446E-02	-1.3750E-02	-8.4837E-03

START OF SUPERSONIC CALCULATION

SUPERSONIC CALCULATION STARTS AT X/L = 0.54232E 00

X/L	RBDY/L	THETABDEG1	CPI(BODY)	CPI(R/D= 1.00)CPI/R/D= 2.00)CPI(A/D= 4.00)CPI/R/D= 5.00)CPI(R/D= 6.00)					
0.5503	0.0374	0.01UPPER1	-2.2116E-01	-2.1671E-01	-5.3007E-02	-5.5999E-02	-4.6073E-02	-3.7416E-02	-3.0085E-02
0.5503	0.0374	0.01LOWER1	-1.2453E-01	-1.0559E-01	-5.3071E-02	-5.5999E-02	-4.6073E-02	-3.7416E-02	-3.0085E-02
0.5503	0.0374	9.0000E 01	-1.7361E-01	-1.4418E-01	-1.0851E-01	-8.4620E-02	-6.7067E-02	-5.4217E-02	-4.4079E-02
0.5503	0.0374	-9.0000E 01	-6.5743E-02	-7.0551E-02	-5.0508E-02	-3.9020E-02	-3.0796E-02	-2.4174E-02	-1.8940E-02
0.6003	0.0319	0.01UPPER1	-1.2235E-01	-1.8424E-01	-2.2199E-01	-5.8233E-02	-5.1298E-02	-4.5209E-02	-4.0103E-02
0.6003	0.0319	0.01LOWER1	-2.8904E-02	-8.1685E-02	6.0715E-04	-5.8233E-02	-5.1298E-02	-4.5209E-02	-4.0103E-02
0.6003	0.0319	9.0000E 01	-8.4287E-02	-1.0637E-01	-9.5302E-02	-8.1400E-02	-7.0081E-02	-6.1156E-02	-5.3986E-02
0.6003	0.0319	-9.0000E 01	-3.2376E-03	-2.9389E-02	-3.2612E-02	-3.1195E-02	-2.9127E-02	-2.4915E-02	-2.4770E-02
0.7003	0.0300	0.01UPPER1	1.4021E-01	-6.7898E-02	-2.0739E-01	-1.3326E-01	-1.0027E-01	-8.6509E-02	-7.8337E-02
0.7003	0.0300	0.01LOWER1	1.3651E-01	-6.9357E-02	-2.0202E-01	-1.3326E-01	-1.0027E-01	-8.6509E-02	-7.8337E-02
0.7003	0.0300	9.0000E 01	1.6740E-01	2.1638E-02	-3.7193E-02	-5.4065E-02	-5.9448E-02	-6.0769E-02	-6.0537E-02
0.7003	0.0300	-9.0000E 01	1.4110E-01	2.2186E-02	-3.7693E-02	-5.4774E-02	-6.0151E-02	-6.1445E-02	-6.1119E-02

DRAG COEFFICIENT = 0.13419E 00
 LIFT COEFFICIENT = 0.17070E 01
 PITCHING MOMENT COEFFICIENT = -0.89056E 00

(b) Output.

Figure 9.- Concluded.

*TRANIN AMACH=1., MOPT=1, TAUB=1, TAUM=.04, XMTB=.5, XMTW=.5, ANGLE=58.,
 SSMAX=.25, XRLE=.25, TR=.2, CRT=.5, XLBASE=.86, XLOUTP=.05, ALPHA=2., AL=3., &END

(a) Input.

CALCULATION OF SURFACE AND FLOW FIELD PRESSURE DISTRIBUTIONS
 FOR FLOW AT FREE STREAM MACH NUMBERS AT OP NEAR ONE, BELOW
 THE LOWER CRITICAL, OR ABOVE THE UPPER CRITICAL MACHUT : FINITE
 THICKNESS WING-BODY COMBINATION WITH THE BODY HAVING
 AN ELLIPTIC CROSS SECTION THAT MAINTAINS A CONSTANT RATIO OF
 MAJOR/MINOR AXES ALONG THE ENTIRE BODY LENGTH WITH THE EQUI-
 VALENT BCCY OF REVOLUTION EITHER USER-SPECIFIED OR HAVING CO-
 ORDINATES R PROPORTIONAL TO $X/L - (X/L)^{m_1}$ OR $1 - X/L - (1 - X/L)^{m_2}$,
 THE WING HAVING A CONSTANT THICKNESS/CHORD RATIO, TAPER RATIO
 BETWEEN 0 AND 1, AND WITH ORIGINATES Z PROPORTIONAL TO $XBAR/C$
 - $(XBAR/C)^{m_3}$ OR $1 - XBAR/C - (1 - XBAR/C)^{m_4}$ BY USING THE TRANSCRIC
 EQUIVALENCE RULE AND THE LOCAL LINEARIZATION METHOD

WING-BODY COMBINATION GEOMETRY AND FLOW FIELD CHARACTERISTICS

RATIO OF SEMIMAJOR/SEMIMINOR AXIS = C.3000E 01
 EQUIVALENT BODY THICKNESS RATIO = C.1000E 00
 EQUIVALENT BODY MAXIMUM THICKNESS AT X/L = C.5000E 00
 EXPONENT N FOR EQUIVALENT BODY COORDINATES = C.2000E 01
 SEB''(X) = 0 AT X/L = C.21132E 00
 WING MAX. THICKNESS AT XBAR/C = C.5000E 00
 WING THICKNESS/CHORD RATIO = C.0000E 01
 EXPONENT FOR WING ULTRALINES = C.2000E 01
 LEADING EDGE OF WING ROOT CHORD AT X/L = C.2500E 00
 TRAILING EDGE OF WING ROOT CHORD AT X/L = C.7500E 00
 PLANFORM TAPER RATIO = C.2000E 00
 LEADING EDGE PIERCES BCCY AT X/L = C.3807E 00
 TRAILING EDGE PIERCES BCCY AT X/L = C.7500E 00
 BODY BASE AT X/L = C.6600E 00
 LEADING EDGE SWEET ANGLE (DEG) = C.5000E 02
 TRAILING EDGE SWEET ANGLE (DEG) = C.0000
 LOCATION OF WINGTIP LEADING EDGE AT X/L = C.6500E 00
 LOCATION OF WINGTIP TRAILING EDGE AT X/L = C.7500E 00
 NORMALIZED MAX. SEMISPAAN SSMAX/L = C.2500E 00
 ANGLE OF ATTACK ALPHAS (DEG) = C.2000E 01
 RATIO OF SPECIFIC HEATS = C.1400E 01
 FREE STREAM MACH NUMBER = C.1000E 01

START OF INTEGRATION FROM SEB''(X) = 0 TO NCSE

X/L	RHOAUX/L	THETA(DEG)	CP(BCCY)	CP(R/D= 1.00)CP(R/D= 2.00)CP(R/D= 3.00)CP(R/D= 4.00)CP(R/D= 5.00)CP(R/D= 6.00)					
0.2113	0.0577	0.0000	2.9647E-02	3.6854E-02	3.5139E-02	3.4458E-02	3.4762E-02	3.4718E-02	3.4695E-02
0.2113	0.1192	9.0000E 01	-4.5801E-03	1.9287E-02	2.7071E-02	2.4726E-02	3.1020E-02	3.1780E-02	3.2278E-02
0.2113	0.0192	-9.0000E 01	3.2254E-02	4.2027E-02	3.9819E-02	3.6496E-02	3.7659E-02	3.7114E-02	3.6733E-02
0.2003	0.0555	0.0000	3.6827E-02	4.2121E-02	3.6053E-02	3.4778E-02	3.5476E-02	3.4733E-02	3.4140E-02
0.2003	0.0185	9.0000E 01	6.7930E-04	2.3926E-02	2.3955E-02	3.1294E-02	3.1705E-02	3.1781E-02	3.1715E-02
0.2003	0.0125	-9.0000E 01	3.5332E-02	4.6871E-02	4.2658E-02	4.0066E-02	3.8338E-02	3.7105E-02	3.6162E-02
0.1503	0.0442	0.0000	4.4855E-02	6.36C-02	4.8461E-02	4.0507E-02	3.5000E-02	3.0769E-02	2.7329E-02
0.1503	0.0147	9.0000E 01	2.9626E-02	4.4900E-02	4.0471E-02	3.5539E-02	3.1418E-02	2.7975E-02	2.5041E-02
0.1503	0.0147	-9.0000E 01	7.4711E-02	6.7389E-02	5.2663E-02	4.2751E-02	3.7610E-02	3.2941E-02	2.9185E-02
0.1003	0.0313	0.0000	1.4130E-01	7.6617E-02	5.1753E-02	3.6437E-02	2.5786E-02	1.7556E-02	1.0844E-02
0.1003	0.0104	9.0000E 01	6.6913E-02	3.2481E-02	4.5266E-02	3.2466E-02	2.2920E-02	1.5317E-02	9.0091E-03
0.1003	0.0104	-9.0000E 01	1.1441E-01	8.2507E-02	5.5140E-02	3.7939E-02	1.5338E-02	1.2362E-02	
0.0503	0.0166	0.0000	2.1901E-01	8.0565E-02	4.0477E-02	1.7155E-02	7.0433E-04	-1.2047E-02	-2.2460E-02
0.0503	0.0055	9.0000E 01	1.2382E-01	7.2489E-02	3.6474E-02	1.4920E-02	-9.3070E-04	-1.1333E-02	-2.3520E-02
0.0503	0.0045	-9.0000E 01	1.6182E-01	8.4504E-02	4.2265E-02	1.8913E-02	-2.0667E-03	-1.0935E-02	-2.1521E-02
0.0043	0.0015	C.0CCC	4.2062E-01	4.6119E-02	-7.5084E-03	-3.5150E-02	-6.1932E-02	-7.9323E-02	-9.3532E-02
0.0043	0.0005	9.0000E 01	3.0927E-01	4.5501E-02	-8.2121E-03	-3.4711E-02	-6.2092E-02	-7.5443E-02	-9.3632E-02
0.0043	0.0005	-9.0000E 01	3.7323E-01	4.6691E-02	-7.6170E-03	-3.7314E-02	-6.1784E-02	-7.9244E-02	-9.3434E-02

START OF INTEGRATION FROM SEB''(X) = 0 TO TAIL

X/L	RHOAUX/L	THETA(DEG)	CP(BCCY)	CP(R/D= 1.00)CP(R/D= 2.00)CP(R/D= 3.00)CP(R/D= 4.00)CP(R/D= 5.00)CP(R/D= 6.00)					
0.2113	0.0577	0.0000	2.9647E-02	3.6854E-02	3.5139E-02	3.4458E-02	3.4762E-02	3.4718E-02	3.4695E-02
0.2113	0.0192	9.0000E 01	-4.5801E-03	1.9287E-02	2.7071E-02	2.4726E-02	3.1020E-02	3.1780E-02	3.2278E-02
0.2113	0.0192	-9.0000E 01	3.2254E-02	4.2027E-02	3.9819E-02	3.6496E-02	3.7659E-02	3.7114E-02	3.6733E-02
0.2503	0.0650	0.0000	-3.3385E-04	1.7161E-02	2.3564E-02	2.7547E-02	3.0411E-02	3.2644E-02	3.4472E-02
0.2503	0.0217	9.0000E 01	-2.3538E-03	3.0961E-03	1.6359E-02	2.2843E-02	2.6929E-02	3.2190E-02	
0.2503	0.0217	-9.0000E 01	8.6659E-03	2.4441E-02	3.8741E-02	3.1337E-02	3.5068E-02	3.6522E-02	

Figure 10.- Sample input/output for a wing-body combination having an elliptical body and with $TR \neq 0$, $\beta_{te} \leq 0$, $\alpha \neq 0$.

0.3003	0.0720	0.0000	-3.4176E-02	-9.3541E-03	0.8810E-03	1.5561E-02	2.1635E-02	2.6324E-02	3.0145E-02
0.3003	0.0243	9.0000E 01	-4.4569E-02	-1.6684E-02	1.6510E-03	1.1869E-02	1.8844E-02	2.4036E-02	2.8227E-02
0.3003	0.0243	-9.0000E 01	-1.8815E-02	1.6199E-03	1.2553E-02	1.9422E-02	2.4553E-02	2.8666E-02	3.2100E-02
0.3503	0.0788	0.0000	-6.3453E-02	-3.5815E-02	-1.0851E-02	1.7634E-03	1.0372E-02	1.6986E-02	2.2306E-02
0.3503	0.0263	9.0000E 01	-6.3149E-02	-3.4999E-02	-1.3465E-02	-5.9658E-04	8.4323E-03	1.5357E-02	2.0967E-02
0.3503	0.0263	-9.0000E 01	-4.3844E-02	-2.0613E-02	-4.7157E-03	5.5071E-03	1.3089E-02	1.9109E-02	2.4117E-02
0.4003	0.0830	0.0(UPPER)	-1.3558E-01	-7.7849E-03	-1.9949E-02	-8.7076E-03	2.3704E-04	7.4149E-03	1.3370E-02
0.4003	0.0830	0.0(LOWER)	4.4171E-02	-1.7349E-03	-1.9949E-02	-8.7076E-03	2.3704E-04	7.4149E-03	1.3370E-02
0.4003	0.0277	9.0000E 01	-1.3518E-01	-7.8563E-02	-4.1570E-02	-2.2118E-02	-9.4300E-03	-1.1666E-04	7.2124E-03
0.4003	0.0277	-9.0000E 01	-7.8030E-02	-3.2850E-02	-1.2226E-02	-1.5539E-03	6.5047E-03	1.2771E-02	1.8015E-02
0.4503	0.0834	0.0(UPPER)	-2.2484E-01	-1.9656E-01	-5.1038E-02	-3.7551E-02	-2.4492E-02	-1.3921E-02	-5.1265E-03
0.4503	0.0836	0.0(LOWER)	-9.5429E-02	-4.7413E-02	-5.3038E-02	-3.7551E-02	-2.4492E-02	-1.3921E-02	-5.1265E-03
0.4503	0.0275	9.0000E 01	-1.5877E-01	-1.3567E-01	-8.6272E-02	-5.8245E-02	-3.9544E-02	-2.3715E-02	-1.4844E-02
0.4503	0.0279	-9.0000E 01	-1.2538E-01	-7.2552E-02	-4.2151E-02	-2.0271E-02	-1.4680E-02	-5.47C7E-03	2.2317E-03
0.5003	0.0801	0.0(UPPER)	-2.6787E-01	-2.3975E-01	-7.2912E-02	-5.8920E-02	-4.4316E-02	-3.2241E-02	-2.2133E-02
0.5003	0.0861	0.0(LOWER)	-1.5022E-01	-1.1636E-01	-7.2912E-02	-5.8920E-02	-4.4316E-02	-3.2241E-02	-2.2133E-02
0.5003	0.0267	9.0000E 01	-2.3275E-01	-1.6946E-01	-1.1677E-01	-8.4960E-02	-6.3288E-02	-4.7152E-02	-3.4355E-02
0.5003	0.0267	-9.0000E 01	-1.5503E-01	-1.0022E-01	-6.5108E-02	-4.5939E-02	-3.2469E-02	-2.1853E-02	-1.3033E-02

START OF SUPERSUNIC CALCULATION

SUPERSONIC CALCULATION STARTS AT X/L = 0.54232E 00

X/L	RBODY/L	THETA(IDEGR)	CP(R/CY)	CP(R/D= 1.00)CP(R/D= 2.00)CP(R/D= 3.00)CP(R/D= 4.00)CP(R/D= 5.00)CP(R/E= 6.00)					
0.5503	0.0729	0.0(UPPER)	-2.4483E-01	-2.3568E-01	-6.7498E-02	-6.7246E-02	-5.4718E-02	-4.3983E-02	-3.4932E-02
0.5503	0.0729	0.0(LOWER)	-1.3406E-01	-1.2342E-01	-6.7498E-02	-6.7246E-02	-5.4718E-02	-4.3983E-02	-3.4932E-02
0.5503	0.0243	9.0000E 01	-2.1879E-01	-1.6978E-01	-1.2705E-01	-9.6074E-02	-7.6015E-02	-6.0956E-02	-4.5027E-02
0.5503	0.0243	-9.0000E 01	-1.3948E-01	-9.5664E-02	-6.7159E-02	-5.1242E-02	-4.0027E-02	-3.1143E-02	-2.3682E-02
0.6003	0.0631	0.0(UPPER)	-1.3192E-01	-1.7966E-01	-2.2356E-01	-5.9157E-02	-5.2225E-02	-4.5961E-02	-4.0752E-02
0.6003	0.0631	0.0(LOWER)	-2.8191E-02	-7.5253E-02	-2.4762E-04	-5.9157E-02	-5.2225E-02	-4.5961E-02	-4.0752E-02
0.6003	0.0210	9.0000E 01	-1.1992E-01	-1.1682E-01	-9.9784E-02	-8.4131E-02	-7.1961E-02	-6.2514E-02	-5.4961E-02
0.6003	0.0210	-9.0000E 01	-3.8163E-02	-4.0630E-02	-3.7462E-02	-3.4207E-02	-3.1237E-02	-2.8456E-02	-2.5839E-02
0.7003	0.0550	0.0(UPPER)	1.3230E-01	-3.9002E-02	-1.5151E-01	-1.2484E-01	-9.4236E-02	-8.2051E-02	-7.5077E-02
0.7003	0.0550	0.0(LOWER)	1.2609E-01	-4.0953E-02	-1.8671E-01	-1.2484E-01	-9.4236E-02	-8.2051E-02	-7.5077E-02
0.7003	0.0183	9.0000E 01	1.5910E-01	2.1566E-02	-3.1702E-02	-4.8917E-02	-5.5222E-02	-5.75C0E-02	-5.8C83E-02
0.7003	0.0183	-9.0000E 01	1.6097E-01	2.1883E-02	-3.2230E-02	-4.9629E-02	-5.5919E-02	-5.8138E-02	-5.8657E-02

DRAG COEFFICIENT = C.12462E 00
 LIFT COEFFICIENT = C.17073E 01
 PITCHING MOMENT COEFFICIENT = -0.2694E 00

(b) Output.

Figure 10.- Concluded.

STRANIN AMACH=1., MOPT=1., TAUB=.1., TAUN=.04, XMTB=.5, XMTW=.5, ANGLE=45.,
 SSMAX=.3215, XRLE=.25, TR=.4, CRT=.4, XLBASE=.86, XLOUTP=.05, LEND

(a) Input.

CALCULATION OF SURFACE AND FLOW FIELD PRESSURE DISTRIBUTIONS
 FOR FLOW AT FREE STREAM MACH NUMBERS AL OR NEAR ONE, BELOW
 THE LOWER CRITICAL, OR ABOVE THE UPPER CRITICAL, ABOUT A FINITE
 THICKNESS WING-INCLINED CIRCULAR BODY COMBINATION WITH THE
 EQUIVALENT BODY OF REVOLUTION EITHER USER-SPECIFIED OR HAVING
 ORDINATES R PROPORTIONAL TO $X/L - (X/L)^{1/N}$ OR $1 - X/L - (1 - X/L)^{1/N}$,
 THE WING HAVING A CONSTANT THICKNESS/CHORD RATIO, TAPER RATIO
 $-(XBAR/C)^{1/M}$ OR $1 - XBAR/C - (1 - XBAR/C)^{1/M}$ BY USING THE TRANSONIC
 EQUIVALENCE NURSE AND THE LOCAL LINEARIZATION METHOD

WING-BODY COMBINATION GEOMETRY AND FLOW FIELD CHARACTERISTICS

EQUIVALENT BODY THICKNESS RATIO =	C.1000E 00
EQUIVALENT BODY MAXIMUM THICKNESS AT X/L =	C.5000E 00
EXPONENT N FOR EQUIVALENT BODY COORDINATES =	C.20000F 01
SEB** (X) = 0 AT X/L =	0.2113E 00
WING MAX. THICKNESS AT XBAR/C =	C.5000E 00
WING THICKNESS/CHORD RATIO =	C.4000E-01
EXPONENT M FOR WING COORDINATES =	0.20000E 01
LEADING EDGE OF WING CUT CHORD AT X/L =	C.2500E 00
TRAILING EDGE OF WING ROOT CHORD AT X/L =	C.5500E 00
PLANFORM TAPER RATIO =	C.4000E 00
LEADING EDGE PIERCES BODY AT X/L =	C.25129E 00
TRAILING EDGE PIERCES BODY AT X/L =	C.57156E 00
BODY BASE AT X/L =	C.8600E 00
LEADING EDGE SWEET ANGLE (DEG) =	C.45000E 02
TRAILING EDGE SWEET ANGLE (DEG) =	C.23755E 02
LOCATION OF WINGTIP LEADING EDGE AT X/L =	C.57156E 00
LOCATION OF WINGTIP TRAILING EDGE AT X/L =	C.69156E 00
NORMALIZED MAX. SEMISPAN SSMAX/L =	C.32150E 00
ANGLE OF ATTACK ALPHAS (DEG) =	C.00000
RATIO OF SPECIFIC HEATS =	C.1400E 01
FREE STREAM MACH NUMBER =	C.10000E 01

START OF INTEGRATION FROM SEB** (X) = C TO NOSE

X/L	R BODY/L	THETA (DEG)	CP(BODY)	CP(R/D= 1.00)CP(R/D= 2.00)CP(R/U= 3.00)CP(R/D= 4.00)CP(R/D= 5.00)CP(R/D= 6.00)					
0.2113	0.0333	C.0C00	2.1307E-02	3.3155E-02	3.4270E-02	3.4476E-02	3.4548E-02	3.4582E-02	3.4600E-02
0.2113	0.0333	9.0C00E 01	2.1307E-02	3.3159E-02	3.4270E-02	3.4476E-02	3.4548E-02	3.4582E-02	3.4600E-02
0.2003	0.C320	0.0C00	2.8812E-02	3.8171E-02	3.7124E-02	3.6069E-02	3.5247E-02	3.4587E-02	3.4039E-02
0.2003	0.C320	9.0C00E 01	2.8d13E-02	3.8171E-02	3.7124E-02	3.6069E-02	3.5247E-02	3.4587E-02	3.4039E-02
0.1503	0.0255	0.0C00	6.6692E-02	5.9471E-02	4.7472E-02	4.0071E-02	3.4755E-02	3.0613E-C2	2.7221E-02
0.1503	0.0255	9.0C00E 01	6.6692E-02	5.9471E-02	4.7472E-02	4.0071E-02	3.4755E-02	3.0613E-02	2.7221E-02
0.1003	0.0181	0.0L0C	1.1374E-01	7.5672E-02	5.0874E-02	3.6118E-02	2.56C7E-C2	1.7441E-02	1.0765E-02
0.1003	0.0181	9.0000E 01	1.1374E-C1	7.5672E-02	5.0874E-02	3.6118E-02	2.56C7E-02	1.7441E-02	1.0765E-02
0.0503	0.0096	0.0C00	1.8138E-C1	7.9464E-02	4.0133E-02	1.7038E-02	6.3612E-04	-1.205CE-C2	-2.2450E-02
0.0503	0.0096	9.0000E 01	1.8138E-01	7.9464E-02	4.0133E-02	1.7038E-02	6.3612E-04	-1.2090E-02	-2.2490E-02
0.0043	0.0049	0.0000	3.7747E-C1	4.6107E-02	-7.9117E-03	-3.9512E-02	-6.1932E-02	-7.9323E-02	-9.3533E-G2
0.0043	0.0049	9.0000E 01	3.7747E-01	4.6107E-02	-7.9117E-03	-3.9512E-02	-6.1932E-02	-7.9323E-02	-9.3533E-02

START OF INTEGRATION FROM SEB** (X) = 0 TO TAIL

X/L	R BODY/L	THETA (DEG)	CP(BODY)	CP(R/D= 1.00)CP(R/D= 2.00)CP(R/D= 3.00)CP(R/D= 4.00)CP(R/D= 5.00)CP(R/D= 6.00)					
0.2113	0.C333	0.0C00	2.1307E-02	3.3155E-02	3.4270E-02	3.4476E-02	3.4548E-02	3.4582E-C2	3.4600E-02
0.2113	0.C333	9.0C00E 01	2.1307E-02	3.3159E-02	3.4270E-02	3.4476E-02	3.4548E-02	3.4582E-02	3.4600E-02
0.2503	0.C375	0.0C00	-3.4545E-C3	1.4556E-02	2.3030E-02	2.7311E-02	3.0278E-02	3.2559E-02	3.4413E-02
0.2503	0.C375	9.0C00E 01	-3.4545E-C3	1.4593E-02	2.3030E-02	2.7311E-02	3.0278E-02	3.2559E-02	3.4413E-02
0.3003	0.C420	0.0C00	6.4617E-02	1.2911E-02	1.9734E-02	2.3766E-02	2.7481E-02	3.0616E-C2	3.3278E-02
0.3003	0.C420	9.0C00E 01	-7.8405E-02	-1.1963E-02	1.1116E-02	1.9936E-02	2.5327E-02	2.9237E-02	3.2320E-02
0.3503	0.C440	0.0000	-1.4041E-C1	1.0000E-06	-4.9464E-03	1.9090E-03	5.4194E-03	1.5920E-C2	2.15C5E-02
0.3503	0.C440	9.0000E 01	-1.3218E-01	-6.5572E-02	-2.4868E-02	-6.7934E-03	4.5358E-03	1.2803E-02	1.9335E-02
0.4003	0.C434	0.0C00	-1.6553E-C1	-1.2128E-01	-6.0262E-03	-9.6651E-03	-2.2625E-03	5.01C3E-03	1.1470E-02
0.4003	0.C434	9.0000E 01	-1.4164E-01	-9.0492E-02	-4.6757E-02	-2.4610E-02	-1.0504E-02	-2.3066E-04	1.8310E-03

Figure 11.- Sample input/output for a wing-body combination having a circular body and with $TR \neq 0$, $\beta_0 > 0$, $a = 0$.

0.4503	0.0413	0.0000	-1.555E-01	-1.5350E-01	1.0000E 06	-1.3301E-02	-5.9250E-03	-3.4170E-03	2.4071E-03
0.4503	0.0413	9.0000E 01	-9.6670E-02	-8.2432E-02	-5.2027E-02	-3.2346E-02	-1.9330E-02	-9.5920E-03	-1.0102E-03
0.5003	0.0391	0.0000	-7.4455E-02	-1.4312E-01	-1.2943E-01	-1.6010E-02	-1.9018E-02	-1.4648E-02	-9.4376E-03
0.5003	0.0391	9.0000E 01	-1.5436E-02	-9.1929E-02	-4.5851E-02	-3.5565E-02	-2.5932E-02	-1.8148E-02	-1.1739E-02

START OF SUPERSONIC CALCULATION

SUPERSONIC CALCULATION STARTS AT X/L = 0.54232E 00

X/L	RHO/D/V/L	THETA(DEG)	CPR(BODY)	CPR/D= 1.001CPR/D= 2.001CPR/D= 3.001CPR/D= 4.001CPR/D= 5.001CPR/D= 6.001CPR/D=							
0.5503	0.0390	0.0000	5.1569E-03	-1.2736E-01	-1.9753E-01	1.0000E 06	-1.5947E-02	-3.0560E-02	-3.1166E-02		
0.5503	0.0390	9.0000E 01	7.1914E-02	-1.5654E-02	-4.5427E-02	-4.4275E-02	-1.8527E-02	-7.2306E-02	-2.6452E-02		
0.6003	0.0418	0.0000	5.6515E-02	-1.9614E-01	-1.3863E-01	-2.1714E-01	-1.0002E-01	-7.6649E-02	-6.1059E-02		
0.6003	0.0418	9.0000E 01	1.0884E-02	-3.5788E-02	-1.2692E-02	-2.6592E-02	-3.3339E-02	-3.1867E-02	-3.0595E-02		
0.6503	0.0439	0.0000	-2.6776E-01	-8.5102E-01	-3.9688E-02	-1.2196E-01	-6.9199E-02	-6.0871E-02	-5.5770E-02		
0.6503	0.0439	9.0000E 01	-2.7797E-01	-1.7927E-01	-1.1532E-01	-4.4898E-02	-7.6059E-02	-6.7084E-02	-6.0440E-02		
0.7003	0.0420	0.0000	-1.3105E-01	-1.0778E-01	-4.2537E-02	-8.3971E-02	-7.7990E-02	-7.3247E-02	-6.5512E-02		
0.7003	0.0420	9.0000E 01	-1.3105E-01	-1.0778E-01	-9.2537E-02	-8.3971E-02	-7.7990E-02	-7.3247E-02	-6.5512E-02		
0.7503	0.0375	0.0000	-1.1600E-01	-9.1726E-02	-8.9741E-02	-8.5572E-02	-8.2649E-02	-8.0463E-02	-7.8570E-02		
0.7503	0.0375	9.0000E 01	-1.1600E-01	-9.1726E-02	-8.9741E-02	-8.5572E-02	-8.2649E-02	-8.0463E-02	-7.8570E-02		
0.8003	0.0320	0.0000	-8.8124E-02	-7.9922E-02	-8.0057E-02	-8.1477E-02	-8.2102E-02	-8.2844E-02	-8.3786E-02		
0.8003	0.0320	9.0000E 01	-8.8124E-02	-7.9922E-02	-8.0057E-02	-8.1727E-02	-8.2102E-02	-8.2844E-02	-8.3388E-02		
0.8503	0.0255	0.0000	-3.9935E-02	-6.7040E-02	-5.9191E-02	-6.6680E-02	-7.2057E-02	-7.6247E-02	-7.4676E-02		
0.8503	0.0255	9.0000E 01	-3.9935E-02	-6.7040E-02	-5.9191E-02	-6.6680E-02	-7.2057E-02	-7.6247E-02	-7.4676E-02		

DRAG COEFFICIENT = 0.1044E 00

(b) Output.

Figure 11.- Concluded.

6TRANIN ANACH=1., MOPT=1, TAUB=.1, TAUM=.04, XMTB=.5, XMTW=.5, ANGLE=45.,
 SSMAX=.338, XRLE=.25, TR=.4, CRT=.4, XLBASE=.86, XLOUTP=.05, AL=3., LEND

(a) Input.

CALCULATION OF SURFACE AND FLOW FIELD PRESSURE DISTRIBUTIONS
 FOR FLOW AT FREE STREAM MACH NUMBERS AT OR NEAR ONE, BELOW
 THE LOWER CRITICAL, OR ABOVE THE UPPER CRITICAL ABOUT A FINITE
 THICKNESS WING-INCENTED BODY COMBINATION WITH THE BODY HAVING
 AN ELLIPTICAL CROSS SECTION THAT MAINTAINS A CONSTANT RATIO OF
 MAJOR/MINOR AXES ALONG THE ENTIRE BODY LENGTH WITH THE EQUI-
 VALENT BODY OF REVOLUTION EITHER USER-SPECIFIED OR HAVING CO-
 ORDINATES R PROPORTIONAL TO $X/L - (X/L)^m$ OR $1-X/L - (1-X/L)^m$,
 THE WING HAVING A CONSTANT THICKNESS/CHORD RATIO, TAPER RATIO
 BETWEEN 0 AND 1, AND WITH COORDINATES Z PROPORTIONAL TO $XBAR/C$
 - $(XPAR/C)^m$ OR $1-XBAR/C - (1-XPAR/C)^m$ BY USING THE TRANSONIC
 EQUIVALENCE RULE AND THE LOCAL LINEARIZATION METHOD

WING-BODY COMBINATION GEOMETRY AND FLOW FIELD CHARACTERISTICS

RATIO OF SEMIMAJOR/SEMIPRINCIPAL AXIS = C.30000E 01
 EQUIVALENT BODY THICKNESS RATIO = C.10000E 00
 EQUIVALENT BODY MAXIMUM THICKNESS AT X/L = C.50000E 00
 EXPONENT FOR EQUIVALENT BODY COORDINATES = C.20000E 01
 SEB** (X) = 0 AT X/L = C.21132E 00
 WING MAX. THICKNESS AT XBAR/C = C.53000E 00
 WING THICKNESS/CHORD RATIO = C.40000E-01
 EXPONENT M FOR WING COORDINATES = C.20000E 01
 LEADING EDGE OF WING ROOT CHORD AT X/L = C.25000E 00
 TRAILING EDGE OF WING ROOT CHORD AT X/L = C.55000E 00
 PLANFORM TAPER RATIO = C.40000E 00
 LEADING EDGE PIERCES BODY AT X/L = C.32613E 00
 TRAILING EDGE PIERCES BODY AT X/L = C.53919E 00
 BODY BASE AT X/L = C.96000E 00
 LEADING EDGE SWEET ANGLE (DEG) = C.45000E 00
 TRAILING EDGE SWEET ANGLE (DEG) = C.25054E 02
 LOCATION OF WINGTIP LEADING EDGE AT X/L = C.58800E 00
 LOCATION OF WINGTIP TRAILING EDGE AT X/L = C.70800E 00
 NORMALIZED MAX. SEMISPAN SSMAX/X/L = C.33800E 00
 ANGLE OF ATTACK ALPPA (DEG) = C.00000
 RATIO OF SPECIFIC HEATS = C.14000E 01
 FREE STREAM MACH NUMBER = C.10000E 01

START OF INTEGRATION FROM SEB** (X) = 0 TO ACSE

X/L	RBODY/L	THETA (DEG)	CP(BODY)	CP(R/C= 1.00)CP(R/D= 2.00)CP(H/D= 3.00)CP(R/D= 4.00)CP(R/C= 5.00)CP(R/D= 6.00)					
0.2113	0.0577	C.0000	4.7974E-02	3.7658E-02	3.5267E-02	3.4492E-02	3.4797E-02	3.4740E-02	3.4710E-02
0.2113	0.0142	9.0000E 01	1.2418E-02	3.0253E-02	3.3360E-02	3.4053E-02	3.4306E-02	3.4426E-02	3.4451E-02
0.2003	C.0555	C.0000	5.7104E-02	4.2837E-02	3.8188E-02	3.6535E-02	3.5508E-02	3.4754E-02	3.4154E-02
0.2003	0.0185	9.0000E 01	1.2878E-02	3.5020E-02	3.6160E-02	3.5623E-02	3.4993E-02	3.4423E-02	3.3929E-02
0.1503	0.0442	0.0000	1.0313E-01	6.3999E-02	4.8544E-02	4.0543E-02	3.5020E-02	3.0782E-02	2.7338E-02
0.1503	0.0147	4.0000E 01	5.0961E-02	5.5879E-02	4.6461E-02	3.9611E-02	3.4495E-02	3.0446E-02	2.7104E-02
0.1003	0.0313	0.0000	1.5950E-01	7.6793E-02	5.1634E-02	3.6054E-02	2.5796E-02	1.7562E-02	1.0848E-02
0.1003	0.0144	9.0000E 01	3.1420E-02	7.2880E-02	5.0134E-02	3.5786E-02	2.5419E-02	1.7321E-02	1.0681E-02
0.0503	0.0160	0.0000	2.2788E-01	8.0611E-02	4.4418E-02	1.7164E-02	1.0711E-04	-1.2045E-02	-2.2459E-02
0.0503	0.0055	9.0000E 01	1.5160E-01	7.8353E-02	3.9851E-02	1.6912E-02	5.6524E-04	-1.2136E-02	-2.2522E-02
0.0043	0.0015	0.0000	4.4493E-01	4.6119E-02	-7.5088E-03	-3.5911E-02	-6.1932E-02	-7.9323E-02	-9.3532E-02
0.0043	0.0005	9.0000E 01	3.4040E-01	4.6096E-02	-7.7147E-03	-3.59513E-02	-6.1933E-02	-7.9324E-02	-9.3533E-02

START OF INTEGRATION FROM SEB** (X) = 0 TO TAUL

X/L	RBODY/L	THETA (DEG)	CP(BODY)	CP(R/D= 1.00)CP(H/D= 2.00)CP(H/D= 3.00)CP(H/D= 4.00)CP(R/D= 5.00)CP(R/D= 6.00)					
0.2113	C.0577	C.0000	4.7974E-01	3.7658E-02	3.5267E-02	3.4492E-02	3.4797E-02	3.4740E-02	3.4710E-02
0.2113	0.0142	9.0000E 01	1.2414E-02	3.0253E-02	3.3360E-02	3.4053E-02	3.4306E-02	3.4426E-02	3.4451E-02
0.2503	0.0650	C.0000	1.7943E-02	1.6326E-02	2.3756E-02	2.7627E-02	3.0455E-02	3.2671E-02	3.4452E-02
0.2503	0.0217	9.0000E 01	-8.6543E-03	1.3204E-02	2.2413E-02	2.7017E-02	3.0109E-02	3.2449E-02	3.4337E-02
0.3003	0.0728	C.0000	-1.5879E-02	-7.5935E-03	7.1287E-03	1.5562E-02	2.1691E-02	2.6359E-02	3.0170E-02
0.3003	0.0243	9.0000E 01	-3.2910E-02	-6.0832E-03	6.9124E-03	1.5553E-02	2.1627E-02	2.6317E-02	3.0140E-02
0.3503	0.0784	0.0000	-1.1022E-02	1.0000E-06	1.3079E-03	1.1848E-03	1.3604E-02	1.9140E-02	2.3851E-02
0.3503	C.0261	9.0000E 01	-1.1392E-01	-4.7325E-02	-1.4910E-02	1.2753E-04	9.6454E-03	1.6616E-02	2.2133E-02

Figure 12.- Sample input/output for a wing-body combination having an elliptical body and with $TR \neq 0$, $B_{te} > 0$, $\alpha = 0$.

0.4003	3.0793	-0.0000	-1.8032E-01	-1.6685E-01	-1.7439E-02	-1.6109E-02	-7.2054E-03	1.3027E-03	8.7667E-03
0.4003	0.0244	9.0000E 01	-1.6231E-01	-9.4191E-02	-5.1764E-02	-3.0159E-02	-1.4055E-02	-1.9634E-03	9.1760E-03
0.4503	0.6762	0.0000	-1.7091E-01	-1.6747E-01	-1.0000E-06	-1.0000E-02	-1.4561E-01	-7.5245E-01	-6.1877E-04
0.4503	3.0754	9.0000E 01	-1.7439E-01	-9.5165E-02	-6.2477E-02	-4.0469E-02	-2.5278E-02	-1.4013E-02	-6.0541E-01
0.5003	0.0712	0.0000	-1.3066E-07	-1.0000E-01	-1.2411E-04	-1.1252E-02	-1.6567E-02	-1.24776E-02	-1.06722E-01
0.5003	3.0237	9.0000E 01	-4.5027E-02	-5.0159E-02	-4.7044E-02	-3.4734E-02	-2.4495E-02	-1.7315E-02	-1.1111E-02

START OF SUPERSONIC CALCULATION

SUPERSONIC CALCULATION STARTS AT X/L = 0.54232E 30

X/L	P30BY/L	THETA(DEG)	CP14(CPV)	CP15(DP)	1.001CP14/1.1	1.001CP15/1.1	3.001CP14/D	4.001CP15/D	5.001CP14/C	7.001CP15/C
0.5503	0.0662	0.0000	-1.7010E-03	-9.7047E-02	-1.7118E-01	-1.0000E-06	-1.4561E-02	-3.1435E-02	-2.1591E-02	-2.2333E-02
0.5503	0.0227	9.0000E 01	-9.4924E-02	-2.1245E-01	-3.1473E-02	-3.0016E-02	-1.3193E-02	-2.8017E-02	-2.2333E-02	-2.2333E-02
0.6003	0.0767	0.0000	1.6649E-01	2.7114E-01	-2.1096E-01	-3.0006E-01	-1.4117E-01	-1.3937E-01	-5.5744E-02	-5.5744E-02
0.6003	3.0236	9.0000E 01	9.2173E-01	5.7479E-01	5.6777E-01	1.0577E-02	-1.4471E-02	-2.7133E-02	-2.7111E-02	-2.7111E-02
0.5503	0.0738	0.0000	-1.5205E-01	-1.0000E-01	-9.4140E-02	-2.1564E-01	-1.4045E-02	-7.4065E-02	-6.4270E-02	-5.3844E-02
0.6003	0.0246	9.0000E 01	-1.6556E-01	-1.0000E-01	-9.0352E-02	-6.9336E-02	-6.2452E-02	-5.7995E-02	-5.3844E-02	-5.3844E-02
0.7003	0.0736	0.0000	-9.7124E-01	-3.9777E-01	-1.4117E-01	-9.4602E-02	-1.833CE-02	-2.3764E-02	-3.8054E-02	-3.8054E-02
0.7003	3.0242	9.0000E 01	-4.9145E-01	-3.0177E-01	-2.04943E-01	-1.0415E-01	-1.2397E-01	-1.0524E-01	-9.2679E-02	-9.2679E-02
0.7503	0.0667	0.0000	-9.4607E-01	-3.6334E-01	-8.4059E-02	-8.5293E-02	-8.2671E-02	-8.0286E-02	-7.4658E-02	-7.4658E-02
0.7503	3.0216	9.0000E 01	-1.2134E-01	-9.4944E-02	-9.0414E-02	-8.5469E-02	-8.2819E-02	-8.0513E-02	-7.4658E-02	-7.4658E-02
0.8003	0.0554	0.0000	-5.9736E-02	-7.4748E-02	-7.9031E-02	-8.0760E-02	-8.1841E-02	-8.2637E-02	-8.3270E-02	-8.3501E-02
0.8003	0.0187	9.0000E 01	-5.8217E-02	-6.2086E-02	-6.1064E-02	-5.1674E-02	-5.2357E-02	-5.2968E-02	-5.3501E-02	-5.3501E-02
0.8503	3.0441	0.0000	-2.9819E-03	-9.2523E-02	-5.8121E-02	-6.6209E-02	-7.1753E-02	-7.6076E-02	-7.5562E-02	-7.5562E-02
0.8503	3.0147	9.0000E 01	-5.5355E-03	-9.3621E-02	-6.0200E-02	-6.7134E-02	-7.2317E-02	-7.6614E-02	-7.5759E-02	-7.5759E-02

DRAG COEFFICIENT = 0.54817E-01

(b) Output.

Figure 12.- Concluded.

NATIONAL AERONAUTICS AND SPACE ADMINISTRATION
WASHINGTON, D.C. 20546

OFFICIAL BUSINESS
PENALTY FOR PRIVATE USE \$300

FIRST CLASS MAIL

POSTAGE AND FEES PAID
NATIONAL AERONAUTICS AND
SPACE ADMINISTRATION
481



POSTMASTER: If Undeliverable (Section 1
Postal Manual) Do Not Re-

"The aeronautical and space activities of the United States shall be conducted so as to contribute . . . to the expansion of human knowledge of phenomena in the atmosphere and space. The Administration shall provide for the widest practicable and appropriate dissemination of information concerning its activities and the results thereof."

—NATIONAL AERONAUTICS AND SPACE ACT OF 1958

NASA SCIENTIFIC AND TECHNICAL PUBLICATIONS

TECHNICAL REPORTS: Scientific and technical information considered important, complete, and a lasting contribution to existing knowledge.

TECHNICAL NOTES: Information less broad in scope but nevertheless of importance as a contribution to existing knowledge.

TECHNICAL MEMORANDUMS: Information receiving limited distribution because of preliminary data, security classification, or other reasons. Also includes conference proceedings with either limited or unlimited distribution.

CONTRACTOR REPORTS: Scientific and technical information generated under a NASA contract or grant and considered an important contribution to existing knowledge.

TECHNICAL TRANSLATIONS: Information published in a foreign language considered to merit NASA distribution in English.

SPECIAL PUBLICATIONS: Information derived from or of value to NASA activities. Publications include final reports of major projects, monographs, data compilations, handbooks, sourcebooks, and special bibliographies.

TECHNOLOGY UTILIZATION

PUBLICATIONS: Information on technology used by NASA that may be of particular interest in commercial and other non-aerospace applications. Publications include Tech Briefs, Technology Utilization Reports and Technology Surveys.

Details on the availability of these publications may be obtained from:

SCIENTIFIC AND TECHNICAL INFORMATION OFFICE

NATIONAL AERONAUTICS AND SPACE ADMINISTRATION

Washington, D.C. 20546